Wireless Channel Characteristic and Its Performance for Stratospheric Platform Communication

成層圏飛翔体通信における 無線通信路及びその性能に関する研究

Doctor Dissertation

February 2007

Graduate School of Global Information and Telecommunication Studies
Waseda University

Iskandar

Contents

List of Figures

List of Tables

Glossary

1G	First Generation
2G	Second Generation
3G	Third Generation
3GPP	Third Generation Partnership Project
AWGN	Additive White Gaussian Noise
BER	Bit Error Rate
BTS	Base Transceiver Station
CDMA	Code Division Multiple Access
CDMA2000	Code Division Multiple Access 2000
DPSK	Differential Phase Shift Keying
DQPSK	Differential Quadrature Phase Shift Keying
ETSI	European Telecommunications Standards Institute
FDD	Frequency Division Duplex
GEO	Geosynchronous Earth Orbit
GPIB	General Purposes Interface Bus
GTD	Geometrical Theory of Diffraction
HAPS	High Altitude Platform Station
IMT-2000	International Mobile Communications-2000

ITU	International Telecommunication Union
JAXA	Japan Aerospace Exploration Agency
LEO	Low Earth Orbit
LOS	Line of Sight
PCA	Perspective Continuation Angle
PCS	Personal Communications Systems
PDF	Probability Density Function
MAI	Multiple Access Interference
MEO	Medium Earth Orbit
MS	Mobile Station
NASA	National Aeronautics and Space Administration
NLOS	Non Line of Sight
Rx	Receiver
SCA	Shadowing Continuation Angle
SPF	Stratospheric Platform
TDD	Time Division Duplex
Tx	Transmitter
UMTS	Universal Mobile Telecommunication System
UTD	Uniform Theory of Diffraction
UTRA	UMTS Terrestrial Radio Access (ETSI)
UTRA	Universal Terrestrial Radio Access (3GPP)
WCDMA	Wideband Code Division Multiple Access

Summary

This study aims at evaluating stratospheric platform (SPF) communication channel and its performance. The SPF has been proposed as a novel wireless delivery method which complements to terrestrial and satellite system. Firstly, we propose a definition and describe an analysis of the wireless channel between SPF and terrestrial mobile users based on experiment in which the measurement is only performed for the case of line of sight (LOS) situation in a semi-urban environment. This experiment is intended to characterize multipath channel behavior in various elevation angles from 10^0 to 90^0 in SPF communication. We then evaluate average bit error probability utilizing the proposed channel model to examine the channel performance.

SPF may be used to serve the users in urban environment not only in LOS condition but also in shadow situation. Therefore, our next study is devoted to evaluate propagation characteristic under the condition of LOS and NLOS in a typical urban low rises environment. A typical building geometry model of urban area is developed and then ray tracing scheme is employed to obtain propagation parameters. We obtained propagation parameters in several scenarios and we estimated power transmit requirement by the SPF for application of IMT-2000 services.

The downlink channel performance for the SPF link in urban area is our further evaluation in this study. BER performance on the basis of the SPF channel model previously obtained is then presented. We show that even in LOS conditions refer to elevation angle above 40^0 in the model, multipath fading mitigation techniques would be required because of their high bit error rates.

One of the most promising applications provided by the SPF system is the next generation mobile communications, which basically employ CDMA technology. Therefore, in the last

topic of this study we propose and analyze system capacity for a multibeam SPF CDMA under a comprehensive multiple access interference (MAI) considering fading and imperfect power control. The proposed SPF channel fading characteristic that is firstly obtained in this study is used in the interference analysis to estimate cell capacity with carrying IMT-2000 services. We found that capacity is reduced in multiple SPF model due to prohibitively interference from an overlapped region. One solution is to increase minimum elevation angle defined for each platform in order to reduce an overlapped region and therefore the interference power produced by the users in that region. However, the number of required SPF will increase because with the increasing of minimum elevation angle the platform's coverage area become smaller. This problem, therefore, would be not only costly but also environmentally unacceptable. To cope with this problem we use adaptive antenna array onboard the platform while at the same time we maintain small minimum elevation angle. With this technique we observed that the capacity of multiple SPF model is increased and it is approaching the capacity obtained in the single SPF model.

Acknowledgments

I would like to express my sincere gratitude to my advisor, Prof. Shigeru Shimamoto for his constant support and valuable guidance throughout this project during my time at Graduate School of Global Information and Telecommunication Studies (GITS) of Waseda University. I wish to thank Prof. Yoshiaki Tanaka, Prof. Mitsuji Matsumoto and Prof. Takuro Sato for serving as my dissertation committee and for their contribution to my academic development. I also thank my colleagues in Shimamoto Laboratory for the research discussions.

I would like to thank Hitachi Scholarship Foundation (HSF) for providing financial support throughout my study period. I really appreciate Mr. Tsutomu Gommibuchi, Mr. Mikio Homma, Mr. Hisao Miyake and Miss Nunokami for their excellent assistance especially during the time of my initial living in Tokyo.

Finally, I would like to express my deepest appreciation to my parents for their continuous encouragement to study and hard work, generous support, and abundant love they have given me. I also appreciate my brother and sisters for their steadfast encouragement. My special thanks go to my wife, Dini, for her collective patience extended to me during this work, and to our children Raffa and Raffie for their smiles and cuteness. Without their sacrifices, understanding, love and moral support, I would not have been able to devote the necessary time and concentration to this research.

Chapter 1
Introduction

In this introductory chapter, the author briefly explains the outline of the thesis. In the first section of this chapter, he describes the background and emphasizes the importance of this research. Then research motivation is stated in the next section and finally structure of the thesis is summarized in the last section of this chapter.

1.1 Research Background

Currently, there are two well-established methods for providing wireless communication services. First method is terrestrially based systems, as it is widely used in cellular and personal communications systems (PCS) and the second method is the satellite systems using geosynchronous earth orbit (GEO), medium earth orbit (MEO) and low earth orbit (LEO) satellites. Those wireless systems are currently used world wide for delivering communication services from a low-speed to a very high-speed data rate. Each concept indeed has its specific advantages and disadvantages.

In terrestrial systems, huge number of base stations is required to provide the needed coverage. Meanwhile, to increase the capacity, the cell size must be reduced or antenna sectorizations have to be applied [1]-[3]. Both schemes are allowing the spectrum to be reused more often within a given geographical area called as a frequency reuse technique.

This philosophy leads to the concept of microcells for areas of high user density, with a base-station on perhaps every street corner. However, the increasing demands for communication services grow very rapidly. A pressure on the radio spectrum can therefore be a trigger to a move towards higher frequency bands, which are less heavily congested. The use of millimeter wavelengths implies line of sight propagation, which represent a challenge compared with lower frequencies. The local obstacles will cause problems because each user needs to have a line of sight (LOS) communication towards a base station. This problem again implies a large number of base stations that has to be deployed.

Satellite system is another alternative delivery mechanism, which can provide LOS communication to many users. Certainly, broadband services from GEO satellites are projected to represent a significant market over the next few years [4]-[6]. However, there are many limitations on performance because of prohibitively very long distance, i.e. nearly 40,000 km, could yield the propagation path loss on the order of 200 dB or more, as well as physical constraints of onboard antenna dimensions. The latter problem brings to a lower limit for the size of cell diameter on the ground and therefore constrain the frequency reuse density and hence an overall system capacity. The terminal antenna on the ground must be sizeable to achieve broadband data rates due to very high propagation path loss. A further drawback over GEO satellite system is due to very long propagation delay, i.e. 250 ms. The downside caused by this huge delay not only creating problem for voice or video communication but also producing the difficulties for some data protocols.

MEO and LEO satellites may circumvent some of GEO satellites limitations in principles, for example propagation path loss and delay can be reduced considerably due to the lower altitude compared with GEO satellites [6]. However, the fast moving characteristic especially in LEO satellites could cause complexities of rapid handover not only between cells but also between satellites. The Doppler effect is another significant problem that has to be anticipated in this system. All MEO and LEO satellites are constantly moving relative to each other and to points on the earth's surface. This causes variations in the frequencies and wavelengths of received signal and hence limits the system performance and capacity. On the other hand, the need for large numbers of MEO or LEO satellites to provide continuous coverage is also a significant economic burden. Even though various new technologies have been proposed in order to overcome the main drawbacks of MEO and LEO satellites, such systems have yet to prove commercially successful.

In recent years, a novel wireless concept that has been attracting much the attention of the telecommunications community is proposed [7]. It is based on reusable unmanned or manned aeronautical vehicles, carrying communication apparatus and operating in the stratosphere in a quasi-stationary position at altitudes around 17-22 km above the Earth's surface. Such altitudes have not been used until now by telecommunication services except perhaps for those related to scientific researches. This system is known as a stratospheric platform (SPF) system or a high altitude platform station (HAPS) system. From the geometrical point of view, this system would enable communication services that take much advantage of the best features of both terrestrial and satellite communications. Moreover, the system could bring advantages of its own, not available in current systems. The most important advantages of employing SPF are high elevation angles, broad coverage, low propagation delay, low-cost operation, easy and incremental deployment, and ability to move around in emergency situation. Although immature airship technology, stabilization system, and onboard antenna technology of the platform are challenging that has to be investigated [8], the SPF is expected to avoid some inherent limitations belongs to the traditional systems. Those are in the sense of a huge number of base stations required by the terrestrial system, limitation of the minimum cell size on the ground involved in GEO satellite system, and suffer from handover problem faced by LEO/MEO satellite system. With these great advantages, the International Telecommunication Union (ITU) has allocated the spectrum to this system at 2 GHz for 3G mobile systems [9], 48/47 GHz for the usage worldwide [10], and 31/28 GHz band is allocated to a certain Asian countries [11].

Moreover, the SPF is designed to have capability of flying for long endurance on-station, fed only by solar energy, offering the possibility to play the role of artificial satellites, with the advantages of being close to earth and more flexible. Such platforms are attracting increasing interest for a variety of applications such as delivering of a wide range of communication services to rural areas lacking in telecommunications infrastructure (either wired and wireless), provision of basic emergency communications systems to areas hit by catastrophes or just supply of broadband telecommunication services to residential zones, with a relative low cost, quick deployment and acceptable data rate. It is also expected that the SPF would deliver a high quality TV broadcasting and video. The flexibility of the system allows its utilization for remote sensing and for earth observation purposes as well.

Those attractive features may not be hold by the conventional terrestrial and in some ways by the satellite systems.

Although the SPF may enjoy many advantages not possessed by the terrestrial and satellite systems, there are still unreported important matters that have to be proven before the deployment in real implementation of this system. One among those matters is the channel characteristic of communication link between the SPF and mobile users on the ground. This thesis deals with the channel modeling and characterization as well as investigation to propagation aspects of communication link for mobile users using the concept of SPF.

1.2 Motivation

Wireless mobile communication systems have evolved remarkably since the last decade because of its ability to provide continuous communication between two or more mobile users. There are a lot of researches and investigations on the mobile channel characteristic for the conventional terrestrial and satellite wireless link have been made and published in the literatures. However, wireless mobile channel characteristic and performance evaluation have not been much reported for the case of the SPF communication link. Modeling the wireless channel is a fundamental step in the development of a communication system using SPF. In wireless channel the nature of the channel characteristic basically determines the choices of:

1. The channel coding and error control techniques.
2. The type of modulation schemes.
3. The needed fading margin.
4. The complexity of the signal processing techniques at the receiver, such as equalizers and synchronizers.
5. The architecture of possible advanced signal processing techniques, such as multiple input multiple output (MIMO) coding and smart antennas.

In the first step of this work, we have been motivated to investigate the SPF channel characteristic in semi-urban LOS communication environment and then evaluate its performance. This work is to show a preliminary contribution to the SPF research area based upon the field measurement. The choice of environment type for our experiment is to provide channel behavior information of communication link in the area when a wireless

terrestrial infrastructure is occasionally not installed or because of an excessive cost for the users to have the satellite connection.

In the latest development, ITU has allocated 3G spectrum for the usage in SPF communication sharing with an existing 3G provided in terrestrial or satellite systems [9]. The word sharing here not only frequency sharing but also coverage area can be made overlapped under an acceptable interference level. The work in this thesis is therefore continued with the investigation of propagation characteristic by taking observation areas in urban environment in which most possible mobile users of terrestrial system are exist. Ray tracing scheme is employed in order to characterize the propagation channel in urban environment because of unavailability of the experimental data in the literature for the case of SPF. We first exploit by experimental survey the information of urban characteristics such as building height, building density and street width inside Tokyo area. Our target in this topic is to provide propagation path loss estimation and then the required power transmit for the application of mobile users inside urban environment when they are receiving signal from the SPF.

Indeed, propagation path loss characteristic are essential so that we are able to design the communication link between SPF and mobile users on the ground and to determine the required power transmit and antenna gain on both sides. However, not only propagation path loss but also channel fading due to multipath may corrupt the channel performance in wireless mobile communication. By using the propagation parameters obtained in this work we then continue our investigation on the downlink performance evaluation to the SPF channel communication link. The orientation of how mobile users seeing the SPF represented by two parameters, namely elevation and azimuth angles, are involved in this work. The results show that there is a limitation on elevation and azimuth angles to be established by mobile users in order to achieve a good performance of communication.

1.3 Structure of the Thesis

This chapter is provided to summarize our work in this thesis. Chapter 2 describes the concept of SPF communication system. The beginning of this chapter introduces the basic concept and then continued by the technology example of this system. Communication characteristic of the SPF is compared in general with the conventional terrestrial and

satellite systems. In the last part of this chapter we show the frequency utilization that has been allocated by the ITU for the SPF system.

In chapter 3 the world-first measurement result for channel characterization and performance evaluation of the SPF mobile channel is presented. Experimental setup and data processing to estimate the SPF channel is explained. Propagation parameters in terms of received power level and Ricean factor (*K* factor) is presented as a function of various elevation angles. For channel performance evaluation, DPSK and DQPSK modulation schemes are employed in our simulation. The performance of the channel is then obtained based on the measured propagation parameters.

Chapter 4 examines the propagation path loss in the city center (urban environment) experienced by mobile users when they received the signal from the SPF in many directions. First part of this chapter explains the basic concept of ray tracing scheme that has been employed for propagation evaluation. An experimental result of site survey inside Tokyo area is then presented in the next section of the chapter. Based on experimental result, building geometry model is therefore developed. Finally according to propagation path loss experienced in the SPF link and other parameters specified for SPF communication, the required transmit power is estimated.

In Chapter 5 we evaluate the downlink performance for the SPF link based on the propagation parameters obtained using ray tracing scheme explained in Chapter 4. The target is to reveal the SPF downlink channel performance. Analysis and discussion in the last part of this chapter show the possibility and at the same time the limitation of implementation of the next generation mobile services through the SPF system.

Chapter 6 presents a reverse link capacity evaluation of CDMA system employing single and multiple SPF in terms of outage probability as a function of number of users. An overlapped region is introduced in the case of multiple platform scenarios. It is shown that overlapped region cannot be neglected in the interference analysis. The increasing minimum elevation angle is then proposed to reduce interference effects generated by the user in overlapped region. The result shows a non-trivial improvement in capacity due to this method, however the number of the SPF might be increased because of the coverage area become smaller. Finally chapter 7 concludes our research and makes suggestions for further research directions.

Chapter 2
An Overview of Stratospheric Platform (SPF) Communication

2.1 Introduction to SPF

In ITU, the terminology of a stratospheric platform (SPF) or a high altitude platform station (HAPS) is defined as *a station located on an object at an altitude of 20 to 50 km and at a specified, nominal, fixed point relative to the earth* [12]. In the definition, it has not been mentioned yet if the object is manned or unmanned or even how is it powered. Thus, several countries are now proposing several alternative technologies for the development of such an object. The SPF is to be positioned well above commercial airplane at an altitude that is high enough to provide service to a large footprint, providing telecommunication, broadcasting and environment observation services with minimal ground network infrastructure. The common vision predicts that this system will consist of one or more quasi-stationary SPF as depicted in Figure 2.1. Each platform provides communication with several ground stations and with numerous mobile and fixed subscriber stations. Each platform will be equipped with a multi-beam array antenna, which capable of projecting numerous spot beams within its potential coverage area.

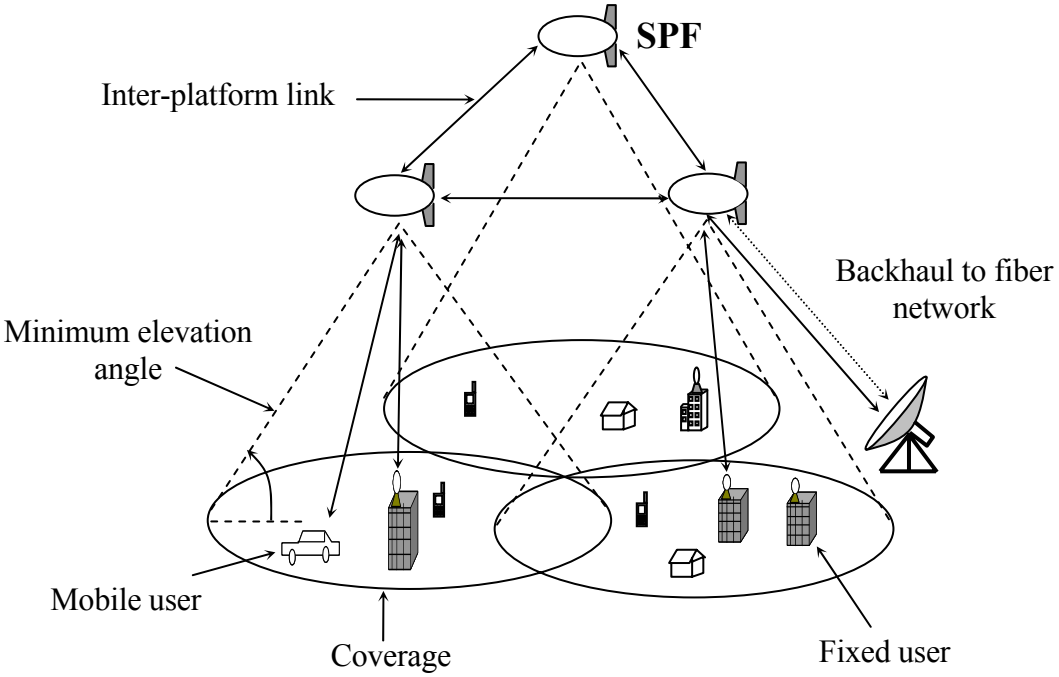

Figure 2.1 SPF basic configuration.

Moreover, the platforms will inter-connected among themselves, and with other networks, such as terrestrial, satellite, public and private. The system concept of this new communication infrastructure is global in nature, but national or regional in service provision.

The SPFs are to operate at unusually high altitudes. Such altitudes have not been used until now by telecommunication systems except perhaps for those related to scientific research. In the following sub section, a brief look into the condition of these altitudes is presented.

2.1.1 The Stratosphere

Earth's atmosphere consists of several distinct layers and one of them is the stratosphere layer. Figure 2.2 shows the first two layers of the earth's atmosphere. The lowest one is the troposphere layer. It extends from the earth's surface to the tropopause about 10 to 18 km in altitude, depending on the season and geographical position. The air pressure at the top of the troposphere is only 10% of that at sea level. In the troposphere, the air temperature generally decreases with height. Rain and almost all weather phenomena occur in the lower part of this layer and approximately 80% of the total air mass resides here.

Above the troposphere is the stratosphere, where it extents from the tropopause to the stratopause at an altitude about 50 km above the ground. The ozone layer resides in the upper stratosphere and more than 99% of the total air mass is concentrated in the first 40 km from the earth's surface. This layer is primarily responsible for absorbing the ultraviolet radiation from the Sun. The stratosphere is characterized by a high static stability associated with increase of temperature with height. The pressure decreases further to reach about 1 hPa at the stratopause. Above the stratosphere is the mesosphere layer, which extends from the stratopause to the mesopause at about 90 km, where the pressure is 0.01 to 0.001 hPa. Most of meteors burn up in the mesosphere as a result of collisions with gas particles there. Higher, up to 300 km, the thermosphere is located. Here, aurora phenomena occur. The exosphere located above the thermosphere is the most distant atmospheric region, a transitional zone between the earth's atmosphere and interplanetary space.

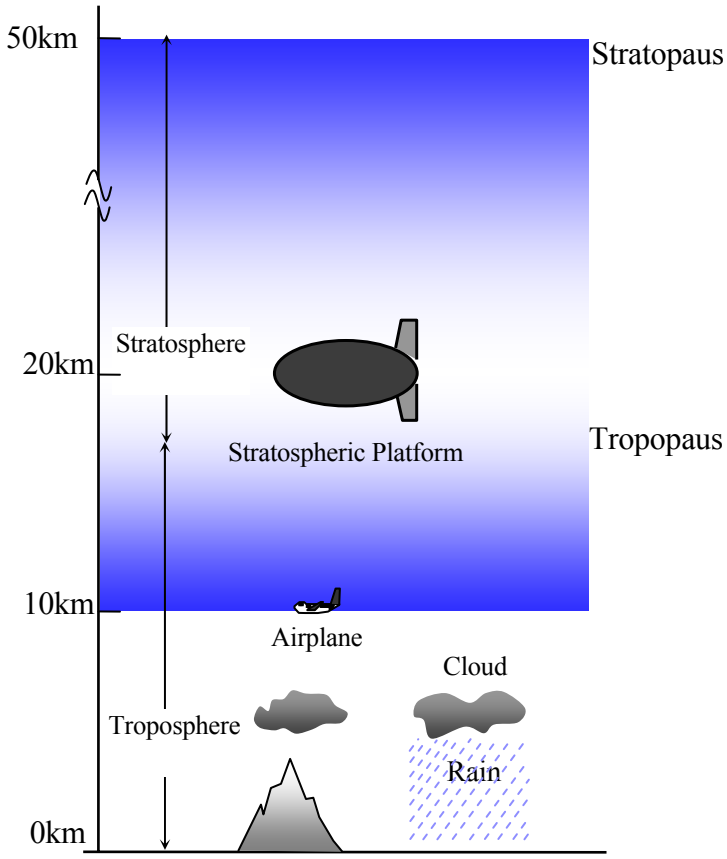

Figure 2.2 The first two layers of the earth's atmosphere.

The wind speeds in the atmosphere vary according to the season, geographic position and temperature gradient. They are highest at altitudes of about 12 km, 70 km, and 100 km. At altitudes of about 20 km and about 90 km, the air masses are relatively stationary and predictable, with very slow winds only. That is why most of stationary stratospheric platforms are to be located at the altitude of about 20 km. The average wind velocities are shown in Figure 2.3 [90]. In fact, wind velocity values vary with season and location, but generally follow this curve. From the figure, the most preferable altitudes fall from 19 to 25 km, while from 17 to 19 km the velocities are little high. Generally, wind velocities increase over the altitude of 25 km up to 70 km and then above 70 km up to 90 km wind speeds decrease. The next lowest wind speeds are occurred at 90 km altitude. Beside wind speed, another important thing for placing SPF is the air density. It is known that as the altitude increases the air density is reduced, making the placement of the vehicle very difficult. For example, at 12 km (the maximum altitude of airplane lanes) the density is about 25 percent compared to that at the sea level, while at 24 km it is only about 3.6 percent. Therefore, even though at the altitude of 90 km wind velocities are very low, however the air density will very low. So that the best places for SPF is at the altitude of around 17-22 km above sea level.

2.1.2 Platform Range

The communication range between the SPF and the user on the ground depends on the platform altitude, signal arrival elevation angle and the earth's dimensions. The service area covered from the platform is then heavily dependent on the minimum elevation angle definition. Figure 2.4 shows the maximum diameter of the LOS coverage area for station altitudes from 10 m up to GEO satellites altitude as a function of minimum elevation angle. The diagram was created exploiting the approximation that microwaves propagate along almost straight lines, like the visible light. It can then be said that the higher is the antenna located on the station, the greater is the station range, but there is a limit. The maximum diameter of the coverage area is somewhat less than the earth's diameter.

In general, terrestrial stations employ the antennas at an altitude of less than 300 m above the ground. Therefore they have LOS range limited to few dozens of kilometers. The coverage area of this system is dependent heavily on the terrain topography. The signal generally propagates in low angle of arrival from base transceiver station (BTS) to the

users, and moreover is affected by attenuation, shadowing, and reflections due to terrain irregularities, buildings, trees, etc. In hilly regions, it is often practically impossible for terrestrial systems to guarantee a uniform coverage without black holes where the signal intensity is too weak to assure their normal operation.

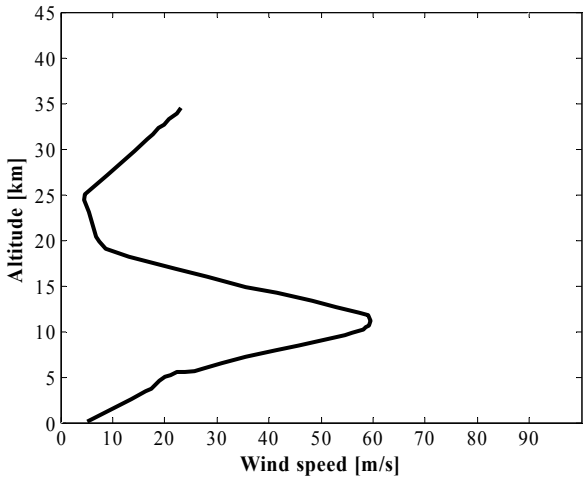

Figure 2.3 Wind speed with refer to altitude [90].

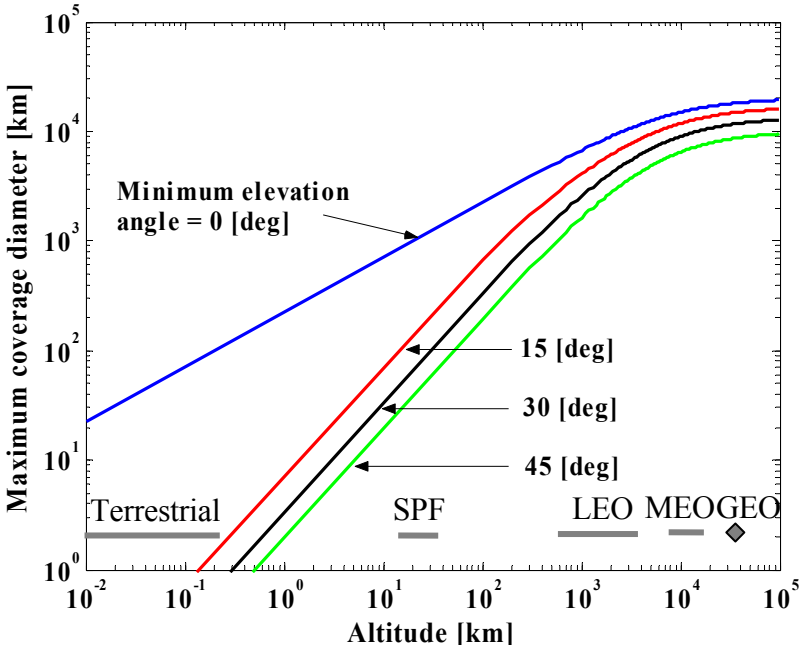

Figure 2.4 Coverage diameter for altitude from 10 m up to 100,000 km.
Note logarithmic scale on both axes.

The SPF and satellite systems suffer less from the shadowing and multipath distortions because they use high elevation angle of arrival signals. LEO satellites reside typically between 500 and 1,500 km above the earth, while MEO satellites are limited to about 5,000 up to 12,000 km. GEO satellites is located in extremely high altitude nearly 36,000 km above the earth and therefore have a very high round trip delay propagation. The coverage of GEO satellites approaches 40% of the earth's surface. However, the northern and southern regions cannot use signals from the geostationary orbit because of their low arrival angle above horizon.

The SPF stations are located somewhere between the terrestrial and the satellite systems. Located at about 20 km altitude they have coverage areas of about 1,000 km in diameter and 800 thousands km^2, for zero-elevation angle. From its geometrical situation, the SPF communication may enjoy high angle signal arrival and the propagation delay in this system almost is not an issue. Within the maximum LOS coverage area, there may be numerous cells served by separate antenna beams. Therefore the spot beams or cells can be created on the ground as following the cellular concept of as in terrestrial mobile systems. The frequency reuse can then be applied in order to increase the network capacity.

2.2 Technology Examples

Studies on the SPF have been started over the last few years in several countries all over the world. For example, in Japan, National Institute of Information Communications Technology (NICT) has taken an initiative of a national R&D project on stratospheric platforms, which has been started since 1998 [8], [13]. A similar ongoing project has also been undertaken in the European countries through the CAPANINA project [14]. In the U.S., they have the Aerovironment/SkyTower project [15] and also the stratospheric platforms program in Korea with KARI and ETRI [16]-[17]. Those investigations are devoted to put the SPF into operation for the new wireless communications infrastructure. As the work is progressing, numerous applications have been identified. Some of the potential applications such as digital TV broadcasting, broadband fixed services and 3G mobile communication IMT-2000 have been experimentally studied [18]-[20].

The idea of the SPF is to keep unmanned Zeppelin-like balloons geostationary at the stratosphere altitude. Each platform shall provide mobile and fixed telecommunication

services to an area of about 150 to 1,000 km in diameter, depending on the minimum elevation angle accepted from the user's location. One of the main challenges is to keep the platforms stationary under the wind speeds of up to 55 m/s, which may occur at these altitudes.

The expected requirements for a stratospheric platform in order to be used as a novel wireless communication infrastructure are as follows:

1. Capable of reaching the stratosphere (an altitude of 20 km or so) and staying at a fixed point within a prescribed range.
2. Capable of round-the-clock continuous operation for a long duration.
3. Capable of bearing large weights, so as to accommodate numerous types of application apparatuses and at the same time supply sufficient power to these apparatuses.
4. Onboard radio equipment may be retrieved on the ground or on the sea, as necessary.
5. Is environmentally friendly in terms of the stratosphere.

Based on the above requirements, we summarize three candidates of vehicle technology that is now being proposed and developed in several countries throughout the world.

2.2.1 Unmanned Airship

These vehicles, which basically balloon, are equipped with a propulsion system, semi-rigid or non-rigid, huge and solar-powered, over 100 m long with a payload of about 800 kg, and intended to stay aloft up to 3 years or more. There are several systems example of this technology, such as Sky Station planned by a company in the US, Stratsat developed by the UK based company, Stratospheric Platform System from Japan and The Airborne Relay Communications (ARC) Systems planned by the US company.

2.2.2 Solar-powered Unmanned Aircraft

This platform technology uses electric motors and propellers as propulsion system. Solar cells are mounted on the wings and stabilizers provide power during the day and charge the onboard fuel cells. Flight duration of such vehicles has not been specified. These vehicles are also known as High Altitude Long Endurance Platforms (HALE Platforms). Although the average flight duration of such vehicles has not been specified yet, some proposals

make claims of continuous flight up to six months or more. The systems examples of this technology are Helios, Pathfinder Plus (AeroVironment) and Heliplat (European Project).

2.2.3 Manned Aircraft

These vehicles have average flight duration of several hours due to fuel constraint and human factors. The system example of this proposal is HALO (Angle Technologies) M-55 (Geoscan Network). A more recent stratospheric airplane, i.e. Proteus, is capable to lift 1000 kg payload to an altitude of 20 km and circulate there for 14 hours or so.

Table 2.1 shows a rough comparison of these aerial vehicles. Considering the mission equipment weight, influence on the environment, and so on. The unmanned airship system is expected to be the candidate with the most potential. However, the airship must be very large in order to be capable of fulfilling these requirements and at the same time capable to reach the stratosphere.

Table 2.1

Technology comparison of the SPF system [8].

Parameter	Large-scale airship (unmanned)	Solar plane (unmanned)	Jet (manned)
Size	Length 150 ~ 200 m	Wingspan 35 ~ 70 m	Length ≈ 30 m
l weight	≈ 30 ton	≈ 1 ton	≈ 2.5 ton
Propulsion energy source	Solar cell	Solar cell	Fossil fuel
Environmentally friendly	Yes	Yes	No
Response in emergency situations	No	Yes	Yes
Flight duration time	About 3 years	Unknown	8 hours
Station keeping range (radius)	~ 1 km	~ 1.5 km	~ 10 km
Mission equipment weight	~ 1000 kg	~ 100 kg	~ 1000 kg
Mission allowable electric power	~ 10 kW	~ 1 kW	~ 20 kW
System example	Japan, Korea, China, Sky Station and other companies in the U.S.	Helios, Pathfinder Plus (AeroVironment), Heliplat (European)	HALO (Angle Technology Corporation, in U.S.)

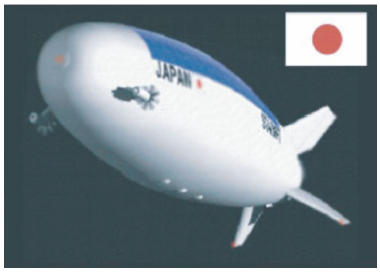

(a). Large-scale airship (designed by JAXA)

(b). Solar-powered unmanned aircraft (AeroVironment/NASA)

(c). Manned aircraft (Jet) Angle Technologies HALO (Proteus 9)

Figure 2.5 Systems examples of the platform technology [8].

One example of the unmanned airship system is developed in Japan. A conceptual drawing of the system was created in the feasibility study carried out by Japan Aerospace Exploration Agency (JAXA) in 1999 as shown in Figure 2.5 (a) [13]. The body of the airship is equipped with a number of helium gasbags, a solar cell panel on its top face, and three propulsion engines. A regenerative fuel cell is installed on the platform for operation at night. Analysis indicated that the length of the airship would be 245 m, the weight would be 32.4 tons, and the power required to propel it would be approximately 200 kW. It was calculated that the equipment load capacity (mission payload) was about 1 ton and the allowable power for maximum dissipation was 10 kW.

2.3 Communication Characteristics

In this section, characteristics and features of radio communications offered by the SPF are summarized, evaluated and in some way the comparison to conventional wireless terrestrial and satellite systems are made.

2.3.1 System Geometry

It is important first to look at the system geometry of SPF before we evaluate its communication characteristic so that the difference from other system is clearly shown. Figure 2.6 describes the geometry of the SPF system by involving the earth's curvature. SPF is positioned at an altitude h (point C) with the sub-platform point, that is the point vertically below the intended platform location, is in point B. In Figure 2.6, point A denotes the position of a user served by the SPF having elevation angle α. Point O in the

figure represents the earth center and R_e is the earth's radius. From the principle of trigonometry we can express that

$$\frac{OA}{\sin\beta} = \frac{OC}{\sin(90+\alpha)} = \frac{OC}{\cos\alpha}, \tag{2.1}$$

$$\sin\beta = \frac{R_e}{R_e + h}\cos\alpha . \tag{2.2}$$

Assuming the earth surface is perfect sphere, the arc AB indicates the radius (d) of SPF coverage on the ground and might be expressed through the following equation

$$AB = R_e\ \gamma . \tag{2.3}$$

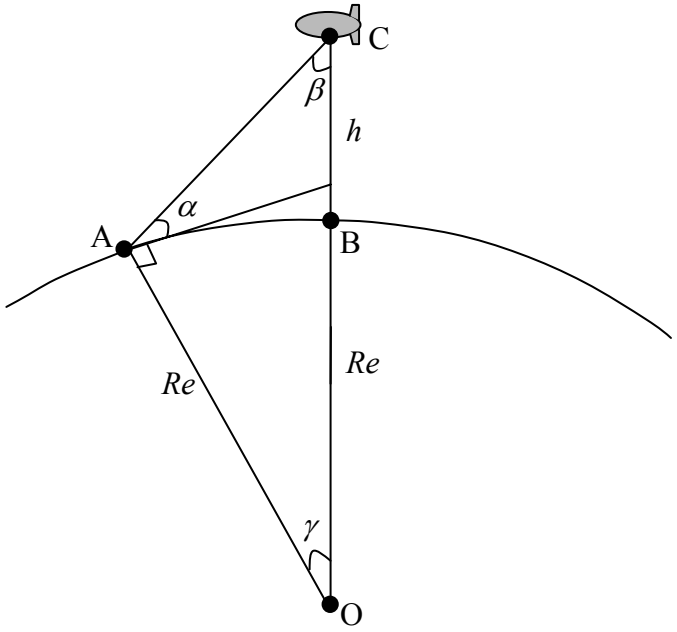

Figure 2.6 Geometrical parameters in SPF communication.

Let us consider the triangle OAC, the total angle of the triangle is 180^0 so that the angle γ can satisfy this equation

$$\gamma = 90^0 - \beta - \alpha . \tag{2.4}$$

After substitution of (2.2) to (2.4), we are able to rewrite the radius of the SPF coverage in (2.5) as follow

$$d = R_e \cdot \left\{ \cos^{-1}\left(\frac{R_e}{R_e + h} \cos\alpha \right) - \alpha \right\}. \tag{2.5}$$

According to the above geometrical analysis, the SPF at 20 km altitude has the capability to cover an area on the ground up to 504 km in radius for 0^0 of elevation angle. Figure 2.7 shows a radius of coverage area as a function of elevation angle with the assumption of platform altitude of 20 km. In this altitude, the SPF can therefore be considered as an ultra-high-altitude tower compared with terrestrial radio tower. As a result, the SPF can easily provide LOS communication with a high elevation angle, whereby the links are relatively free of the influence of obstacles. The antenna and the radio equipment can be made smaller because the electric power required for transmission can be decreased. Furthermore, there is minimal voice delay when used for voice telephone or the like, because the stratospheric platform is much closer to the ground than satellites, and hence the delay propagation is almost not an issue in this system.

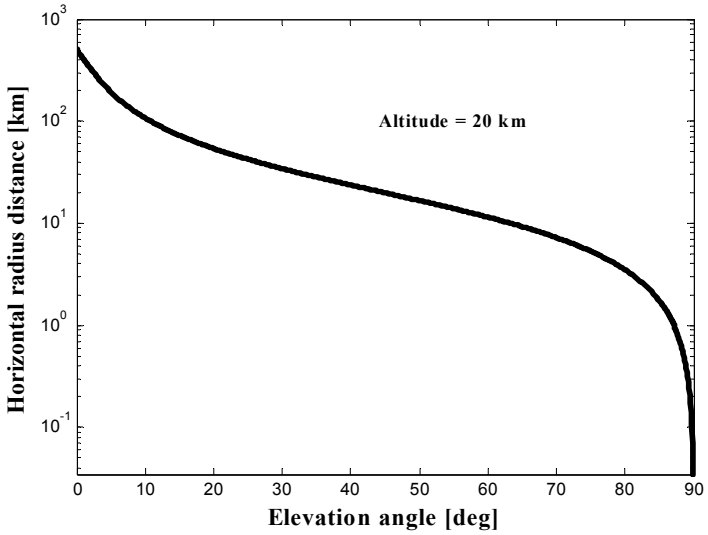

Figure 2.7 Radius of coverage area vs. elevation angle.

2.3.2 Electromagnetic Environment

Analysis of electromagnetic environment as well as sharing frequencies between different systems is now becoming very important because the demand for radio communication is

rapidly increasing. In terrestrial wireless communications such as mobile communication or broadcasting, the signal is transmitted using electromagnetic wave traveling very close to the ground. That signal is subject to reduce in power level not only by the distance but also due to attenuated by buildings, trees, terrain features, etc. Therefore, the signal must be transmitted with sufficiently high transmission power to maintain the link quality. Terrestrial system therefore offers very limited area because there is restriction on the regulation of maximum transmitted power the system can transmit.

The SPF system offers more far away in distance for the same amount of electromagnetic transmit power than the terrestrial system. Thus, the transmission power from SPF can be much lower than from terrestrial to cover the same area. As a result electromagnetic waves are minimally irradiated to the surroundings and consequently hence to the human health.

2.3.3 LOS Path and Propagation Delay

Considering the above geometry, SPF system has much higher LOS probability with a high elevation angle compared with the terrestrial system. The paths are relatively free from the influence of obstacles. In semi-urban or rural environment, obstacles may be trees, buildings or residential houses which mostly only one or two storey building. However, when SPF is used to serve an area in urban environment the building can be very high or even sometime there are many skyscraper building. In this condition, LOS propagation would be very difficult to be achieved in a low elevation angle. If we assume that the average building height in particular area of urban environment is 20 m and has Rayleigh distribution then the probability of LOS path and shadow path for 20 km altitude of SPF can be described as in Figure 2.8. From the figure we can see that for probability of LOS situation is higher than 50% then the required minimum elevation angle is 40^0. The probability of LOS goes down when the average building height is increase for example in a high rises urban environment.

Propagation delay in SPF communication is not an important issue because it closes to earth. Maximum round trip propagation delay is depending on the minimum elevation angle. For example, if the minimum elevation angle is 10^0 then the maximum round trip propagation delay is only 0.7 ms. Therefore, it will not become a serious problem in the designing of advanced data communication which basically use IP protocol.

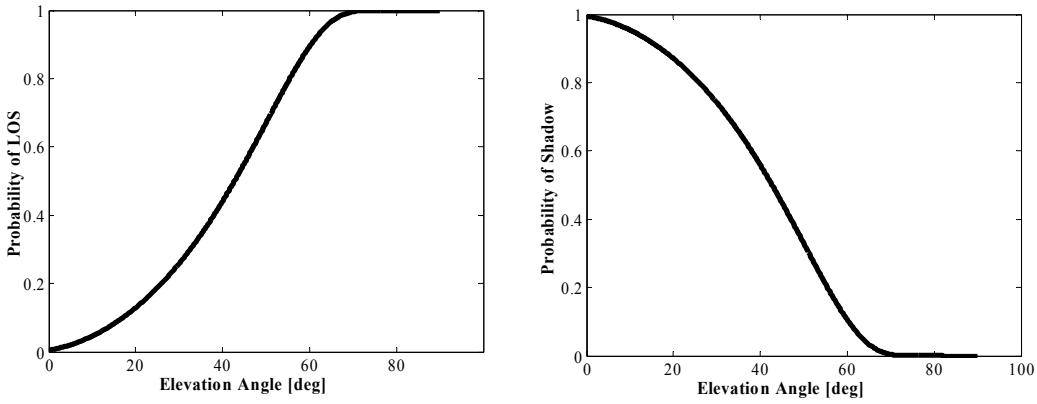

Figure 2.8 Probability of LOS and shadow situation for a Rayleigh distributed building height with average 20 m. SPF is assumed 20 km altitude.

2.3.4 Flexibility

The system can provide flexibility in allocation of platforms and provision of communication links according to need, responding to disasters and other such extraordinary events. It is also expected that in the event the onboard equipment malfunctions or when upgrades become necessary, the onboard equipment can be temporarily retrieved on the ground, therefore providing greater flexibility than a satellite system.

The telecommunication and broadcasting concept using the stratospheric platform provides that a number of stratospheric platforms will be arranged in the sky in a mesh manner, with a spacing of a few tens to a few hundreds of kilometers, set to serve as relay stations or a base station. With this concept, there can be envisioned a variety of applications, not only for fixed communications but also for mobile communications, broadcasting, global environment measurements, radio monitoring, and so on. Among others, a broadband access network that uses high frequencies (in the millimeter wave band, for example) and provides transmission speed of 20 Mbps or more in a single channel, aimed at personal users, is considered to be one of the applications that will make the most of the features of the stratospheric platform. It raises the possibility that high-quality digital services, such as a high-speed Internet and a high-quality digital broadcasting (whereby motion pictures and a large volume of contents can be exchanged without taxing the user's system) may be realized without relying on satellites or on the terrestrial infrastructure, such as optical

fibers. Further, by connecting the platforms with optical wireless links, it will be possible to establish links by wireless only over a wide area.

In Table 2.2, a general comparison in many aspects among the existing terrestrial and satellite systems with the proposed SPF system is shown.

2.4 Frequencies Allocation

Until 1997, there is no international telecommunication regulations were addressing the SPF specifically. In February 1997, at the request of some countries, the ITU Radio Regulations Board (RRB) has recognized SPF as separate category of radio stations and decided upon a new provisional rule of procedure. It was the very first international regulatory decision concerning this system. The decision of RRB has been confirmed by the World Radio communication Conference (WRC), Geneva 1997. At this occasion, the conference introduced a formal definition of this system into the Radio Regulations, and made provisions for operation of the SPF within the fixed service in the bands of 47.2 – 47.5 GHz and 47.9 – 48.2 GHz.

At the same time, the WRC-97 has initiated specific technical studies and other actions. The ITU studies have been continued until now, focusing on protection against interference and on efficient use of the radio frequency spectrum. Proposal to modify Resolution 221 in WRC-2000 held in Istanbul, has decided that the following frequency bands may be used for the usage of next generation mobile communication based on SPF system worldwide on a co-primary basis.

In region 1 and 3:

- 1885 – 1980 MHz : 95 MHz bandwidth
- 2010 – 2025 MHz : 15 MHz bandwidth
- 2110 – 2170 MHz : 60 MHz bandwidth

In region 2:

- 1885 – 1980 MHz = 95 MHz bandwidth
- 2110 – 2160 MHz = 50 MHz bandwidth

Table 2.2

Comparison of wireless system.

Issue	Terrestrial Wireless	Satellite	SPF/HAPS
Availability and cost of mobile terminals	Huge cellular/PCS market drives high volumes resulting in small low-cost, low-power units	Specialized, more stringent requirements leads to expensive bulky terminals with short battery life	Terrestrial terminals applicable
Propagation delay	Low	Causes noticeable impairment in voice communications in GEO (and MEO to some extent)	Low
Health concerns with radio emissions from handsets	Low-power handsets minimize concerns	High-power handsets due to large path losses (possibly alleviated by careful antenna design)	Power levels like in terrestrial systems (except for large coverage area)
Communications technology risk	Mature technology and well-established industry	Considerable new technology for LEOs and MEOs; GEOs still lag cellular/PCS in volume, cost, and performance	Terrestrial wireless technology, supplemented with spot-beam antennas; if widely deployed, opportunities for specialized equipment (scanning beams to follow traffic)
Deployment timing	Deployment can be staged; substantial initial build-out to provide sufficient coverage for commercial service	Service cannot start before the entire system is deployed	One platform and ground support typically enough for initial commercial service
System growth	Cell-splitting to add capacity, requiring system reengineering; easy equipment update/repair	System capacity increased only by adding satellites; hardware upgrade only with replacement satellites	Capacity increase through spot-beam resizing, and additional platforms; equipment upgrades relatively easy
System complexity due to motion of components	Only user terminals are mobile	Motion of LEOs and MEOs a major source of complexity, especially when inter-satellite links are used	Motion low to moderate (stability characteristic to be proven)
Operational complexity and cost	Well-understood	High for GEOs, and especially LEOs due to continual launches to replace old or failed satellites	Some proposals require frequent landings of platforms (to refuel or to rest pilots
Radio channel “quality”	Rayleigh fading limits distance and data rate; path loss up to 50 dB/decade; good signal quality through proper antenna placement	Free-space-like channel with Ricean fading; path loss roughly 20 dB/decade; GEO distance limits spectrum efficiency	Free-space-like channel at distance comparable to terrestrial
Indoor coverage	Substantial coverage achieved	Generally not available (high-power signals in Iridium to trigger ringing only for incoming calls)	Substantial coverage possible
Breadth of geographical coverage	A few kilometers per base station	Large regions in GEO; global for LEO and MEO	Hundreds of kilometers per platform
Cell diameter	0.1 – 1 km	50 km in the case of LEOs and more than 400 km for GEOs	1 – 10 km
Shadowing from terrain	Causes gaps in coverage; requires additional equipment	Problem only at low look angles	Similar to satellite
Communications and power infrastructure; real estate	Numerous base stations to be sited, powered, and linked by cables or microwave	Single gateway collects traffic from a large area	Comparable to satellite
Esthetic issues and health concerns with towers and antennas	Many sites required for coverage and capacity; “smart” antennas might make them more visible; continued public debates expected	Earth stations located away from populated area	Similar to satellite
Public safety concern about flying objects	Not an issue	Occasional concern about space junk falling to Earth	Large craft floating or flying overhead can raise significant objections

The conference decided also to study additional frequency allocations for the SPF communication between 16 and 32 GHz. Finally, in the WRC-2000, use of the 31 GHz and 28 GHz bands was permitted for the fixed services (FS) by using SPF in some countries as follows:

- 27.5 – 28.35 GHz (850 MHz bandwidth for downlink)
  Sharing with conventional FS, mobile services (MS), and uplink fixed satellite services (FSS).
- 31.0 – 31.3 GHz (300 MHz bandwidth for uplink)
  Sharing with conventional FS and MS. Adjacent with science services (SS) using passive sensors in the bands of 31.3 – 31.8 GHz.

Figure 2.9 shows the frequency allocation table for the SPF communication all over the world according to WRC 1997 and 2000.

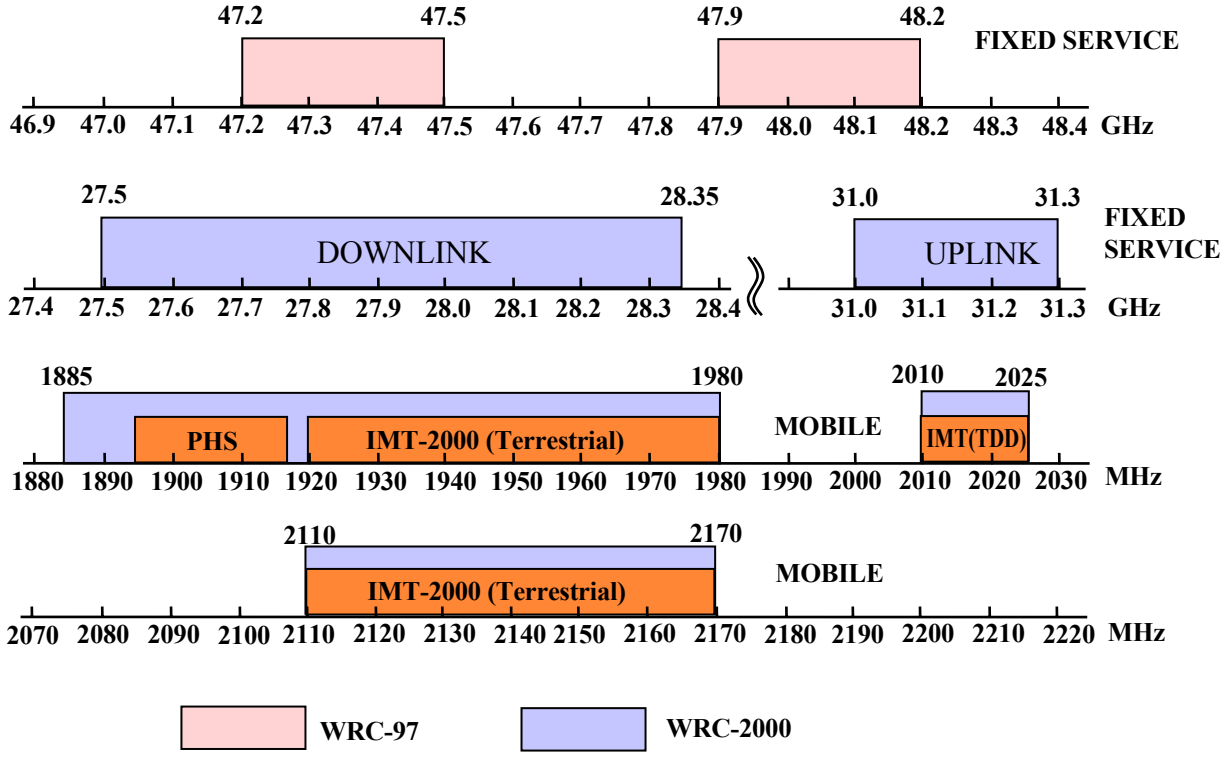

Figure 2.9 Frequency allocation table for the SPF communication.

Chapter 3
Mobile Channel Characterization

In this chapter we introduce a channel characterization and performance evaluation of the SPF communication link. We propose a definition and describe an analysis of the wireless channel for the link between SPF and mobile users based on experimental measurements in semi-urban environment [97]-[99].

3.1 Introduction

Unlike in wired channel signal transmitted through the wireless channel will experience multipath propagation problem, which places fundamental limitations on the performance and capacity of wireless communication systems. Moreover, in mobile wireless communication channel, signal at the receiver will suffer from deep fade due to the motion of both the transmitter and the receiver. This condition is then causing problems that the radio channels are particularly random in nature and do not offer an easy analysis. Therefore, modeling and characterization of the wireless channel has become one of the most important parts of wireless system design.

In order to maintain a robust and reliable wireless communication, in which the channel is strongly affected by poor propagation condition, investigation to a proper technology is very important and challenging. In most cases wireless channel would require a

complicated signal design, powerful signal processing and sophisticated transmission and reception technologies. To define a proper technology that is appropriate for a particular wireless channel condition, wireless channel modeling and characterization must be accurately investigated.

Many research activities on the channel modeling and characterization have already been done in the case of wireless terrestrial and satellites channel. Traditionally, channel modeling and characterization have focused on predicting the average signal strength as well as its variability in spatial distance relative to a particular location. This is called as a large-scale propagation model that predicts the mean signal strength and its variation between an arbitrary Tx and Rx separation distance. Typically, in terrestrial radio channel, received signal is characterized by rayleigh distribution because of suffering from unavailability of LOS link between BTS and MS. There are a plethora propagation models have been proposed for conventional terrestrial systems [21]-[30]. Among the models Okumura's model is one of the most widely used models for signal prediction in urban areas [26]. After more than one decade, Hata [27] proposed an empirical formulation of the graphical path loss data provided by Okumura. Besides Hata also supplied correction equations for application to other situations. Those prominent results are then known as a very useful model in outdoor propagation loss prediction since 1G, 2G and even 3G mobile cellular communications were deployed.

In satellite systems, a ground terminal and the associated satellite are reciprocally visible and propagation of radio waves mostly takes place through an unobstructed LOS path [31]-[33]. Free space attenuation is the major factor in link design for fixed satellite system. Considering land mobile satellite system, free space attenuation and multipath fading effects are the major factor [34]-[36]. Both fixed and mobile satellite propagation link are also introduced by atmospheric conditions such as atmospheric refraction, precipitation (rain, fog, snow), and cloud cover, resulting to an additional loss in the direct signal. In fact, satellite radio channel characteristic generally follows the Ricean fading channel because mostly the links between satellite and MS users on the ground are usually LOS.

From the entire model available nowadays for propagation path loss prediction either for terrestrial or satellite system, the general equation is presented by the following expression

$$L_T = L_{FSL} + L_S + L_F , \tag{3.1}$$

where L_T is the total propagation path loss, L_{FSL} represents free space path loss as a function of Tx-Rx separation distance, L_S denotes the shadowing loss, and L_F is fading loss. Free space path loss is dependent to only frequency and separation distance between transceiver as typically expressed by the following equation

$$L_{FSL} = 10\log\left[\frac{Gt\,Gr\,\lambda^2}{(4\pi d_l)^2}\right]. \tag{3.2}$$

Here G_t is transmitter antenna gain, G_r is the receiver antenna gain, λ is a wavelength in meter, and d represents the distance between Tx and Rx in meter. This free space path loss equation is only valid predictor for values of d_l, which are in the far-field of the transmitting antenna. The local mean received signal will have almost constant average value over the local area. As the receiver moves farther away from the transmitter over much larger distance, the local mean received signal will gradually decrease, and it is known as a large-scale propagation model.

Large-scale propagation model deals only with propagation path loss and shadowing for the distance between Tx-Rx is large enough. However in terrestrial and satellite channel there is still significant variation in the received signal as the receiver moves over very small distances. This phenomenon is called as small-scale fading model in which signal variation is so rapid that it can only usefully be predicted by statistical means. Many physical factors in the radio propagation channel influence small-scale fading such as multipath propagation, speed of the transceiver, speed of surrounding objects, and the transmission bandwidth of the signal [3].

While large-scale propagation model is related to narrowband channel characteristic, the small-scale fading model is a wideband channel characterization and contains all information necessary to simulate or analyze any type of radio transmission through the channel. The information of small-scale propagation characteristic in the wireless channel is very important and can be directly related to the impulse response of the radio channel.

Although there are a lot of references in wireless channel characterization dedicated for conventional terrestrial and satellite links, however investigations in channel

characterization have not been much reported for novel wireless communication infrastructure using the so-called stratospheric platform (SPF). Here in this chapter, for the first time we investigate the narrowband channel characteristic of SPF communication link and evaluate its performance under a particular modulation scheme for a specific area in which the measurements were conducted.

Stratospheric platforms have been recently proposed as a new wireless infrastructure for realizing the next generation of communication systems. To provide high quality services and to choose a proper technology that is going to be used in platform communication, an investigation of the wireless stratospheric platform channel is essential. In this chapter, narrowband SPF channel characteristics are presented in terms of Ricean factor (*K* factor) and local mean received power over a wide range of elevation angles ranging from 10^0 to 90^0. Eventually, we evaluate average bit error rate (BER) based on the proposed channel model to examine the channel performance. For the environment in which the measurements were conducted, we find that elevation angles greater than 40^0 yield better performance.

3.2 Related Work

We demonstrate in Figure 2.1 Chapter 2 a model of stratospheric platforms configuration. The model shows inter-platform communication links and the links between platform and terrestrial fixed or mobile users. It is obvious with their unique positioning the stratospheric platforms allow truly ubiquitous wireless communications to users anywhere and anytime by arranging multiple SPF on the sky. However channel characterization of this system is considered as a matter of urgency in order to define a proper technology that is appropriate for the SPF channel condition. We concentrate our examination here to the channel characterization of the link between platform and terrestrial mobile user based on elevation angle dependency. To the best of our knowledge, we found an examination for the channel characterization of the stratospheric platform communication link has been scarcely addressed. F. Dovis et al. show the performance of small-scale high altitude platform channel in [37]. However, in their model an influence of platform elevation angle has not been considered for the performance evaluation.

In Figure 2.6 Chapter 2, the coverage area is a function of platform altitude (h), earth radius (R_e) and elevation angle (α). The diameter (D) of coverage area of the stratospheric platform can be easily approached by the following expression

$$D = 2R_e.\left(\cos^{-1}\left(\frac{R_e}{R_e+h}\cos(\alpha)\right) - \alpha\right). \tag{3.3}$$

From (3.3), let we assume that the platform stays at a fixed altitude. Therefore elevation angle is the only one important parameter for determining the coverage area. The lower the elevation angle is, the larger the coverage area will be obtained. However, the performance of communication link as a function of elevation angle has to be carefully examined. We will show in the next section a proposed channel characteristic that has direct relationship between elevation angle and the channel characteristic. Moreover, the performance evaluation to the proposed channel characteristic will be reported as well.

We have investigated several fade and non-fade duration distributions as a function of various elevation angles for the stratospheric platform communication by using the data of experiments. However, fade and non-fade duration are only determined by introducing a perspective continuation angle (PCA) and a shadowing continuation angle (SCA) [38]. Both PCA and SCA are introduced by using the system that is equipped by the camera in order to predict the visibility.

Our further investigation presented here includes a result of the instantaneous power level measurement that is received from the stratospheric platform. Frequency bands of 1.2 and 2.4 GHz are used in the experiment. We consider these frequencies to become a representation of 2 GHz band, over which the ITU has allocated that band for the application of the next generation mobile communication based on stratospheric platform [9]. Thus, this work deals with the measurement for a definition and an analysis of narrowband channel for the link between the stratospheric platforms and the terrestrial mobile users over wide range of elevation angles. The experiment has been carried out for every 10^0 intervals of elevation angle ranging from 10^0 to 90^0, at which all communication links are line of sight (LOS). As we know, multipath fading should be examined for both of LOS as well as non-line of sight (NLOS) communication link. Since the stratospheric platform is proposed to be employed in high probability of LOS situation, this experiment

is aimed to examine the multipath fading in a clear LOS link. Preliminary result of these field tests indicates a very little multipath for very high elevation angles while deep fades were experienced for the lower elevation angles. Especially if contribution of reflected waves from the ground, structures as well as from the trees nearby the receiver is significant. Further analysis to the result of these field tests is presented in more detail in terms of *K* factor and local mean received power in the next section.

3.3 Experimental Model

In this section we explain experimental setup of our measurement and data analysis technique in order to obtain the propagation parameters.

3.3.1 Measurement Configuration

Our motivation of this measurement emerges to point out the influence of elevation angle to the performance of the stratospheric platform channel in LOS situation. The propagation measurements were conducted in Hokkaido area (Northern part of Japan). The field tests were conducted on the long highways with the environment nearby the experimental site consists of trees and residential structures. In this case, the propagation path between the stratospheric platform (as a transmitter) and mobile terminal (as a receiver) is always in LOS situation. The environment in the field tests which is characterized by the trees and mostly one or two stories of structures can be considered to represent the typical semi-urban areas.

In Figure 3.1, we describe the model of our experiments. Transmitter equipment and antenna are mounted on the balloon as a "flying platform" which is fixed positioned at an altitude of around 200 m above the ground. The mobile receiver was installed in a vehicle, which is connected to a spectrum analyzer and interfaced to the computer using general purposes interface bus (GPIB) in order to maintain high accuracy and easy measurement. We use the same antenna type and characteristic on both sides of the stratospheric platform and the mobile terminal. The specifications of antenna are as follows:

- Turnstyle loop antenna
- 0 dBi gain
- Circular polarization

- Omnidirectional radiation pattern

The equipments on board the platform have a capability to operate at a continuous wave frequency of 1.2 and 2.4 GHz, which are arranged by the remote carrier control machine from the ground.

The data was collected by driving the van equipped with a mobile receiver in several different spatial positions with respect to any particular elevation angle (α) in a step of 10^0. In this case, the elevation angle is the angle between the horizon and the line connecting the receiver and the platform as depicted in Figure 3.1. Due to a fixed position of the stratospheric platform and a slow movement of the mobile receiver during the field tests, no Doppler shift of communication channel frequency is expected. We repeat the data collection for other elevation angle by changing the position of the vehicle with respect to the platform position as shown in Figure 3.2. Note we do not consider azimuth angle in the measurement so that the position of vehicle is only determined by elevation angle with respect to the platform.

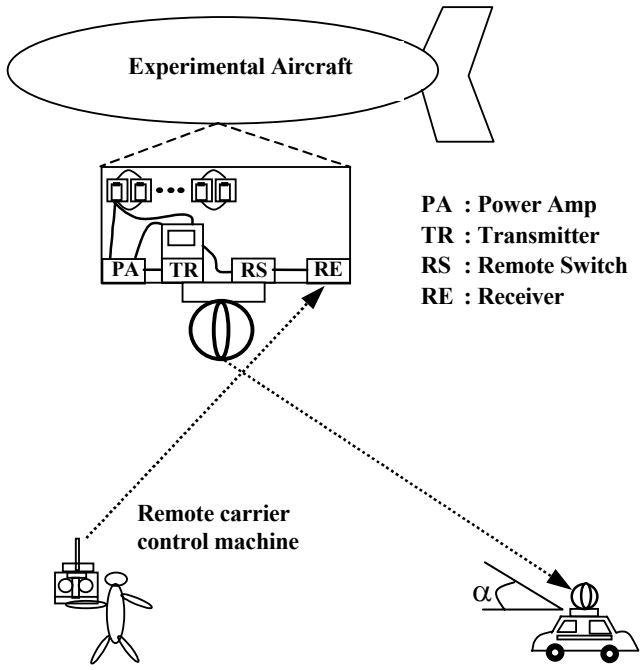

Figure 3.1 Channel characterization experimental configuration.

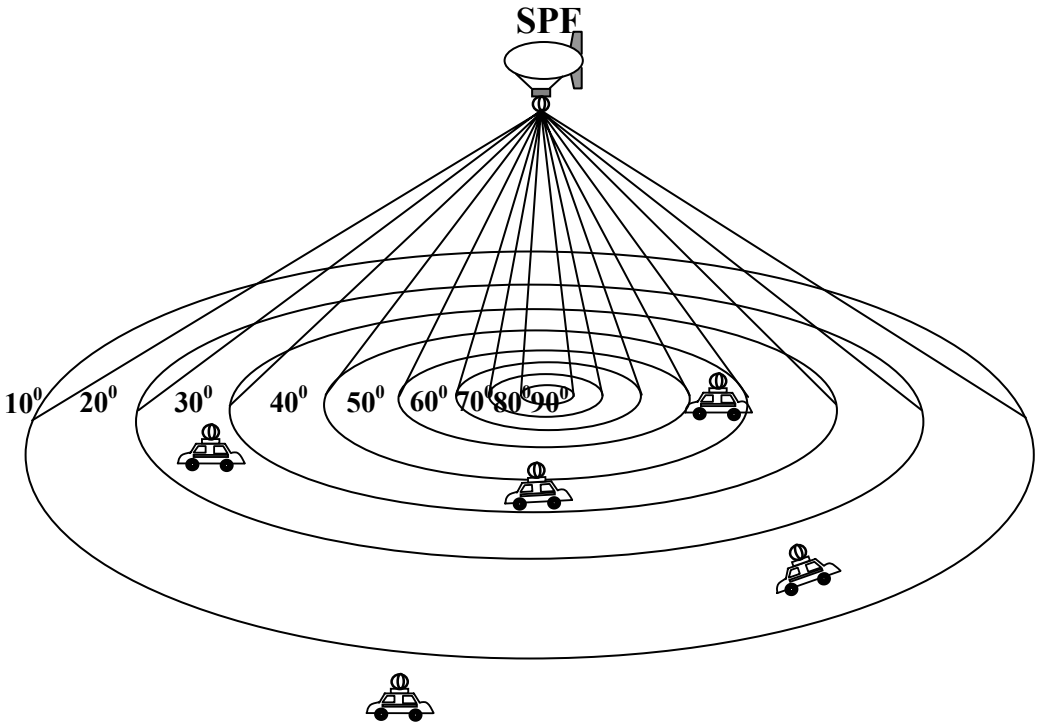

Figure 3.2 Data measurement in various elevation angles.

During intensively signal measurement, the data acquisition system measures the power level in dBm and provides a real-time display of the received power level on the computer. The data are then sampled at 100 times per second and stored in the computer's memory for the further analysis. Since the antenna has 0 dBi gain on both sides of transmitter and receiver, there is no necessary to modify the data from that we read in the acquisition system.

3.3.2 Data Analysis Technique

We collected row data from measurement in the unit of dBm, which means instantaneous received power. Two different frequencies have been used in the measurement. From this data we then compute a cumulative probability as follows. *N* samples of received power over elevation angle $\alpha=90^0$, $P_{r_i}^{90}$, were first collected

$$P_{r_i}^{90} = P_{r_i}, \quad i = 1,2,3,\ldots,N. \tag{3.4}$$

Then the measured data of the received power obtained from other elevation angles $P_{r_i}^{\alpha}$, in which $\alpha = 80^0, 70^0, \ldots, 10^0$, were normalized to the RMS value of the received power when $\alpha=90^0$ in order to get fading depth of received signal $P_{r_i}^{Fade}$ over all the elevation angles in the measurement. It is given by

$$P_{r_i}^{Fade} = \frac{P_{r_i}^{\alpha}}{P_{r_i}^{90}}. \tag{3.5}$$

Since the received power collected during the fade, $P_{r_i}^{Fade}$, is smaller relative to the 90^0 data, we note that

$$P_{r_i}^{Fade} < 1. \tag{3.6}$$

We can therefore define a fade level, F_i, in [dB] as

$$F_i = 10\log\left(P_{r_i}^{Fade}\right). \tag{3.7}$$

The cumulative fade depth distribution or cumulative probability is then computed by dividing the range interval of the fade data into N_F power bins of the size ΔF. Thus

$$\Delta F\, N_F = \max\left\{\left|F_i\right|\right\},\ i = 1 \le i \le N. \tag{3.8}$$

The selection of the size of ΔF is to produce a smooth and continuous distribution curve. The variable D_j is then chosen to represent the number of fade samples as follow

$$F_i\,(1 \le i \le N), \tag{3.9}$$

in which (3.9) satisfying the inequality of $0 > F_i > x_j$, where $x_j = j\,\Delta F$. This is repeated for $j = 1$ to NF. The cumulative probability is finally computed as D_j / N.

3.4 Propagation Parameter

When the stratospheric platform is employed as a very high altitude base station, the possibility of LOS link between the platform and the mobile users is high. Therefore, within the coverage of the platform, the channel is expected to be the Ricean channel and

closer to the Gaussian channel rather than to the Rayleigh fading channel. However, LOS link between the platform and the mobile receiver must be verified. In the field tests, received power consists of the LOS signal and the multipath scattered signal. Thus, Rice distribution can be employed to describe the statistics of the channel.

3.4.1 Cumulative Probability of Received Signal

We describe in Figure 3.3 and 3.4 an example of a time variation signal observed at 1.2 GHz and 2.4 GHz attained from 10^0, 50^0, and 90^0 elevation angle, respectively for the instantaneous received power over 200 samples of data. We analyze two points from the figure. First, the instantaneous received power varies more significant in the case of low elevation angles (i.e. elevation 10^0) rather than in high elevation angles (i.e. elevation 50^0 and 90^0). This fact can provide an indication that the contribution of multipath power components to the total received power is higher in low elevation angle than that in high elevation angle [39]. The higher the fluctuation of the received signal is, the higher the fading depth, which means the worst the signal is. Note in the measurement there is always LOS path available so that the Rice channel distribution may be applied. In the next sub section we extract the parameter of Ricean distribution using the measured data.

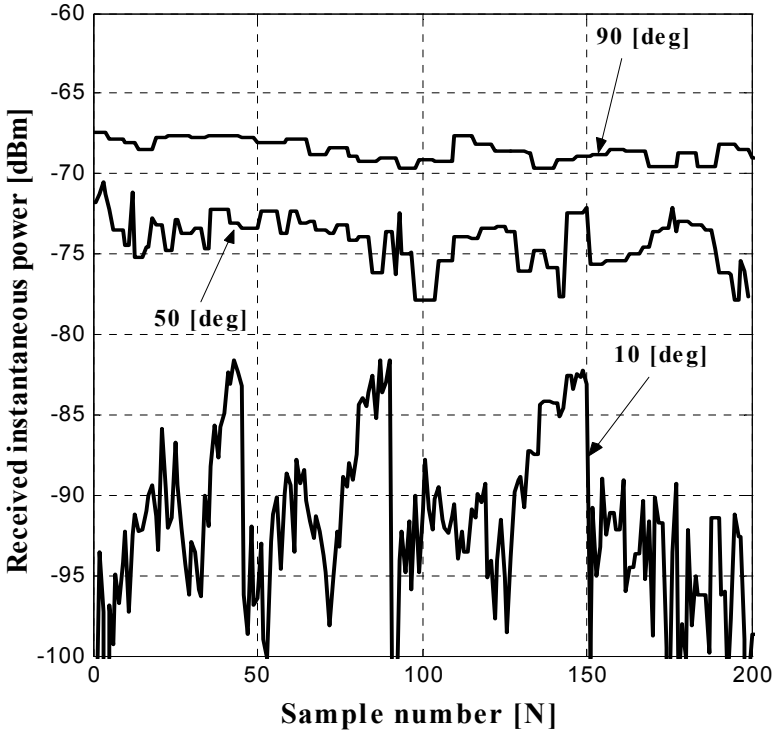

Figure 3.3 Partial data of received instantaneous power at 1.2 GHz (elevation angle is 10^0, 50^0 and 90^0).

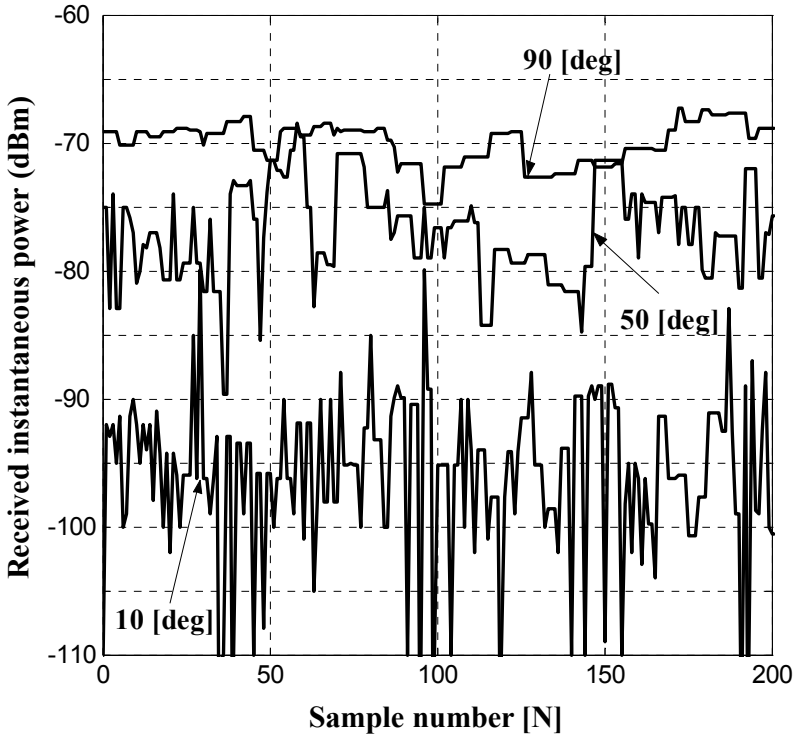

Figure 3.4 Partial data of received instantaneous power at 2.4 GHz (elevation angle is 10^0, 50^0 and 90^0).

Secondly, the local mean received power in low elevation angle is smaller than that in high elevation angle. This is because of the distance between transmitter and receiver is much longer in low elevation angle rather than in high elevation angle. In this case free space attenuation, which depends on Tx-Rx separation distance must be taken into account.

We generate a cumulative probability of received power in order to understand more easily about measurement result using the method that has been explained in sub-section 3.3.2. In Figure 3.5, cumulative probabilities of received power at a frequency of 1.2 GHz that is measured in various elevation angles are reported. Figure 3.6 shows the measurement result for 2.4 GHz. Note during the measurement, only the total received power was collected. There is no separate information regarding the LOS power or the multipath scattered power. It can be seen from the figures, fading depth in a very high elevation angle (i.e. $\alpha=90^0$) is found to be very small. It is only on the order of 1-2 dB. However, in other elevation angles, the curves exhibit a fading depth greater than 2 dB. For example, in the elevation angles of 80^0 to 40^0, the fading depth is observed about 2-25 dB and more than 25 dB of fading depth is observe in the elevation angles lower than 40^0. For both operating frequencies that we used in the experiment, the fading depth in a particular

elevation angle is found to be almost similar. This fact leads to our preliminary conclusion as follow. Even though in low elevation angle the LOS link between the stratospheric platform and the mobile terminal can be achieved, however multipath mechanism, which is caused by the ground, structures and trees exhibits a major contribution to the total received power. Therefore, the stratospheric platform channel operated in low elevation angle may suffer from a serious multipath problem. We perform an analysis in the following sub-section in order to characterize the stratospheric platform channel behavior over various elevation angles.

3.4.2 *K* factor and Local Mean Received Power

In this sub-section the measured propagation parameters are presented and evaluated. An appropriate data conversion from a power level (dBm) into an amplitude level for each data sample is performed in this sub-section. If there is a single dominant signal, for example from LOS path as suggested in our measurement, the composite received signal envelope at the receiver can be described by the probability density function (PDF) of Ricean distribution as described in the following expression [40]-[41]

$$p(R) = \frac{R}{\sigma^2}\exp\left(-\frac{R^2 + A^2}{2\sigma^2}\right) I_0\left(\frac{R\,A}{\sigma^2}\right), \tag{3.10}$$

where R denotes the envelope of the received signal, σ^2 is the variance or average power of the multipath components, A represents the amplitude of the LOS path or dominant signal and $I_0(.)$ is the zero-th order modified Bessel function of the first kind.

In order to find K factor from measured data, let we start from the moment of original Rice distribution that follows this equation

$$E[R^n] = (2\sigma^2)^{n/2}\,\Gamma(\frac{n}{2}+1)\,e^{-K}\;{}_1F_1\left(\frac{n}{2}+1;1;K\right). \tag{3.11}$$

where n is the order of the moment. K factor is the ratio between average LOS power and average multipath power and can be expressed as

$$K = \frac{A^2}{2\sigma^2}. \tag{3.12}$$

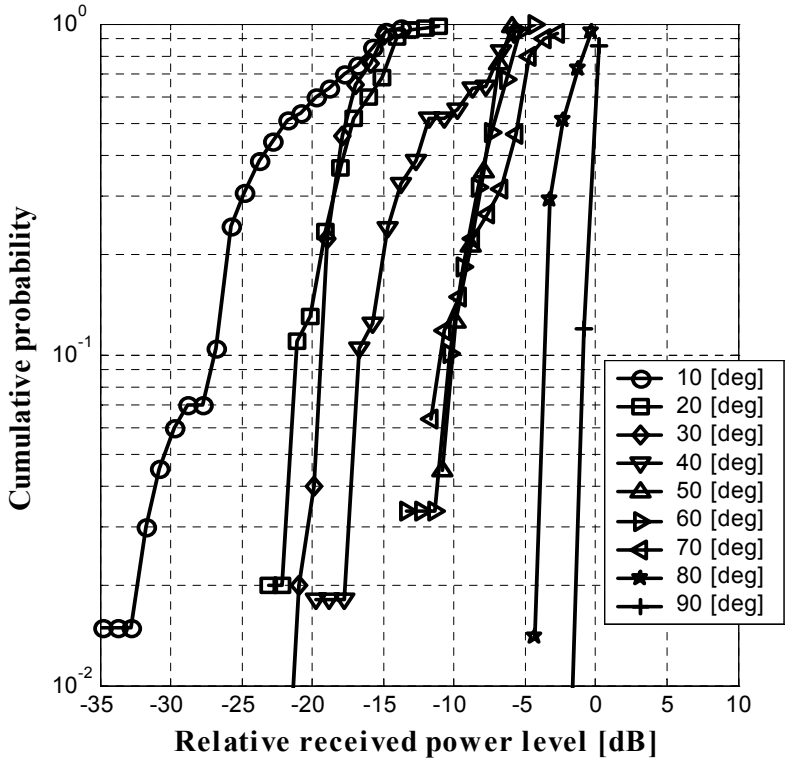

Figure 3.5 Comparison of received power cumulative probability at 1.2 GHz for various elevation angles from 10^0 to 90^0.

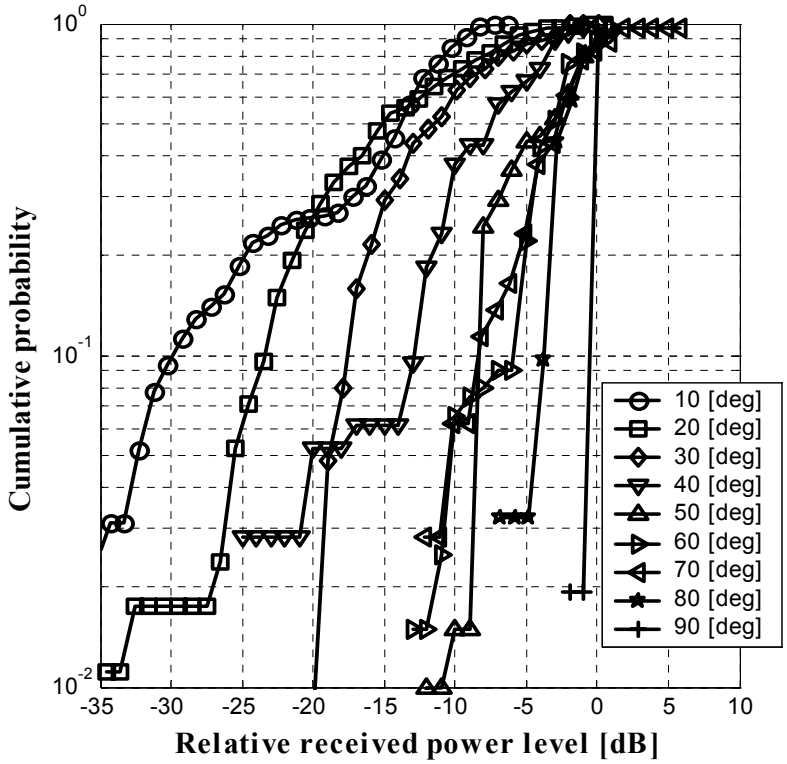

Figure 3.6 Comparison of received power cumulative probability at 2.4 GHz for various elevation angles from 10^0 to 90^0.

From (3.11) we can write first moment and second moment of Rice distribution, respectively as follow

$$E[R] = (2\sigma^2)^{1/2}\,\Gamma(\frac{3}{2})e^{-K}\;{}_1F_1\left(\frac{3}{2};1;K\right), \tag{3.13}$$

$$E[R^2] = (2\sigma^2)\,\Gamma(2)e^{-K}\;{}_1F_1\left(2;1;K\right), \tag{3.14}$$

where $E[R]$ is the expected value and $E[R^2]$ is expressed by

$$E[R^2] = A^2 + 2\sigma^2 \;=\; 2\sigma^2(K+1). \tag{3.15}$$

Since R that denotes the envelope of the received signal is measured in our experiment, from the data of measurements we have both value of $E[R]$ and $E[R^2]$ through the following equation

$$E[R] \;=\; \frac{1}{N}\sum_{j=1}^{N} R_j\,, \tag{3.16}$$

$$E[R^2] \;=\; \frac{1}{N}\sum_{j=1}^{N} R_j^2\,, \tag{3.17}$$

where R_j denotes the j^{th} data sample in amplitude and N is the total of data sample which we use 1,000 data sample in this evaluation.

Now let we arrange (3.13) and (3.14) through one equation, as follow

$$\begin{aligned}\frac{E[R]}{\sqrt{E[R^2]}} &= \frac{(2\sigma^2)^{1/2}\,\Gamma(\frac{3}{2})e^{-K}\,F\left(\frac{3}{2};1;K\right)}{2\sigma^2(1+K)} \\ &= \frac{\sqrt{\pi}}{2}\frac{e^{-K}}{\sqrt{K+1}}F\left(\frac{3}{2};1;K\right) \\ &= \frac{\sqrt{\pi}}{2}\frac{1}{\sqrt{K+1}}F\left(-\frac{1}{2};1;-K\right)\end{aligned}\quad . \tag{3.18}$$

We can solve (3.18) by using the confluent hypergeometric function definition expressed as follows

$$F(a;\, c;\, z) = e^{z}\, F(c-a;c;-z)\,, \tag{3.19}$$

$$a\,F(a+1;\, c+1;\, z) = (a-c)\;F(a;c+1;z) + c\,F(a;c;z)\,, \tag{3.20}$$

$$z\,F(a+1;\, c+1;\, z) = c\,(F(a+1;c;z) - F(a;c;z))\,. \tag{3.21}$$

From (3.19) to (3.21), we can write

$$\begin{aligned}
F\left(-\frac{1}{2};\,1;\,z\right) &= -z\,F\left(\frac{1}{2};2;z\right) + F\left(\frac{1}{2};1;z\right) \\
&= \frac{z^2}{2}F\left(\frac{3}{2};3;z\right) - z\,F\left(\frac{3}{2};2;z\right) + F\left(\frac{1}{2};1;z\right) \\
&= \frac{z^2}{2}F\left(\frac{3}{2};3;z\right) + z\,F\left(\frac{1}{2};2;z\right) + (1-2z)F\left(\frac{1}{2};1;z\right) \\
z\,F\left(\frac{1}{2};2;z\right) &= -\frac{z^2}{4}F\left(\frac{3}{2};3;z\right) + zF\left(\frac{1}{2};1;z\right) \\
F\left(-\frac{1}{2};1;z\right) &= \frac{z^2}{4}F\left(\frac{3}{2};3;z\right) + (1-z)F\left(\frac{1}{2};1;z\right) \\
F\left(-\frac{1}{2};1;-K\right) &= \frac{K^2}{4}F\left(\frac{3}{2};3;-K\right) + (1+K)F\left(\frac{1}{2};1;-K\right)
\end{aligned} \tag{3.22}$$

It is known that

$$I_0(\frac{K}{2}) \;=\; e^{K/2}\,F(\frac{1}{2};1;-K)\,, \tag{3.23}$$

$$I_1(\frac{K}{2}) \;=\; \frac{K}{4}e^{K/2}\,F(\frac{3}{2};3;-K)\,. \tag{3.24}$$

Therefore

$$F\left(-\frac{1}{2};1;-K)\right) = e^{-K/2}\left(K\,I_1\left(\frac{K}{2}\right) + (1+K)\,I_0\left(\frac{K}{2}\right)\right). \tag{3.25}$$

By substituting (3.18) with (3.25) we obtain

$$\frac{E[R]}{\sqrt{E[R^2]}} \;=\; \frac{\sqrt{\pi}}{2}\exp\left(-\frac{K}{2}\right)\frac{1}{\sqrt{K+1}}\left((1+K)\,I_0\left(\frac{K}{2}\right)+K\,I_1\left(\frac{K}{2}\right)\right), \tag{3.26}$$

where $I_1(.)$ is modified first order Bessel function of the first kind.

Now we can extract K factor from measured received signal through equation (3.26). This equation expresses the variation of channel between Rayleigh (K = 0) and the Gaussian like distribution ($K = \infty$) and Figure 3.7 shows (3.26) graphically. We use Figure 3.7 as a best-fit test to the samples data of received power after we converted to the amplitude. The same data of observed samples as in local mean power calculation is also used for K factor estimation.

Figure 3.8 shows the result of K factor estimation for the link between stratospheric platform and terrestrial mobile terminal as a function of elevation angle. The K factor obtained from two different frequencies is presented on the figure. For both curves, K factor increases when the elevation angle of the platform increases. The small value of K factor describes the strong contribution of the multipath scattered power in low elevation angle. In this experiment, the value of K factor is small when the elevation angle is low (i.e. lower than 40^0). In the case of high elevation angle (i.e. greater than 40^0), the value of K factor is gradually increasing and that means the total received power is dominated by direct power. From this observation the coverage area of the platform should be carefully designed with respect to the minimum performance requirement, which will be described in next Section of this chapter.

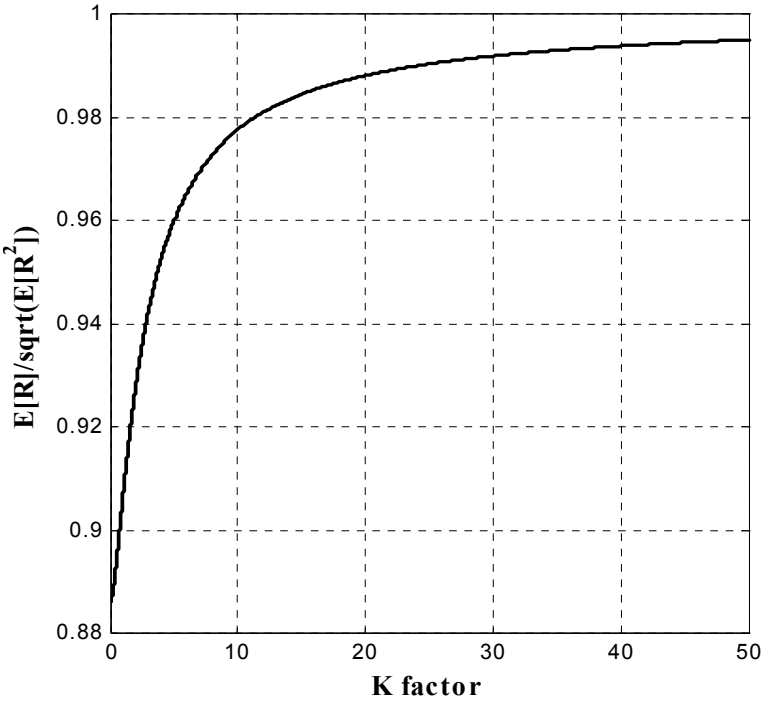

Figure 3.7 Variation of the statistics received amplitude and the K factor.

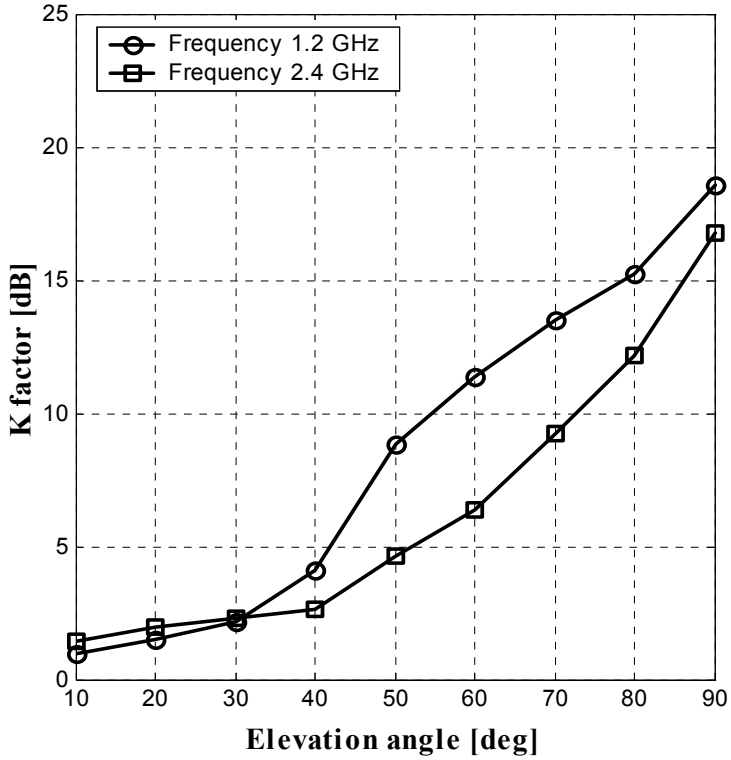

Figure 3.8 The measured *K* factor as a function of elevation angle.

The local mean received power is extracted by averaging the instantaneous received power over N = 1,000 samples within a spatial distance about 25 m (> 200 λ) for each elevation angle. This spatial distance is long enough to contain signal variations at a large scale [39].

Detail measured propagation parameters are displayed in Table 3.1 and Table 3.2 for 1.2 GHz and 2.4 GHz frequency, respectively. The parameters are *K* factor, local mean received power, and the standard deviation of local mean received power. Local mean received power is observed with respect to the elevation angle we used in the measurement. We found local mean received power varies about 20 dB between the lowest (10^0) and the highest (90^0) of elevation angle. The standard deviation of local mean received power is large in low elevation angle (i.e. 10^0) and decreases as the elevation angle increases. This statistical representation of local mean received power is very useful in estimating the coverage of the platform and in predicting the level of co-channel interference at a mobile terminal.

Table 3.1

Propagation parameters for each elevation angle of the platform

(Measurement result in Hokkaido at 1.2 GHz frequency).

Elevation angle [degree]	1.2 GHz		
	K factor [dB]	Local mean received power [dBm]	Standard deviation of local mean received power [dB]
10	0.9	-88.6	5.2
20	1.5	-84.1	2.7
30	2.2	-84.4	1.8
40	4.1	-78.6	3.9
50	8.9	-74.9	1.5
60	11.4	-74.5	2.0
70	13.5	-74.0	2.8
80	15.2	-69.4	1.3
90	18.6	-67.3	0.5

Table 3.2

Propagation parameters for each elevation angle of the platform

(Measurement result in Hokkaido at 2.4 GHz frequency).

Elevation angle [degree]	2.4 GHz		
	K factor [dB]	Local mean received power [dBm]	Standard deviation of local mean received power [dB]
10	1.4	-89.8	7.6
20	2.0	-84.8	7.0
30	2.3	-81.4	5.0
40	2.7	-78.2	5.1
50	4.6	-74.3	3.3
60	6.4	-73.5	2.9
70	9.2	-73.2	3.6
80	12.2	-72.3	1.6
90	16.8	-70.1	0.5

The antenna characteristics used during the measurement plays an important role in affecting the results presented in Table 3.1 and 3.2. Since we use the 0 dBi gain of antenna during experiment, the local mean received power is directly dependent to the elevation angle and to the power transmit. Moreover, omnidirectional antenna is widely used at mobile user side so that we use this antenna pattern in our measurement. Multipath power

contribution through the use of omnidirectional antenna is quite significant compared with the use of directional antenna. As a result, the *K* factor cannot be as high as if we use directional antenna. This is due to the fact that multipath power contribution is much higher when we employ omnidirectional antenna than that use directional antenna.

The above results are obtained when the platforms position is fixed during measurement. In case of the real implementation, may be there is a movement of the platforms in a horizontal or vertical displacement and a movement on their attitude in terms of pitch, roll and yaw. Such movements have two effects to the result presented in Table 3.1 and 3.2. Firstly, it can cause the changing of relative angle with respect to the mobile users position on the ground. We found that horizontal displacements of the platform have a big impact to the channel performance in high elevation angle, while the vertical displacements have an effect mostly in low elevation angle. Figure 3.9 shows the model of horizontal and vertical platform displacement. Assuming both horizontal and vertical platform displacement is 4 km (worst case) with altitude equals 20 km. We summarize in the Table 3.3 the variation of elevation angle due to the platform displacement.

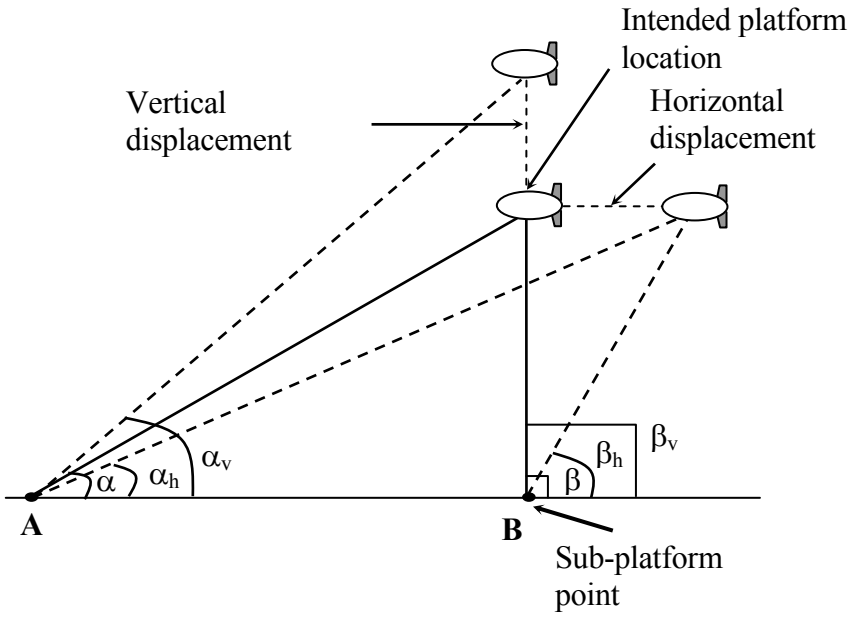

Figure 3.9 A model of platform movement.

Table 3.3

Effect of horizontal and vertical platform displacement on elevation angle.

User position	Original angle	Horizontal displacement		Vertical displacement	
		New angle	Difference from original angle	New angle	Difference from original angle
A	$\alpha = 10^0$	$\alpha_h = 9.7^0$	$\Delta\alpha = 0.3^0$	$\alpha_v = 11.9^0$	$\Delta\alpha = 1.9^0$
B	$\beta = 90^0$	$\beta_h = 78.7^0$	$\Delta\beta = 11.3^0$	$\beta_v = 90^0$	$\Delta\beta = 0^0$

Based on the above analyses, those *K* factor and local mean received power would vary to decrease or increase with respect to the elevation angle variation caused by platform movement. For example, in horizontal displacement, elevation angle variation will be much higher for an area below the sub-platform point (the point vertically below the intended platform location) than that for an area further away from sub-platform point. In this case, both *K* factor and local mean power would vary in high elevation angle but nearly constant in low elevation angle. In vertical displacement, the opposite condition will be observed that is *K* factor and local mean power would vary in low elevation angle but nearly constant for high elevation angle.

Secondly, the platform movement could introduce the frequency Doppler spread that leads to the fast fading channel characteristic. In the stratospheric platform communication, the Doppler spread is a function of the relative velocity between both the platform and the mobile terminal on the ground. It causes the frequency dispersion, which leads to the signal distortion. Some configurations of stabilization mechanism must be equipped to reduce the platform movement. Moreover, the use of beam steering antenna is another proposed solution to compensate the problem, which is caused by the platform movement.

3.5 Performance Evaluation

The measurement results show that the fast amplitude fluctuations of the proposed stratospheric platform channel are described by a Ricean density function. The *K* factor varies between 0.9 and 18.6 dB at frequency 1.2 GHz and between 1.4 and 16.8 dB at

frequency 2.4 GHz. The proposed channel model can be evaluated by utilizing the measured propagation parameters. Therefore, by using the measured propagation parameters, the bit error probability performance for DPSK and DQPSK modulation scheme is evaluated in this section with different elevation angles.

3.5.1 Under DPSK Modulation Scheme

Because of the platform is fixed positioned and the mobile receiver moved slowly during the field tests, the bit error probability has been suggested to be evaluated under the frequency non-selective slow fading channel. To evaluate the SPF channel performance in closed form, we first transform (3.10) to an expression where the random variable is the E_b/N_0 instead of the received signal envelope, R, where E_b is energy bit and N_0 is one sided power spectral density of the AWGN in units of W/Hz. Note the instantaneous E_b/N_0, which we denote as Γ, is proportional to R^2. We assume AWGN noise only, therefore the transformation could resulting the following equation

$$P(\Gamma) = \frac{1+K}{\overline{\Gamma}} \exp\left(-\frac{\Gamma(1+K)+K\overline{\Gamma}}{\overline{\Gamma}} \right) I_0\left(\sqrt{\frac{4(1+K)K\Gamma}{\overline{\Gamma}}} \right). \qquad (3.27)$$

Since we assume the fading is slow and flat for SPF channel in the measurement, the average BER can be expressed as [42]

$$P_e(\overline{\Gamma}, K) = \int_0^\infty \varepsilon(\Gamma)\, p(\Gamma)\, d\Gamma, \qquad (3.28)$$

where $\varepsilon(\Gamma)$ is the BER as a function of the E_b/N_0. For Ricean fading channel as it suggests in SPF channel, we can actually find $P_e(\overline{\Gamma}, K)$ for the general expression

$$P_e(\Gamma, k_1, k_2) = k_1 \exp(-k_2\Gamma), \qquad (3.29)$$

which covers DPSK and non-coherent binary FSK. Substituting (3.27) and (3.29) into (3.28) we can evaluate the integral in closed form as follow

$$P_e(\overline{\Gamma}, K) = \frac{k_1}{1+\upsilon} \exp\left(-\frac{K\upsilon}{1+\upsilon} \right), \qquad (3.30)$$

where $\upsilon = k_2 \overline{\Gamma}/(1+K)$. For DPSK k_1 = 1/2 and k_2 = 1, therefore for DPSK modulation scheme, the performance of SPF channel in term of BER can be expressed by

$$P_e, DPSK(\overline{\Gamma}, K) = \frac{1+K}{2(\overline{\Gamma}+1+K)} \exp\left(-\frac{K\overline{\Gamma}}{\overline{\Gamma}+1+K}\right), \tag{3.31}$$

where $\Gamma = \overline{\beta^2} E_b / N_0$ is the average value of the signal to noise ratio and $\overline{\beta^2}$ is unit variance of amplitude values of the fading channel.

3.5.2 Under DQPSK Modulation Scheme

We have evaluated BER for the SPF channel under DPSK modulation scheme, however there is no closed form solution for DQPSK so that we use numerical integration to evaluate bit error probability. We employe the same propagation parameters as used in DPSK to evaluate the SPF channel performance under DQPSK modulation scheme. From equation (3.10), we first define Γ as

$$\Gamma = \frac{\left(\frac{A^2}{2}+\sigma^2\right)T}{N_0}. \tag{3.32}$$

For DQPSK, the BER for AWGN channel is given by [42]

$$P_e = Q(a,b) - \frac{1}{2} I_0(a,b) \exp\left(-\frac{1}{2}(a^2+b^2)\right), \tag{3.33}$$

where $Q(a,b)$ is the Marcum Q function, $I_0(.)$ is the zeroth order modified Bessel function and the parameters a and b are defined as

$$a = \sqrt{2\delta_g\left[1-\frac{1}{\sqrt{2}}\right]}, \tag{3.34}$$

$$b = \sqrt{2\delta_g\left[1+\frac{1}{\sqrt{2}}\right]}. \tag{3.35}$$

Since we assume the SPF channel in our measurement is slow and flat fading channel, the received carrier envelope within any symbol interval will be a random variable R having the PDF given in (3.10). Therefore the BER condition for a particular R will have the same form as that of the AWGN channel but with A replaced by R and σ_g replaced by Γ. From (3.33) and using the series expansion for the Marcum Q function, the conditional BER is

$$P_{e/R} = \exp\left[-\frac{1}{2}(a^2+b^2)\right]\left\{\sum_{m=1}^{\infty}\left(\frac{a}{b}\right)^m I_m(ab)+\frac{1}{2}I_0(ab)\right\}, \tag{3.36}$$

where $a^2+b^2=4\Gamma$, $ab=\sqrt{2}\,\Gamma$, and $a/b=\sqrt{2}-1$. Integrating (3.36) over the Ricean density function (3.10) yields the probability of error as

$$P_e = \int_0^{\infty} e^{-2\Gamma}.\left\{\frac{1}{2}I_0\left[\sqrt{2}\,\Gamma\right]+\sum_{m=1}^{\infty}\left[\sqrt{2}-1\right]^m I_m\left[\sqrt{2}\,\Gamma\right]\right\} p(R)\,dR. \tag{3.37}$$

To solve (3.37), first we have to look at the following integral equation

$$J_m = \int_0^{\infty} e^{-2\Gamma} I_m\left[\sqrt{2}\,\Gamma\right] p(R)\,dR. \tag{3.38}$$

Then substitute (3.10) into ((3.37) by using the integral representation of the mth order modified Bessel function and we write as

$$J_m = \frac{1}{\pi\sigma^2}\exp\left(-\frac{A^2}{2\sigma^2}\right)\int_0^{\pi}\cos(m\theta)\,d\theta\int_0^{\infty} R\,e^{-a^2R^2} I_0\left(\frac{RA}{\sigma^2}\right)dR, \tag{3.39}$$

where

$$a^2 = \frac{T}{N_0}\left[1-\frac{1}{\sqrt{2}}\cos\theta\right]+\frac{1}{2\sigma^2}. \tag{3.40}$$

After using a series representation for the modified Bessel function $I_0(.)$ in equation (3.39) we have

$$J_m = \frac{1}{\pi}\int_0^{\pi}\frac{(1+K).\cos(m\theta).e^{-E}}{1+K+[2-\sqrt{2}\cos\theta]\,\Gamma}\,d\theta, \tag{3.41}$$

where

$$E = \frac{[2-\sqrt{2}\cos\theta]K\,\Gamma}{1+K+[2-\sqrt{2}\cos\theta]\,\Gamma}. \tag{3.42}$$

Finally, substituting (3.41) in to (3.37), we have an expression of BER for DQPSK modulation scheme as follow

$$P_{e,DQPSK} = \frac{1}{2\pi}\int_0^{\pi}\frac{(1+K)\,e^{-E}}{1+K+[2-\sqrt{2}\cos\theta]\,\Gamma}d\theta + \sum_{m=1}^{\infty}[\sqrt{2}-1]^m\frac{1}{\pi} \; x\int_0^{\pi}\frac{(1+K).\cos(m\theta).e^{-E}}{1+K+[2-\sqrt{2}\cos\theta]\,\Gamma}d\theta \tag{3.43}$$

Performance evaluations of the proposed stratospheric platform channel in 1.2 GHz frequency for both DPSK and DQPSK are shown from Figure 3.10 to Figure 3.11, respectively, while for 2.4 GHz frequency are shown in Figure 3.12 and Figure 3.13. We can see in the figures, both modulation schemes show a comparable performance. Bit error probability at frequency 1.2 GHz exhibits slightly better performance compared with 2.4 GHz, particularly in a high elevat ion angle (i.e. greater than 40^0). In general, the performance of the proposed channel for both modulation schemes is getting worse for an elevation angle lower than 40^0. However, we can see that the performance is getting better for elevation angles greater than 40^0, which means the multipath scattered power does not contribute significantly in a high elevation angle.

The results of bit error probability evaluation for LOS situation in our experiment show that an error floor has been occurred due to the presence of the diffuse multipath components. As an example, prediction to the values of the signal to noise ratio (E_b/N_0) necessary to achieve an average bit error probability of 10^{-3} is reported in Table 3.4 and Table 3.5 for DPSK and DQPSK modulation scheme, respectively. From the tables, we can see that the necessary of signal to noise ratio to achieve 10^{-3} of bit error probability in case of elevation angle lower than 40^0 is much higher than that in the situation of elevation angle greater than 40^0.

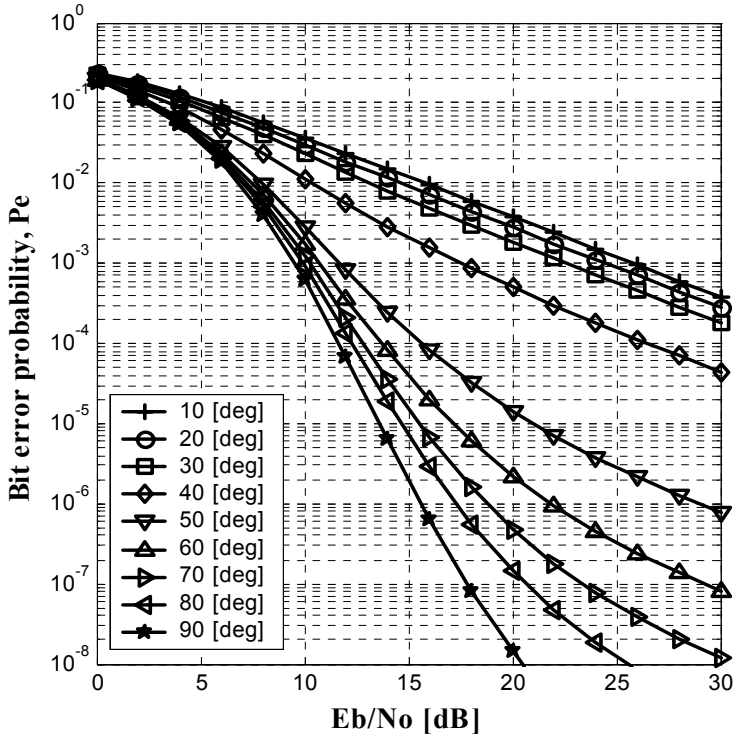

Figure 3.10 Bit error probability, *Pe*, for various elevation angles (α) from 10^0 to 90^0 at frequency of 1.2 GHz in the experiments (DPSK).

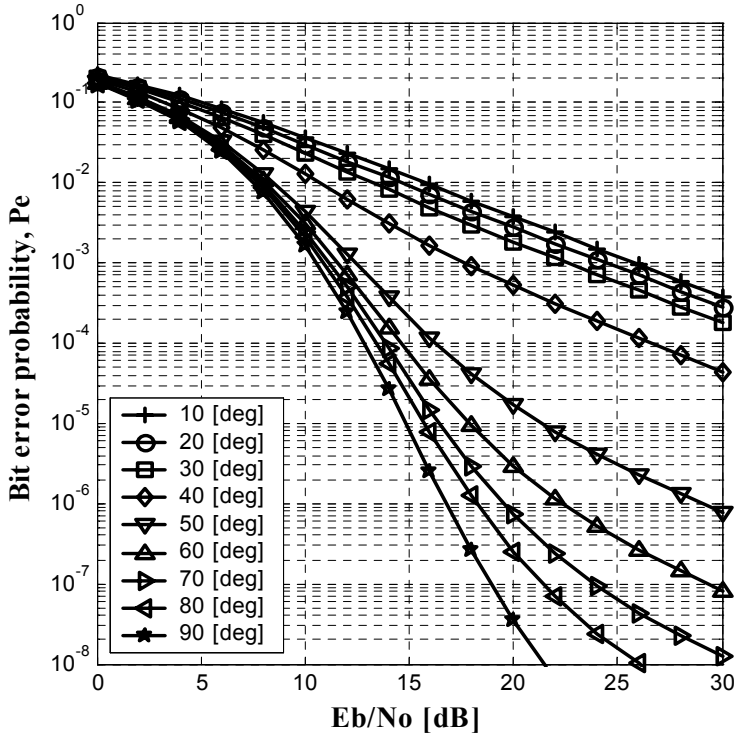

Figure 3.11 Bit error probability, *Pe*, for various elevation angles (α) from 10^0 to 90^0 at frequency of 1.2 GHz in the experiments (DQPSK).

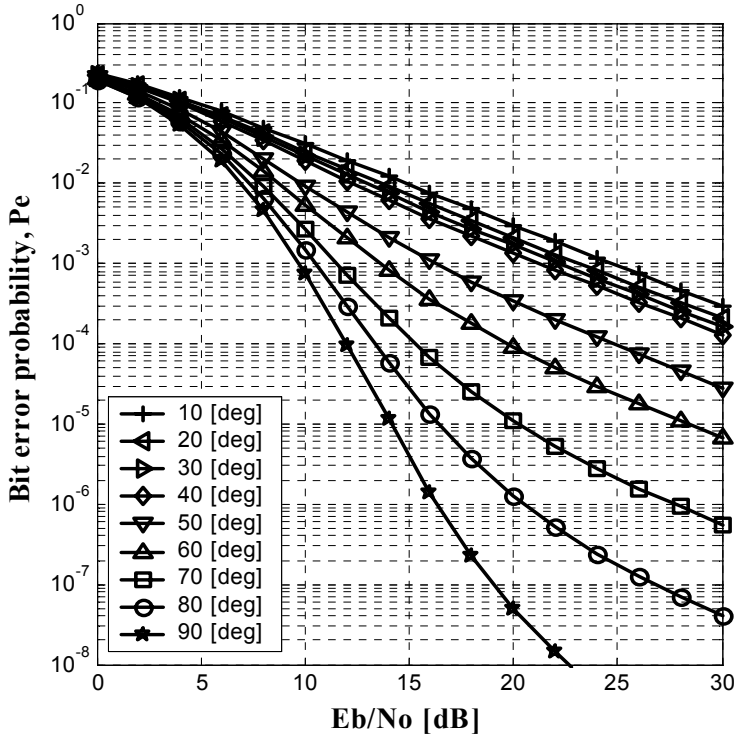

Figure 3.12 Bit error probability, P_e, for various elevation angles (α) from 10^0 to 90^0 at frequency of 2.4 GHz in the experiments (DPSK).

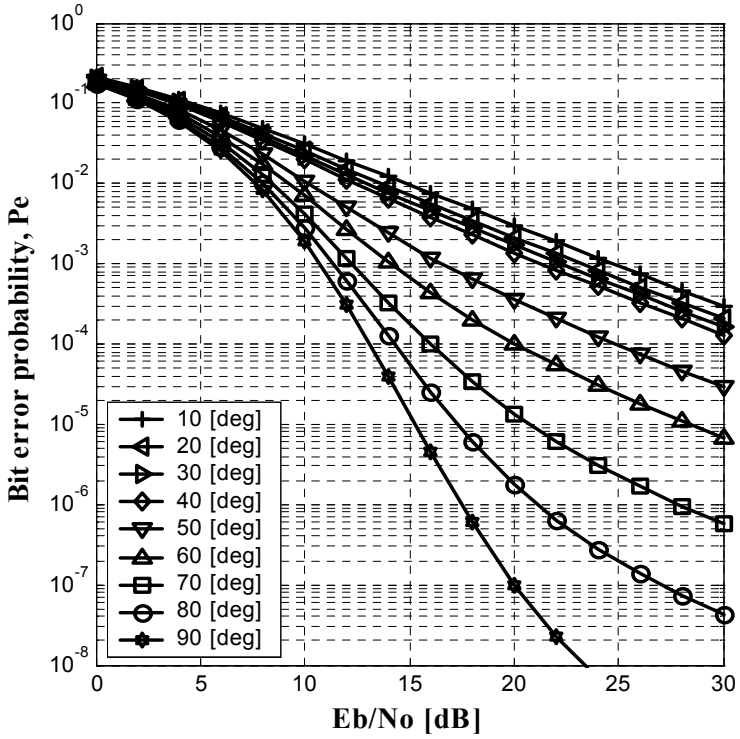

Figure 3.13 Bit error probability, P_e, for various elevation angles (α) from 10^0 to 90^0 at frequency of 2.4 GHz in the experiments (DQPSK).

Table 3.4

Predicted signal to noise ratio (E_b/N_0) necessary to achieve a bit error probability of 10^{-3} over wide range of elevation angles for DPSK modulation scheme.

f [GHz]	E_b/N_0 [dB]								
	Elevation Angle								
	10^0	20^0	30^0	40^0	50^0	60^0	70^0	80^0	90^0
1.2	25.7	24.3	22.4	17.3	11.6	10.7	10.2	9.9	9.5
2.4	24.6	23.0	22.1	21.1	16.2	13.5	11.5	10.5	9.7

Table 3.5

Predicted signal to noise ratio (E_b/N_0) necessary to achieve a bit error probability of 10^{-3} over wide range of elevation angles for DQPSK modulation scheme.

f [GHz]	E_b/N_0 [dB]								
	Elevation angle								
	10^0	20^0	30^0	40^0	50^0	60^0	70^0	80^0	90^0
1.2	25.6	24.3	22.4	17.5	12.4	11.5	11.1	10.9	10.5
2.4	24.5	23.0	22.1	21.1	16.4	14.0	12.2	11.4	10.7

In order to provide an appropriate required bit error probability for a particular application, the stratospheric platform coverage would have to be adjusted by selecting a suitable elevation angle. To increase the coverage area of the platform, multipath fading mitigation techniques are required, particularly in low elevation angle, which correspond to a small value of the K factor. Furthermore, the use of channel coding, equalization, diversity technique or employ OFDM technique may be required to realize reliable and robust communication in the stratospheric platform environment.

The stratospheric platform channel presented in this analysis is an approach model in order to investigate the effect of elevation angle to the channel performance. We notice from the results that the performance is proven as an increasing function of elevation angle. As previously mentioned, in our analysis the received signal amplitude is modeled as Ricean distributed due to the presence of LOS link. The *K* factor is mainly governed by the

elevation angle and the type of environment during experiment. In one hand, for a certain elevation angle, both LOS power ($A^2/2$) and multipath scattered power (σ^2) are subject to proportionally decrease from the results presented in this study in case of the actual 20 km platform altitude. This is because both LOS signal and multipath signal will experience the longer distance through the same atmospheric condition before they arrive at the ground. As a result, the *K* factor is expected to be nearly constant for each specific elevation angle. By contrary we observe the *K* factor would have to vary for different elevation angle even if for a particular altitude of the platform as is shown in our results. This is due to multipath power varies along with the variation of elevation angle. Based on the above analysis, it may be expected to characterize the platform channel at 20 km altitude by using these results under the limitation of the similar condition and the similar geometry (i.e. similar elevation angle and similar type of environment). On the other hand, these results would need to be adjusted to estimate the actual system channel performance due to the different antenna type and taking into consideration the co-channel interference. Moreover, the performance of the stratospheric platform channel needs quantifying a more complex channel model that consider different type of environment (i.e. in built-up or rural area), and also taking into consideration an effect of wideband channel characteristic. However, the tendency of the platform channel performance over the variation of elevation angles can be observed by using this result. According to the result we are able to carefully design the suitable coverage area of the stratospheric platform.

3.6 Summary

In this chapter, we have presented and analyzed the first channel measurement results for the case of stratospheric platform communication link. Area in which the measurement was conducted is similar to a typical semi-urban environment. In the measurement, links between stratospheric platform and mobile user on the ground are mostly LOS link even though for a very low elevation angle. The measurement itself is intended to characterize the stratospheric platform mobile communication channel and its multipath behavior.

According to the results, multipath fading is observed and shown that the fading depth would have to vary between 1 dB and more than 25 dB depending on the elevation angle. Note that in the measurement we used an omnidirectional antenna. We then characterize the stratospheric platform channel by using method of moment to find *Rice parameter* (*K*).

Another propagation parameter that we have found from the data of measurement is local mean received power. Both *K* factor and local mean received power are evaluated under the variation of elevation angle. Our evaluation show that the *K* factor would have to vary from 0.9 to 18.6 dB for a frequency carrier of 1.2 GHz in the measurement and 1.4 to 16.8 dB at frequency 2.4 GHz. Standard deviation of local mean received power is found to decrease as elevation angle increase indicating little multipath in high elevation angle. Up to this point we have described the channel characteristic in stratospheric platform communication.

We then evaluated bit error probability performance for such a channel using DPSK and DQPSK modulation scheme through simulation for both frequency carriers. Simulation result show the performance in elevation angle lower than 40^0 is intolerable error. This is due to a significant multipath scattered power contribution from the ground reflection and other potential scattered power such as trees and structure nearby the receiver. As a preliminary conclusion, minimum elevation angle plays an important role in the designing the coverage area of the stratospheric platform communication. Though the lower the minimum angle the larger the coverage area, it is still difficult to obtain high performance in fringe of the coverage. Therefore, it is required a multipath mitigation technique as a performance improvement method, especially for an area with very low elevation angle, for example at the edge of coverage.

Chapter 4

SPF Radio Propagation Modeling with Ray Tracing

In Chapter 3 we have examined and characterized SPF channel for mobile communications based on measurement for an area of semi-urban environment over which all communication links are LOS. In this chapter mobile SPF channel is evaluated in terms of propagation path loss and required transmitted power in the area of urban low rises environment. Both LOS and NLOS link are analyzed with considering various elevation and azimuth angles of SPF that is seen from mobile station. A building geometry model, which its characteristics has been developed based on the experimental result in urban environment, is proposed for radio propagation evaluation in SPF system. The evaluation is based on a well-known ray tracing algorithm which is applied to the proposed building geometry model. Predicted results of propagation loss using ray tracing algorithm are then compared with a physical-statistical model for comparison and verification. Both methods show a good agreement in all scenarios. Finally, the required transmit power from SPF is estimated for the application of third generation IMT-2000 services over various scenarios of SPF position.

4.1 Introduction

Before cellular mobile systems are introduced in the early 1980s the commercial use of radio spectrum was dominated by broadcast radio and television. In broadcast systems the target is to cover an entire area from a single transmitter using assigned frequency channel. Therefore, these systems design goal is to achieve the largest possible coverage area in which the received power is sufficiently strong compared to background noise. To achieve this goal, transmitting antenna should be located on a tall of buildings or towers with the maximum allocated power. At the end of coverage area, receiving antenna is also located at the top of buildings whenever possible. In order to support broadcast system, propagation mechanism of the signal was studied over long distance of 100 km or more, considering earth curvature, refraction in the atmosphere, and large-scale terrain features.

Cellular mobile systems are completely different with broadcast systems in the matter of the coverage size. Cellular mobile systems were designed to only cover short distance communication, for example communication from mobile user to base transceiver station (BTS) or vise versa. The nature of the decrease of the radio signal with distance allows the spectrum to be reused elsewhere within the same area. Therefore, in cellular mobile systems, the target is to make the received signal power adequate to overcome the background noise, while minimizing interference to other more distant links operating at the same frequency. To achieve this target, it is a complicated task because in one hand the signal should have enough power over the desired links, but on the other hand it should avoid interference to other links. This problem has motivated the cellular concept to accommodate as many users as possible through spatial reuse of the limited allocated spectrum. Up to this point we have introduced the necessary of radio propagation evaluation in cellular mobile systems as a fundamental feature in determining system design.

Many literatures have addressed the propagation characteristics for terrestrial cellular mobile systems. In the initial deployment of cellular systems, radio link has covered up to about 20 km from a BTS. However, to anticipate the growing of subscriber, it is needed to make the coverage area of each BTS smaller in order to reuse the allocated spectrum. As a result, a newer cellular systems has significantly reduced their coverage to the maximum distance may be no more than hundred meters. Since the allocated spectrum to cellular

mobile systems lie in the frequency of 450 MHz, 900 MHz, and the band around 2 GHz, the wave length of the signal is smaller than the typical dimension of the building but larger than the roughness of the building materials. Thus, the propagation mechanism can be explained mathematically in terms of the processes of reflection, transmission at the walls and diffraction by building edges. In modern communication, this subject has experimentally investigated and can be found in many literatures for the case of terrestrial cellular systems in which the BTS antenna is located slightly higher, at the same height, or lower than the average building height.

This chapter, however, is intended to evaluate radio propagation characteristics in terms of path loss model and Rice factor for a new wireless system that is called the SPF system operating in urban environment. We begin with a radio propagation modeling that appropriates for the SPF communication. Then it is followed by main content of this chapter that explains detailed SPF radio propagation evaluation with focusing to the ray tracing method.

4.2 Radio Propagation Model for the SPF Communication

4.2.1 Review of Existing Model

In conventional terrestrial and satellite wireless systems, a various radio propagation models for different environment and different wireless services have been proposed and developed. While in satellite system we have to deal with megacells ranging for various types of environments, in terrestrial cellular system we may classify the propagation model for urban environment into three distinct models. These include propagation model in:

- *Macrocells*—In macrocells urban environment the antenna BTS is often placed well above an average rooftop so that the propagation path is dominated by the over the rooftop path. The important parameter for the macrocell propagation model is the overall area covered, rather than the specific field strength at particular location. The model of macrocellular system is often dependent to parameters such as antenna heights, environment, and distance.

- *Microcells*—The reason of creating microcells is motivated by a desire to reduce cell sizes in areas where large numbers of users require access to the system.

Therefore, limited radio spectrum is required to be reused over very short distances. In microcells the antenna BTS is often located well below the average rooftop so that the propagation path is dominated by reflections and diffractions from building walls and streets.

- *Picocells*—Picocells is created when a BTS antenna is located inside a building for high-traffic areas such as railway stations, office buildings, or airport. The propagation mechanism is mainly dominated by the reflections and diffraction by the objects inside the building. Penetration through the walls is also major mechanism in picocells as well as propagation into buildings from outdoor resources such as macrocells and microcells.

In general, there are two different models to model radio propagation that might often be used in mobile system design. Each method has a specific advantages and disadvantages over the other method. Moreover, each method has its specific application in terms of the types of environments and the types of services. Those methods are:

- *Empirical or statistical models*—These models are based on the statistical characterization of the received signal. Thus, they are easier to implement, require less computational effort, and are less sensitive to the environment's geometry. Moreover, these models are able to provide parameters suitable to simulate propagation channels and to estimate the performance of the system but suffer from a number of disadvantages. Those are they can only be used over parameter ranges included in the original measurement set, environments must be classified subjectively according to categories such as urban or semi-urban which have different meanings in different countries, and they provide no physical insight into mechanisms by which propagation occurs. Examples of these models are Okumura model [26], Hata model [27], COST 231 model [43]-[44], Lee model [1], and Ibrahim and Parson model [45].

- *Site-specific or deterministic models*—Site-specific or deterministic propagation models are based on the theory of electromagnetic wave propagation. These models do not rely on extensive measurements just like in statistical models, but on knowledge of greater detail of the environment. They provide accurate predictions of the signal propagation and also provide delay spread information.

In principle, the propagation characteristics of electromagnetic waves could be computed exactly by solving Maxwell's equations. However, this approach requires very complicated mathematical operations and requires considerable computing power. Therefore this approach has been applied to simplified environment. These models include ray tracing method, finite-difference time-domain (FDTD) method, moment-method model, artificial neural-network model and some new methods such as vector parabolic-equation model, fast far-field approximation model, waveguide model, and Boltzmann model. Examples of these models include Allsebrook and Parson model [46]-[47], Ikegami model [48], rooftop diffraction model [49], flat edge model [50]-[51], Walfisch-Bertoni model [52], and some of many other models that use deterministic model are proposed in [53]-[61].

4.2.2 Model for SPF

Compared with the traditional terrestrial radio tower, the propagation characteristic in SPF communication is inherently different. In traditional terrestrial radio towers, BTS antennas are usually located about or less than 50 m in height above the average rooftop level. Therefore their communications with distant users are essentially horizontal in nature. Thus multiple screen diffraction past rows of buildings of similar heights becomes a dominant attenuation mechanism. However, the SPF can be considered to be an extremely tall BTS, where the propagation path consists of free space LOS propagation between the SPF and the rooftops nearest the MS, a combination of diffraction from rooftop to the street and multiple reflections from the sides of the nearby buildings. Therefore, multiple screen diffraction is negligible for SPF propagation except for very small elevation angle, i.e. less than 3^0.

In Figure 4.1 the basic propagation model in SPF communication is demonstrated. Based on the model, theoretically propagation loss in SPF communication can be calculated as the sum of the free space loss (L_{fs}), the rooftop scattering loss (L_{rts}) and the multiple screen diffraction loss (L_{msd}). The total propagation loss is then expressed as

$$L_{total} = L_{fs} + L_{rts} + L_{msd} . \quad (4.1)$$

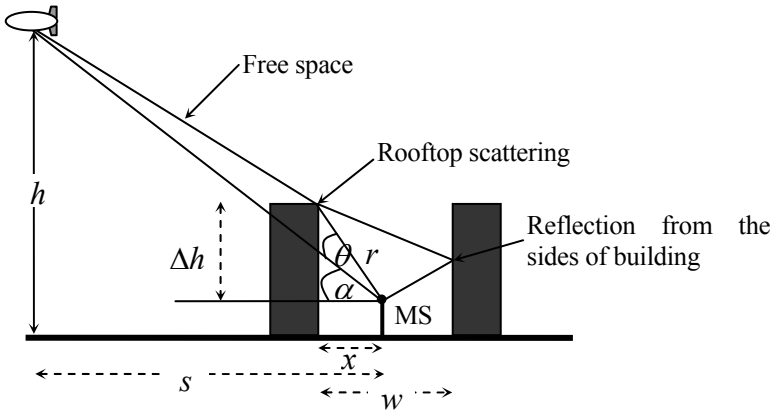

Figure 4.1 Basic propagation model in SPF communication.

4.2.3 Free Space Loss (L_{fs})

The free space loss, which for HAP this is usually the dominant propagation loss is given by the common expression as

$$L_{fs} = 10\log_{10}\left(\frac{\lambda}{4\pi d}\right)^2, \tag{4.2}$$

where λ is the wave length and d is the distance between Tx and Rx.

4.2.4 Rooftop Scattering Loss (L_{rts})

The diffraction from rooftop down to the street level or MS level leads to the excess loss to the MS as expressed as

$$L_{rts} = Min\left\{10\log_{10}\left[\frac{\lambda}{2\pi^2 r}\left(\frac{1}{2\pi\theta}\right)^2\right], L_{mrl}\right\}, \tag{4.3}$$

where L_{mrl} is the excess propagation loss due to multiple reflections from the sides of buildings surrounding the MS. From Figure 4.1 we can express

$$\theta = \left|\tan^{-1}\frac{\Delta h}{x1} - \alpha\right|, \tag{4.4}$$

$$r = \sqrt{\left(\Delta h^2 + x^2\right)}, \text{ and}$$

$$x1 = x \;; \qquad if\ \Delta h\cot\alpha \le x$$

$$x1 = 0 \;; \qquad if\ \Delta h\cot\alpha \ge x'$$

where,

Δh : difference height between the building mean and the MS

x : horizontal distance between MS and the diffraction edge (shadow)

α : elevation angle of SPF with respect to MS

w : width between two buildings across the street.

For all deployment scenarios, x is given as the smaller between $w/2$ and Δh cot a or it can be expressed as

$$x = Min\left\{\frac{w}{2}, \Delta h \cot(\alpha)\right\}. \tag{4.5}$$

The second term $\Delta h \cot(\alpha)$ is essentially the width of the shadow cast by the surrounding buildings onto the street level (or the level of MS). When SPF elevation angle is close to 90^0, the shadow cast is narrow and in this case the rooftop diffraction loss is relatively small. For smaller elevation angles, which means the rooftop diffraction loss can be very high, the MS may receive stronger signals from multiple reflections from the sides of nearby buildings. The condition for multiple side-reflections is satisfied if

$$w \le \Delta h \cot(\alpha). \tag{4.6}$$

The number of reflections (N) between opposing building can be estimated by

$$N = \text{int}\left(\frac{\Delta h}{w \tan(\alpha)} - 1\right), \tag{4.7}$$

where int(X) means the largest integer that is smaller or equal to X. The excess propagation loss due to reflection can be computed if the incident angle and the real and imaginary parts of the dielectric constant of the building material are known. However, except for "grazing" reflection where the microwave essentially propagates parallel to the building surface, the excess loss can be taken to be 10 dB. Hence the multiple reflection loss is

$$L_{mrl} = -10N. \tag{4.8}$$

The rooftop diffraction loss is typically of the order of 10-40 dB, except for the case where there is a clear line of sight between the SPF and the MS. In case of multiple side

reflections from opposing buildings does not occur, i.e. the following condition is satisfied when

$$w > \Delta h \cot(\alpha). \tag{4.9}$$

It is assumed that at least two reflections must take place before the signal can reach the MS since one of them must be a reflection from the ground.

In typical urban high rises, both the street width and building height are of the order of 25 m. Accordingly, N does not exceed 2 until elevation angle is below 19^0. In urban or suburban low rises, with building height lower than 10 m and street width of around 35 m, elevation angle will be less than 5.5^0 before N becomes greater than 2. Hence in both cases, the excess loss should be of the order of 20 dB or less. In typical residential and rural areas, outdoor radio propagation is dominated by line of sight propagation and rooftop diffraction. Multiple reflections between two adjacent buildings are rarely effective because of the distances between buildings. The absence of multiple reflections means that the MS on the shady side of the radio transmission from SPF will have to rely on rooftop diffraction to provide coverage. The excess diffraction loss from rooftop scattering is typically between 20-40 dB, means more power is needed for communications between MS and SPF in the shady area.

4.2.5 Multiple Screen Diffraction Loss (L_{msd})

Multiple screen diffraction loss from the SPF is very different from multiple screen diffraction loss from the traditional radio tower BTS antennas pass rows of buildings, especially in the case where the elevation angle is not very small. According to the SPF propagation model in Figure 4.1, multiple screen diffraction loss takes the following general form

$$L_{msd} = 10\log_{10}\left(Q^2\right). \tag{4.10}$$

In the case of SPF, the factor Q depends on the elevation angle of the SP relative to the location of the MS. For most elevation angles, L_{msd} is essentially zero. At very small elevation angles, L_{msd} increase rapidly. At zero elevation angle, L_{msd} becomes arbitrarily

large so that practically only line of sight propagation is possible between the SPF and the MS. In the following, we examine the two cases of multiple screen diffraction separately.

A. Multiple screen diffraction loss for small elevation angles

This model is applicable in cases where the elevation angle α is less than 3^0 but greater than 0^0. From the consideration of diffraction fringes between two successive screens, it leads to the following dimensionless variable

$$\chi = \tan(\alpha)\sqrt{\frac{w\cos(\alpha)}{\lambda}}, \tag{4.11}$$

where w is again the average separation between rows of buildings. The condition that α must be small reduces χ to

$$\chi = \alpha\sqrt{\frac{w}{\lambda}}. \tag{4.12}$$

This should be compared with the combination of

$$\frac{\Delta h}{s}\sqrt{\frac{w}{\lambda}}, \tag{4.13}$$

when the BTS antenna is well above average rooftop level. In fact $\Delta h/s$ can be considered to be the tangent of the effective elevation angle between MS and BTS antenna. Therefore

$$Q = 2.35\left(\alpha\sqrt{\frac{w}{\lambda}}\right)^{0.9}. \tag{4.14}$$

The total transmission loss for this case then becomes

$$\begin{aligned} L_{tot} &= 10\log_{10}\left(\frac{\lambda}{4\pi d}\right)^2 + Min\left\{10\log_{10}\left[\frac{\lambda}{2\pi^2 r}\left(\frac{1}{2\pi\theta}\right)^2\right], 10*\mathrm{int}\left(\frac{\Delta h}{w\tan(\alpha)} - 1\right)\right\} \\ &\quad + 10\log_{10}\left(2.35^2\left(\alpha\sqrt{\frac{w}{\lambda}}\right)^{1.8}\right) \end{aligned} \tag{4.15}$$

B. Multiple screen diffraction loss for other elevation angles

When the elevation angle between SPF and MS is greater than about 3^0, which corresponds roughly to χ being greater than 1 (for typical average building separation w of about 50 m), the multiple screen diffraction loss becomes effectively zero. Then in this cases the total transmission loss becomes

$$L_{tot} = 10\log_{10}\left(\frac{\lambda}{4\pi d}\right)^2 + Min\left\{10\log_{10}\left[\frac{\lambda}{2\pi^2 r}\left(\frac{1}{2\pi\theta}\right)^2\right], 10\,\mathrm{int}\left(\frac{\Delta h}{w\tan(\alpha)} - 1\right)\right\}. \quad (4.16)$$

The SPF typically has its main coverage zones within a 200 km radius, which corresponds to an elevation angle of 6^0 or higher. Therefore multiple screen diffraction is not a significant loss factor for SPF in the main service area. Fringe coverage, especially those with elevation angle lower than 3^0, however, becomes more difficult for SPF, requiring, in most cases, strategically placed repeaters to enhance the link margin to sufficient degrees.

The above propagation model for the case of SPF communications is theoretically based on their geometrical feature with only two buildings is considered. In the following section, however, it aims at evaluating the propagation parameters of SPF communication based on ray tracing scheme with the building geometry model represents a typical urban environment, which is developed based on the result of experiment inside and nearby Tokyo city. We start with the basic concept of ray tracing method, in which the method is going to be used in the estimation.

4.3 Ray Tracing Model

An overview and the basic concept of the ray tracing techniques used for propagation prediction in SPF system are presented in this section. Wireless system planning and propagation prediction has been an active area of research for the past three decades. As mentioned in Section 4.2, earlier prediction model were based on empirical measurements. These models were not site-specific in nature and the predictions were primarily based on the distance between the transmitter and the receiver. These empirical models can only be used to predict the narrow band characteristics of the channel such as the mean signal strength. By the last decade, several researchers developed more complicated models, which were used to predict the signal strength more accurately. Some of these models did in fact use site-specific information while statistical in nature and predicted the signal only

within a certain margin error. These models were only useful in predicting the narrow band characteristics of the channel and did not provide any information regarding the wide band characteristics such as the power delay profile and the angle of arrival information. A more promising approach for predicting the propagation characteristics deterministically was introduced in the early 1990's, using a technique called ray tracing [62]-[63].

Ray tracing is a site-specific method of propagation modeling. Electromagnetic analysis employed by this method is based on geometrical optic (GO) and geometrical theory of diffraction (GTD) as an extension of GO to include diffraction. GTD was therefore extended to the uniform theory of diffraction (UTD) when the transition functions are included in the diffraction coefficients [65]. The ray tracing algorithm is a very high accuracy method in predicting propagation parameters. However, this method has been limited by the requirement of the detailed geometrical data in the region under study and the computation time.

Ray tracing at the beginning constitutes a technique to computer graphics where it is used to render the scenes to synthesize realistic images. Various researches conducted by independent researchers have been proved that the ray tracing technique could be used to predict the propagation characteristics of a wireless channel [51], [56], and [60]-[64]. Propagation prediction using ray tracing is theoretically applicable to a wide variety of environments ranging from dense urban surroundings to indoor maze like scenarios. Moreover, the ray tracing technique can be used as a tool to determine the optimal position of the BTS antenna, the optimal antenna radiation pattern and to find the coverage of wireless systems.

4.3.1 Basic Concept

In ray tracing scheme three basic propagation mechanisms such as reflection, diffraction and scaterring are employed. In the ray tracing algorithm individual ray will be traced from Tx to Rx through the above three mechanism. Here we will briefly review those mechanisms.

A. Reflection

Figure 4.2 shows the mechanism of reflection in a smooth surface. Reflection occurs when a radio wave propagates and incidents onto a smooth surface with large dimensions

compared to the signal wavelength (e.g., walls of buildings, road surface, etc.). A single path may experience multiple reflections. There are three basic reflection types such as specular reflection from smooth surfaces, reflections from rough surfaces and geometrical optic (GO) reflections. The normal handling of specular reflection with a single specular point is simplification of the more complete GO approach to reflection. The general reflection coefficient R is

$$R = R_s \, g \,, \tag{4.17}$$

where R_s is the smooth surface reflection coefficient and g is the surface roughness attenuation factor (a scalar quantity) [65]. For parallel and perpendicular polarization, respectively, the smooth surface reflection coefficients are

$$R_{\parallel} = \frac{\eta_2 \sin\theta_t - \eta_1 \sin\theta_i}{\eta_2 \sin\theta_t + \eta_1 \sin\theta_i}, \text{ (parallel polarization)} \tag{4.18}$$

$$R_{\perp} = \frac{\eta_2 \sin\theta_i - \eta_1 \sin\theta_t}{\eta_2 \sin\theta_t + \eta_1 \sin\theta_i}, \text{ (perpendicular polarization)} \tag{4.19}$$

where θ_1 is the angle of incidence relative to a plane tangent at the point of reflection and $\eta_{1,2}$ is the complex permittivity given by

$$\eta_{1,2} = \sqrt{\frac{j\,\omega\,\mu_{1,2}}{\sigma_{1,2} + j\,\omega\,\varepsilon_{1,2}}}\,, \tag{4.20}$$

where σ, ε and μ are the conductivity, permittivity and permeability of the air and the reflecting material and ω is the frequency of the incident radiation in radians.

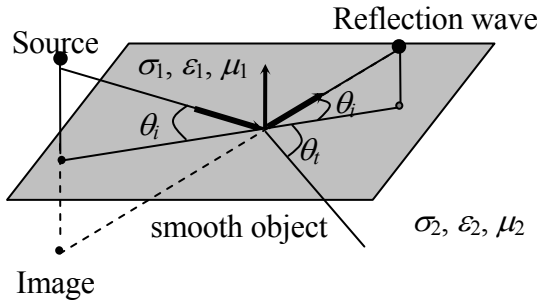

Figure 4.2 Reflection mechanism.

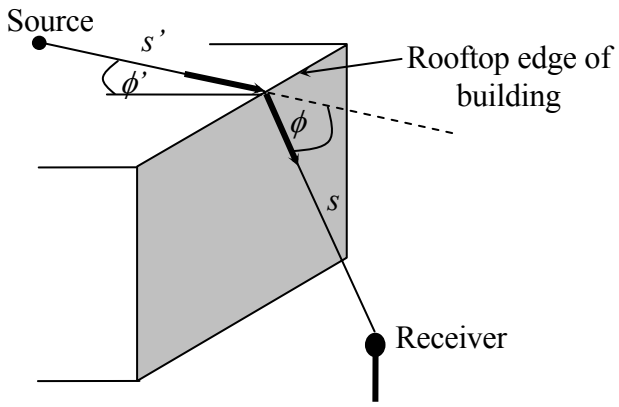

Figure 4.3 Diffraction mechanism.

B. Diffraction

Diffraction occurs when a large body obstructs the radio path between the transmitter and the receiver, causing secondary waves to be formed behind the obstructing body and continue to propagate towards the receiver. This mechanism is often termed as shadowing because it occurs when the propagation path between the transmitter and the receiver is partly shadowed (obstructed), for instance, by hilly terrains or by big structures.

The problem of computing the field scattered from the edge discontinuity has been addressed by a number of researchers, for example in [66] and [67]. Keller's geometric theory of diffraction (GTD) is an extended theory of geometric optics (GO) so that it could treat edge effects, although it still would predict incorrect fields at the singularities occurring at the shadow and reflection boundaries, as shown in Figure 4.3. Using the geometry and notation in the figure, the diffraction coefficients are

$$D_{\parallel}^{\perp} = \frac{-e^{-j(\pi/4)}}{2n\sqrt{2\pi k}\sin\gamma_0}\left[\begin{array}{l} \cot\left(\dfrac{\pi+(\phi-\phi')}{2n}\right)F\left(kLa^{+}(\phi-\phi')\right) \\ +\cot\left(\dfrac{\pi-(\phi-\phi')}{2n}\right)F\left(kLa^{-}(\phi-\phi')\right) \\ +R_{\parallel,0}^{\perp}\cot\left(\dfrac{\pi-(\phi+\phi')}{2n}\right)F\left(kLa^{-}(\phi+\phi')\right) \\ +R_{\parallel,0}^{\perp}\cot\left(\dfrac{\pi+(\phi+\phi')}{2n}\right)F\left(kLa^{+}(\phi+\phi')\right) \end{array}\right]. \qquad (4.21)$$

The Fresnel integral to correct for the singularities at the shadow boundaries is given by

$$F(X) = 2j\sqrt{X}\, e^{jx} \int_{\sqrt{X}}^{\infty} e^{-j\tau^2} d\tau\,, \tag{4.22}$$

where X represents the various possible arguments of $F(\cdot)$ in (2.30). The distance term L is

$$L = \frac{s\, s' \sin^2 \gamma_0}{s + s'}\,, \tag{4.23}$$

where s is the distance from diffracting edge to the field point, and s' is the distance from the edge to the illuminating source, as shown in Figure 4.3.

C. Scattering

Scattering occurs when a radio wave incidents onto a large rough surface, causing the reflected rays to spread out in various directions. Scattering can also take place due to the wave propagating through very dense foliage. We assume all objects have smooth surface in the ray tracing algorithm so that there is always a specular reflection and ignore the scattering mechanism for simplicity of evaluation.

4.3.2 Ray Tracing Techniques

Ray tracing techniques attempts to find ray paths between transmitter and receiver. Power incident at the receiver due to these different ray paths can be calculated using free space model. Power of different ray paths when mapped according to the time of arrival of the rays would provide us with the power delay profile of the wireless channel. Two fundamentally different methods are commonly used for finding the ray paths. They are the method of images and the pin-cushion method.

A. Method of Images

In the method of images, a similar concept to image theory is used in electromagnetics evaluation. This method starts by constructing an image or a projection of the transmitter in all the building surfaces visible to the transmitter. Then the secondary images of the different primary images are constructed on all the surfaces visible to the primary images. This image mapping of the transmitter is carried on until a chosen maximum numbers of reflections are accounted for. A strength line of sight is drawn from all the images to the

receiver. Finally the valid ray paths are selected from the transmitter to the receiver are selected by drawing a straight line from all the images of the transmitter to the receiver. The path is termed as valid if the straight line from the image to the receiver passes through the actual building surface and not just the image plane.

Figure 4.4 shows a simple application of the method of images. In the figure the ray from Tx image 2 to Rx1 is considered valid since it passes through the original building surface, while the ray from Tx image 2 to Rx2 is not valid since it does not pass through the building surface. The image method is successfully used in many wireless prediction tools, which uses two-dimensional ray tracing [57] and [67]-[69]. In urban scenario with 2D building database, this method assumes that the transmitters and the receivers lie well below the lowest rooftops and the sides of the buildings are flat from top to bottom. The method of images has also been used in indoor scenarios with the reflections from the ceilings and the floors taken into account separately. The number of images generated using this method grows exponentially with the number of surfaces. Hence the complexity of a ray tracer based on the method of images does not lend itself to complicated 3D urban scenarios with thousands of surfaces [70]-[71].

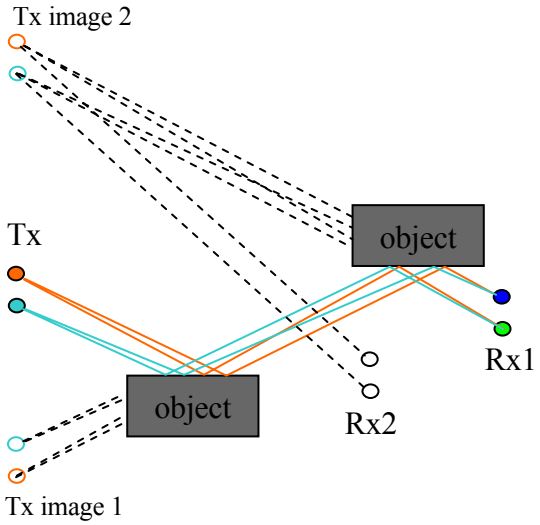

Figure 4.4 Ray tracing using method of image.

B. Pin-Cushion Method

The pin-cushion method launches numerous rays from the transmitter into the environment. Each ray is represented as a straight line. The trajectory of individual ray is followed until it hits a surface. The present ray is then spawned into two. One representing the reflected wave and the other represents the transmitted wave. The direction of the reflected and the transmitted wave is calculated using Snell's law. Each time the ray hits a surface the power of the reflected ray and the transmitted ray is calculated by reducing the reflected power loss and the transmitter power loss from the original power of the ray. The reflected and the transmitted rays are the traced until it hits a pre-determined number of surfaces or until the power reduces below a pre-determined level. There are two types of pin-cushion method. Those are ray launching method and receiver modeling method.

- *Ray Launching Method* is assumed that the number of rays is launched from the transmitter uniformly. The launched point must be uniformly distributed so that all the regions are equally illuminated using the ray tracing technique. Also, to keep the ray manipulations a minimum, the wave front denoted by the ray should have identical shape and size. The wave front of each ray can be interpreted as the area of cross section between a ray and its neighbors. A straightforward method to launch the rays would be to launch the rays from a uniform sphere, by dividing the azimuthal and the elevation angles equally. However, such a division of the spherical surface would have a greater density of the vertices towards the poles and the lesser density of the vertices towards the equator. This would mean that there would be more rays emanating from the poles than from the equator. The better technique for launching the rays into 3D environment was proposed by [51].

- *Receiver Modeling* performs various ray segments of all rays to be checked to see whether they illuminate the receiver or not. Ray that intersect the receiver are analyzed and power delay profile estimate can be developed by mapping the power of various rays with respect to the arrival time information of the different rays. The set of rays originated from the same source and reflected from the same set of surfaces can be considered to the part of the same wave front. In this method one approach is to model the receiver as a sphere with a finite radius, as determined by the unfolded length of the ray. The receiver is considered to be illuminated by the ray if the ray hits the reception sphere. Such an approach would work perfectly for a 2D

case. For example, if the rays were transmitted at equal incremental angles δ, then the neighboring rays would be $S\delta$ distance apart, if the ray has traveled a total distance S from transmitter. So the receiver can be modeled as having a circular diameter of $S\delta$. Thus ensures that only one ray from a wave front intersects with the reception sphere.

Intersection between ray and objects is an important thing in the ray tracing technique in order to determine the point of intersection on the plane and the direction of the next reflected or transmitted wave. There are three types of intersection. Those are ray-plan intersection, ray-sphere intersection and ray-triangle intersection. In this work, however, only ray-plan intersection is considered to model the intersection between the ray and the building and street in the model. In ray-plane intersection a plane is defined by equation or vector. For example let that there is a plan with the vector of $[A\,B\,C\,D]$or with the equation as

$$Ax + By + Cz + D = 0, \tag{4.24}$$

where A, B and C define normal to the plane. If A, B and C define a unit normal then the distance from the origin [0 0 0] to the plane is D. Now let we define the ray by the vector as follow

$$\vec{R}_0 = [X_0\, Y_0\, Z_0] \text{ and } \vec{R}_d = [X_d\, Y_d\, Z_d], \tag{4.25}$$

then

$$\vec{R}(t) = \vec{R}0 + t * \vec{R}d, \qquad t > 0. \tag{4.26}$$

To determine if there is an intersection with the plane, substitute for $\vec{R}(t)$ into the plane equation and get

$$A(X_0 + t * X_d) + B(Y_0 + t * Y_d) + C(Z_0 + t * Z_d) + D = 0, \tag{4.27}$$

which yields

$$\begin{aligned} t &= -(AX_0 + BY_0 + CZ_0 + D)/(AX_d + BY_d + CZ_d) \\ &= -(\vec{P}_n \bullet \vec{R}_0 + D)/(\vec{P}_n \bullet \vec{R}_d) \end{aligned}. \tag{4.28}$$

In order to find that there intersection between ray and the plan, first we compute $\vec{P}_n \bullet \vec{R}_n = V_d$. If $V_d = 0$, it means incident angle is 90^0 then the ray is parallel to the plane and there is no intersection (if ray in the plane then we ignore it). However, if $V_d > 0$ then the normal of the plane is pointing away from the ray. If we use one-sided planar objects then the ray tracing could stop when the condition is fulfilled, or continue if double-sided planar.

Now let we compute the second dot product $V_0 = -(\vec{P}_n \bullet \vec{R}_0 + D)$ and compute $t = V_o / V_d$. If t < 0 then the ray intersects plane behind origin, i.e. there is no intersection of interest. However if the condition opposite means t > 0 then compute the intersection point as

$$\vec{P}_i = [X_i \; Y_i \; Z_i] = [X_0 + t * X_d \;\; Y_0 + t * Y_d \;\; Z_0 + t * Z_d]. \tag{4.29}$$

Up to this point we can determine the point of intersection and the direction of the transmitted ray after it intersects with the plane object.

4.4 Stratospheric Platform Ray Tracing Model

In this chapter stratospheric platform ray tracing model is developed. The building geometry model over which the ray tracing algorithm will be applied is obtained from experiment. The purpose of the experiment is to define the channel situation and to observe building height distribution in urban environment. The result is then used as an approach model to develop a building geometry model. This model is used to characterize propagation path loss and channel characteristics for mobile communication in which the SPF is employed as a new wireless infrastructure. Two channel situations can be defined for each specific area. First is visible situation and the other is shadowing situation. The former is the situation when direct LOS path between SPF and mobile user on the ground can be established, while the latter is the condition where there is no LOS situation can be developed. For both situations we need to examine propagation parameters such as path loss and multipath characteristic of the SPF channel. The propagation parameters can then be used in order to simulate or estimate the channel performance of the SPF communication link. In this following sub section, experimental configuration and its result are presented.

4.4.1 Experimental Configuration

Experiment was carried out in four areas inside and nearby Tokyo Prefecture. Those areas inside Tokyo Prefecture are Shinjuku, Shibuya and Asakusa. The area nearby Tokyo Prefecture is Kiryu in Gunma Prefecture. Areas inside Tokyo are featured with narrow roads and very tall buildings so it is able to represent an urban high rises environment. While Kiryu in Gunma represents an area of urban low rises environment with moderate height of building.

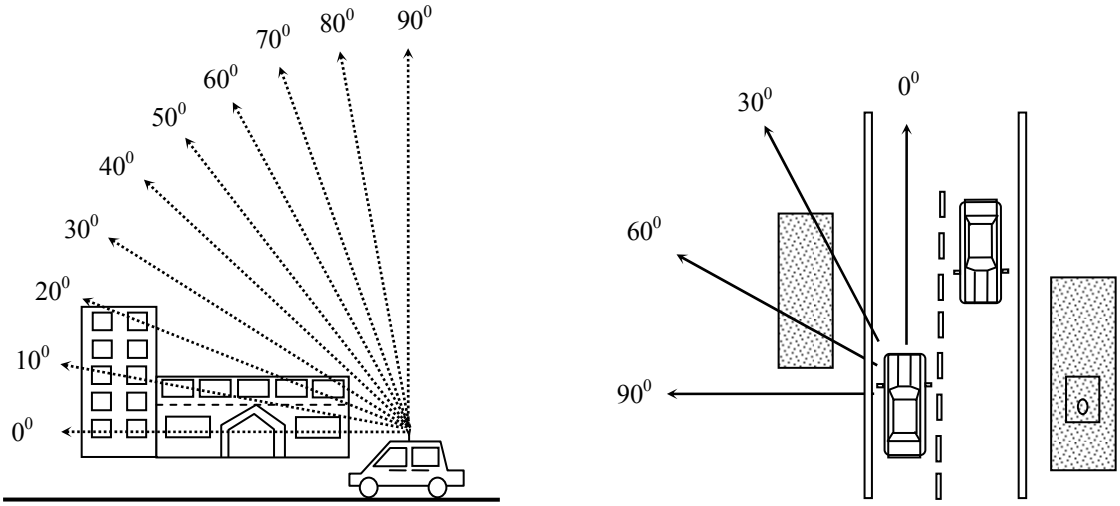

(a) (b)

Figure 4.5 Experiment configuration: (a) Side view; (b) Top view.

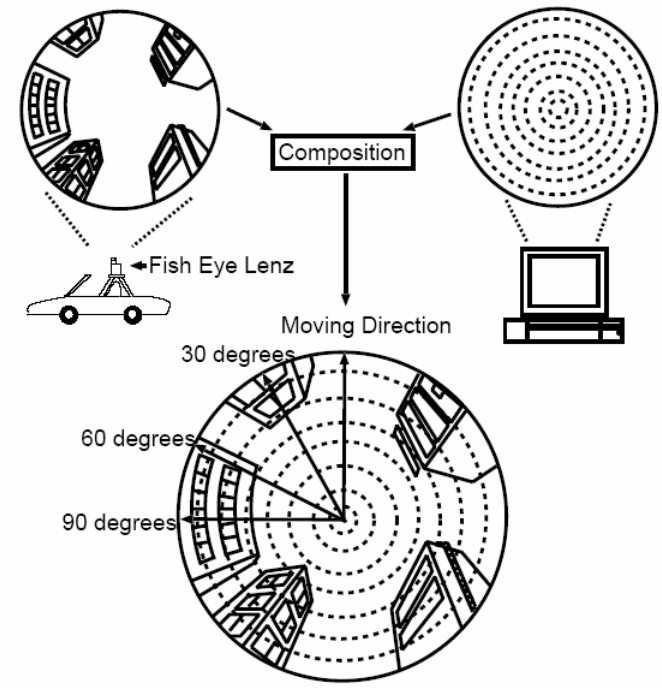

Figure 4.6 Fish eye lens and picture composition.

A car, computer and video camera featured with fish eye lens were used in the experiment. The car, which is equipped with the video camera on the top, moved in various directions in each observed area in the city for about 5 km. Figure 4.5 describes our experiment configuration from a side and top view, respectively.

The video camera was aimed at 0^0, 30^0, 60^0 and 90^0 to the moving direction. The principle of this experiment using fish eye lens can be seen in Figure 4.6. Video camera took the pictures of surrounding buildings and recorded them. In the computer the data for each elevation angle within 360^0 azimuth is assigned with the marker. Then the composition of both recorded picture from video camera and the marker data from computer is performed. The result indicates visible channel probability and shadowing channel probability. As an example, Figure 4.7 shows the situation of how to calculate probability of channel situation. Each visible situation is derived with counting markers, which indicates continuous horizontal visible situation in each elevation angle. And for each shadowing situation is also derived with counting markers, which indicates continuous horizontal shadowing situation in each elevation angle.

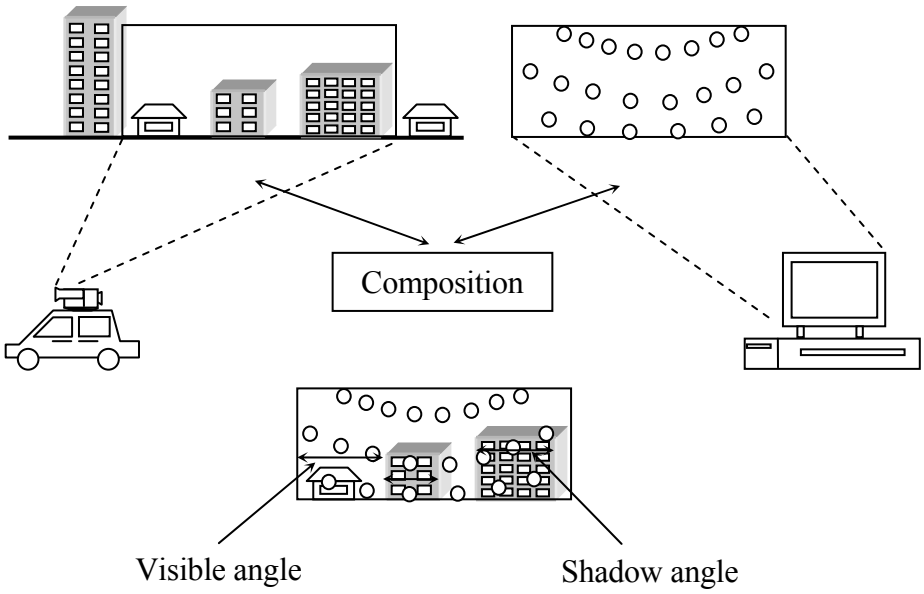

Figure 4.7 Visibility and shadow probability experiment.

4.4.2 Visibility and Building Height Distribution

Now we are able to present in part of the experimental results in terms of visibility and building height distribution. The detailed results of experiment can be found in [72]. Visibility is defined as the probability of the channel of having LOS situation to the total situation (both LOS and NLOS situation) at each elevation within 360^0 azimuth angle. From the field test, visibility graph can be described as a function of elevation angle in a step of 10^0 intervals. In Figures 4.8, the markers (triangles, diamonds, squares and circles) demonstrate the result of experiments for the visibility of surveyed area. The lines (solid, dashed, dotted, and dashed-dot) illustrate an approximation of the visibility by equation. This equation is an empirical approach for visibility, $p_v(\alpha,\theta)$, based on the measurement result as a function of elevation (α) and azimuth angle (θ) [72] which is expressed as

$$p_v(\alpha,\theta) = \begin{cases} (\sin\alpha)^{0.01} & ;\ \theta = 0^0 \\ (\sin\alpha)^{\sin\theta} & ;\ \theta = 30^0, 60^0, 90^0 \end{cases}. \tag{4.30}$$

In this case, θ=0^0 is in the positive y-axis direction and θ=90^0 is in the negative x-axis direction explained in Figures 4.10. We found that the visibility is a decreasing function against azimuth angle. In the figures, Rayleigh distributed model is a good approach for azimuth angle approaching 90^0 in urban high rises environment such as areas inside Tokyo Prefecture. The visibility can theoretically be expressed in terms of the probability density function of the building height $p_b(h_b)$ as

$$P_v(\alpha,\theta) = P_v(h_b > h_T) = \int_{h_T}^{\infty} p_b(h_b)\, dh_b\ , \tag{4.31}$$

where h_b is the building height and h_T is the threshold height which if its value is exceeded then shadowing is occur. If $p_b(h_b)$ is Rayleigh distributed, the visibility can be expressed by

$$P_v(\alpha,\theta) = \int_{h_T}^{\infty} \frac{h_b}{\sigma_b^2}\left(-\frac{h_b^2}{2\sigma_b^2}\right) dh_b = \exp\left(-\frac{h_T^2}{2\sigma_b^2}\right), \tag{4.32}$$

where σ_b is the building height standard deviation. In Figure 4.8 Rayleigh distribution is used with parameters σ_b = 15 m, w = 35 m, d_m = w/2, h_m = 1.5 m and θ = 90^0. We can see

that the visibility can be approached by Rayleigh distribution if the surveyed area is a high rises urban environment, i.e. inside Tokyo Prefecture and azimuth angle is nearly 90^0.

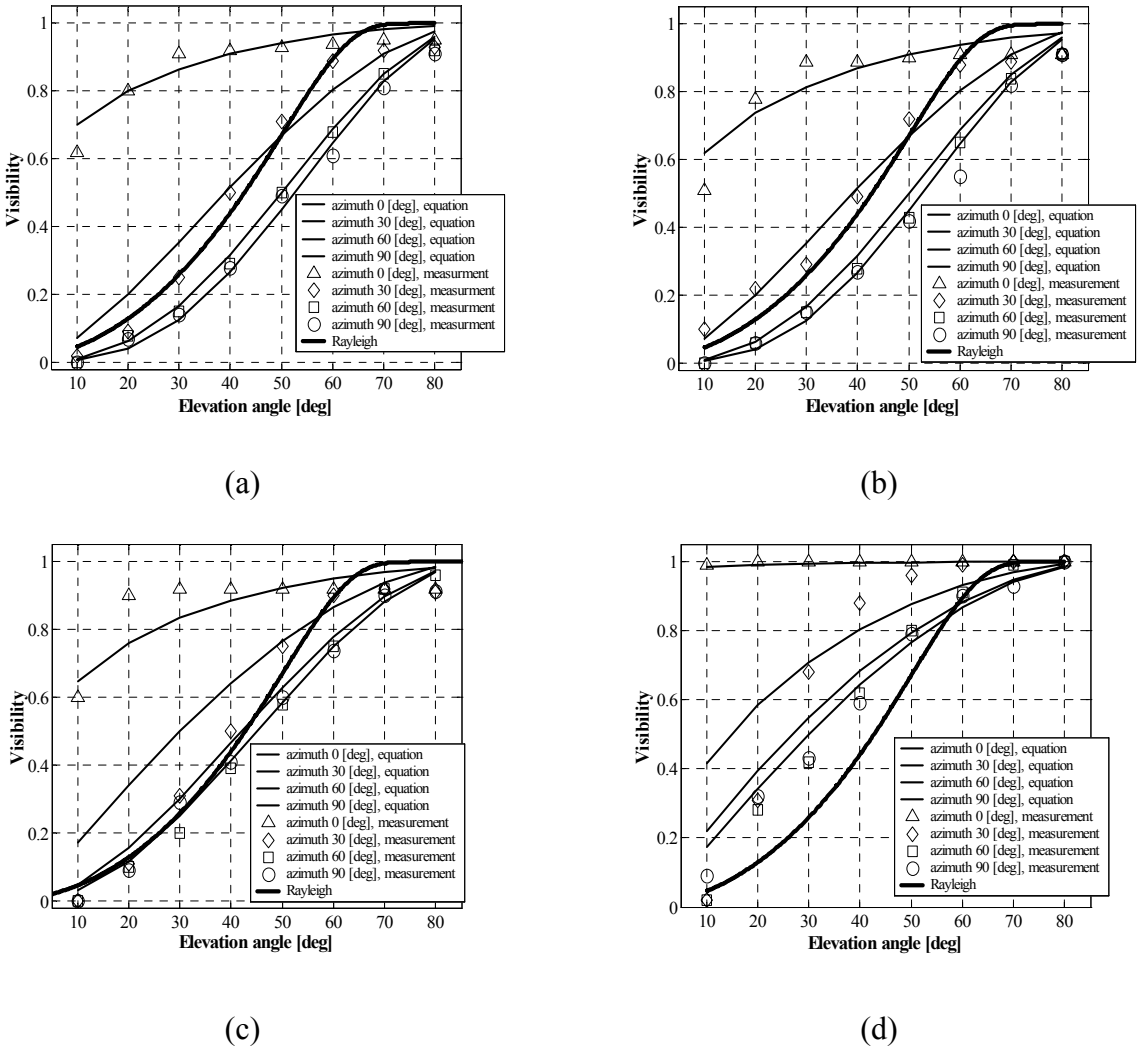

Figure 4.8 Visibility of surveyed areas: (a) Shinjuku; (b) Shibuya; (c) Asakusa; (d) Kiryu.

Another important result from the observed areas is that the cumulative distribution of the building height, which is demonstrated in Figure 4.9. From the figure, we can see that Shinjuku area represents as an area in which the probability of average building height is the highest compared with the other areas. From the survey, we also observed both an average of building height as well as building density [pieces/km^2] and the result is depicted in Table 4.1. With respect to the experimental result, Shinjuku area has the highest average building height of 25.5 m. It is followed with Shibuya of around 25 m, Asakusa of around 22.1 m and Kiryu of around less than 19 m. The building density has

been found in Asakusa is the highest density and followed by that in Shinjuku, Shibuya and Kiryu, respectively.

Table 4.1

Average building height and density.

Area	Average building height [m]	Building density [pieces/km^2]
Shinjuku	25.5	290
Shibuya	25.0	200
Asakusa	22.1	580
Kiryu	19.1	7

4.4.3 Proposed Building Geometry Model

We develop the building geometry model for SPF link outdoor propagation evaluation, in which the model is based on the result of site survey presented above. The building geometry model presented here has been selected as an appropriate model to represent the characteristic of surveyed urban environment in the sense of the street width, average building height and the building density.

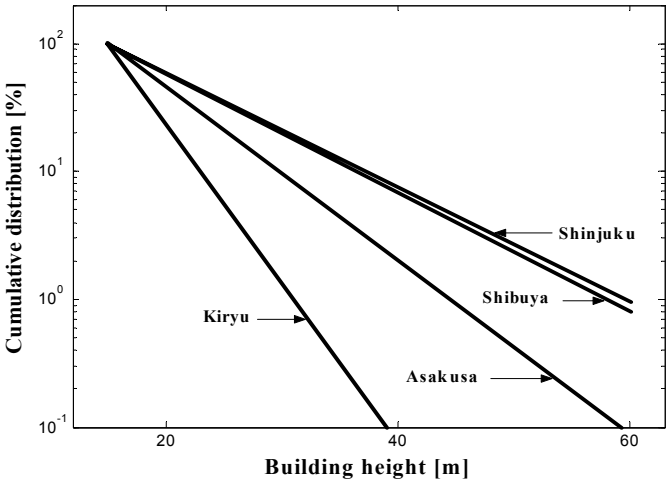

Figure 4.9 Surveyed result of CDF building height.

We develop 8 buildings block model as described in Figures 4.10 (a) and (b) for the top view and the side view, respectively. The block model to be evaluated consists of the buildings with their height is between the average building height of Kiryu and Asakusa areas. The building density in the model, however, closes to Shibuya area. Therefore, we are able to define the building geometry model to be evaluated here as a representation of urban low rise environment.

A MS as a receiver is located in the position at point D amid the street surrounded by the building. In the model, buildings are assumed to have the same height (h_b = 20 m) and the same width (w_b = 25 m), but vary in length, for example we consider the building length of 55 m, 70 m and 85 m as shown in Figure 4.10. All street width (w_s) of 35 m is assumed to be equal in the model under consideration (i.e. slightly wider than the real average street width in the surveyed area). The MS is assumed to have 1.5 m in height and is located at the center of the street ($d_m = w_s/2$). Frequency of 2 GHz has been suggested for the SPF IMT-2000 services [8] and hence we use this frequency in ray tracing simulation. The well-known ray tracing algorithm is then applied to the developed building geometry model with the rays are launched from the SPF as a transmitter and are received by the MS as a receiver.

4.4.4 Virtual Ray Tracing Model

We propose virtual ray tracing model that employs a number of virtual transmitters located above the area under test [73]. The virtual transmitters are introduced in order to overcome the difficulty of applying the ray launching methods for the large separation such as from the SPF to the MS. In our work, however, we include diffraction mechanism effects from building rooftops, which this mechanism has been neglected in [73]. The virtual ray tracing model is depicted in Figure 4.11.

It is known that the wave in the far field region, such as transmitted from the SPF at 20 km altitude to the MS on the ground, will have virtually parallel wave fronts. Therefore, the method used here is to enhance the ray model places an array of virtual transmitters around the building geometry model under test as shown in Figure 4.11. Each virtual transmitter is now used to launch a single ray. Using knowledge of the location of the SPF and the virtual transmitters, a precise ray launch angle for each virtual transmitter can be calculated.

This angle is used to launch a single ray that emulates the path that would have been traced from the SPF. By using an array of virtual transmitters, the software can simulate a number of uniformly launched rays from the SPF. To overcome the path length problem (i.e. the shorter distance from the virtual transmitter), modifications are made in both the ray tracing and field reconstruction modules to add the extra path length from the SPF paths. Using this technique, a number of rays can be launched from the array of virtual transmitters to imitate the set of rays that would have been launched from the SPF. An accurate simulation can be achieved for any point in the test environment by restricting each virtual transmitter to a single ray launch, calculating the launch angle using knowledge of the SPF position and modifying the path length to reflect the distance to the SPF.

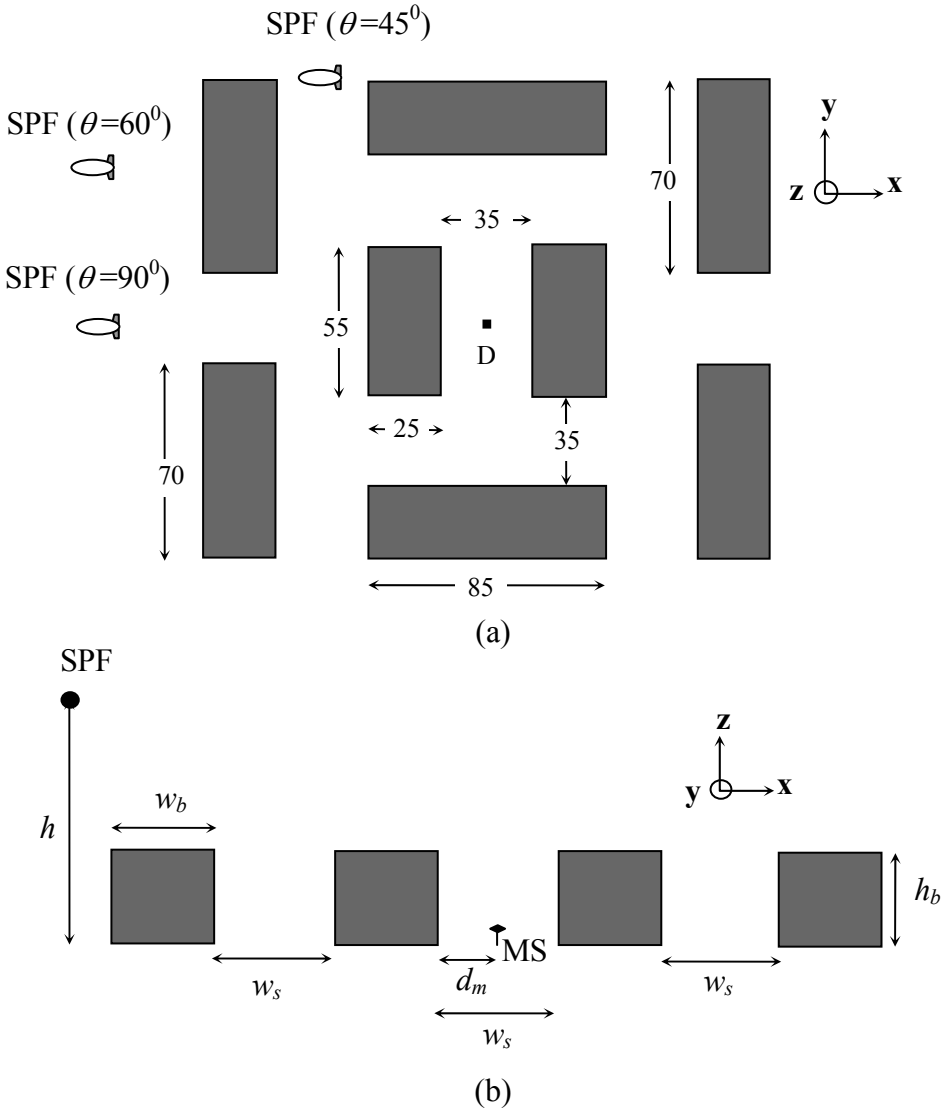

Figure 4.10 The model under test: (a) Top view; (b) Side view.

The generation of virtual transmitters was repeated when the elevation angle is changed. We employ nine categories of ray to be included in our simulation. The variation of SPF elevation angle and the ray path are illustrated in Figure 4.12. These ray categories include

- Line of sight
- Single reflection from building
- Single reflection from street
- Double reflection from building to street
- Double reflection from building to building
- Diffraction from rooftop of building
- Diffraction from rooftop and single reflection from building
- Diffraction from rooftop and single reflection from street
- Diffraction from rooftop and double reflection from building to street.

Rays outside the above categories are assumed to leave the target and terminated from the simulation environment. Since all surfaces in real propagation environments are finite, also edges and corners have to be considered. When a radio wave encounters an edge of a large object, secondary waves to be formed behind the obstructing object and continue to propagate towards the receiver. This mechanism is called diffraction and is found to be important for the case of low elevation angle.

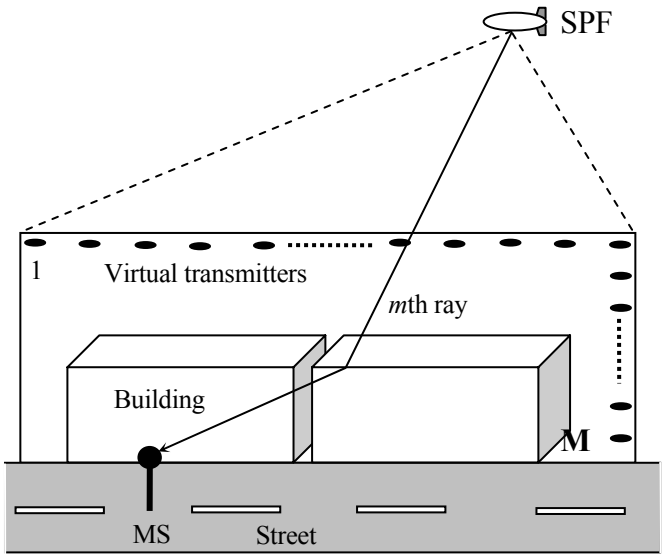

Figure 4.11 Concept of virtual transmitters.

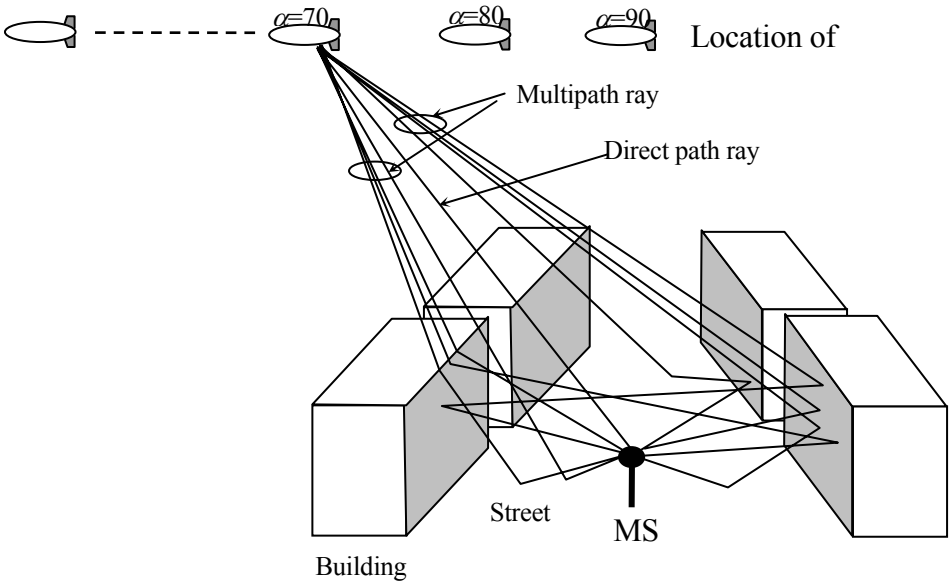

Figure 4.12 Typical multipath propagation in a SPF channel.

Electrical parameters presented in Table 4.2 that involve throughout the prediction in this work are used in the ray tracing simulation. The buildings are assumed made of concrete, in which ε_r and σ are their dielectric constant and conductivity, respectively. In the prediction, two situations were observed, those are LOS and NLOS (the situation that the direct ray is obstructed by the building nearby the MS position). As a result, we are able to obtain the power impinging the MS separately from the direct LOS power, multipath scattered power (total power from rays except direct LOS power) and their total complex vector summation.

Table 4.2

Electrical parameters of the building and the street in the ray tracing simulation [65].

	ε_r	$\sigma[\Omega^{-1}m^{-1}]$
Building	3	0.005
Street	15	7

4.4.5 Analytical Model

To compute loss power when the rays intersect with an object we use ray tracing algorithm that involve the geometrical optics (GO) and the uniform theory of diffraction (UTD).

UTD is a method of an extension of GO to include diffraction. Both of transmitting and receiving antennas are assumed to be an isotropic antenna with a 0 dBi gain. Therefore, an electric field of ray that arrives at the receiving antenna is calculated using the following formulas for direct ray (E_{LOS}), reflected ray (E_R), and diffracted ray (E_D), respectively as

$$E_{LOS} = E_0 \frac{e^{-jkd_0}}{d_0}, \tag{4.33}$$

$$E_R = E_0 \cdot \overline{R} \frac{e^{-jk(s_1+s_2)}}{s_1+s_2}, \tag{4.34}$$

$$E_D = \frac{E_0}{s'} \cdot \overline{D} \sqrt{\frac{s_3}{s(s+s_3)}}\, e^{-jk(s+s_3)}, \tag{4.35}$$

$k=\lambda/2\pi$ denotes the propagation constant, E_0 represents an emitted electric field from transmitter, d_0 corresponds to the direct path length, s_1 indicates the distance from the source to the reflection point, s_2 is the distance from reflection point to the receiver, s_3 represents the path length from the source to the diffraction point, and s is the path length from diffraction point to the receiver. $\overline{R}$ is a representation of a Fresnel dyadic reflection coefficient and $\overline{D}$ denotes the dyadic finite conductivity edge diffraction coefficient. These two coefficients follow the general formulation presented on [65]. Finally, respective rays for each ray category, which there are n = 9 ray categories, were added at the MS and expressed as

$$E_i = \sum_{j=1}^{n} E_j . \tag{4.36}$$

E_j is the received electric field of the jth ray for ith category.

Although the precision can be improved by additional ray category such as double diffraction in combination with multiple reflections from wall and street, however we have to compensate by computational complexity and therefore it leads to huge computation and hence time consuming. Generally, ray after diffracted by the building edge and then undergo for more than two reflections will be very weak in power. Therefore, there is no significant ray's power is expected for those who had experienced of single diffraction and

more than two reflections. In this work, the total electric field contribution consists of vector summation of 9 ray categories and can be expressed by

$$E_{Tot} = \sum_{i=1}^{9} E_i \,. \tag{4.37}$$

Finally, the total propagation loss (L) is expressed as

$$L = 20\log\left(\frac{\lambda}{4\pi}\frac{|E_{Tot}|}{|E_0|}\right). \tag{4.38}$$

From (4.38), now we are able to demonstrate the result of propagation loss estimated for the above-mentioned model as a function of elevation and azimuth angle as presented in the following section.

4.5 Physical-Statistical Approach

When there is no measurement result to predict the propagation loss in urban environment for the case of SPF communication, one can be used is a physical-statistical model that is proposed in [74] for comparison with the ray tracing result. The model allows a prediction to be made for a system operated in areas where direct measurements are unavailable. We apply the method to the same building geometry model as described in Figure 4.10 by adjusting the scale, which appropriates to the SPF geometry.

A physical-statistical model is originally proposed to predict propagation parameters of land-mobile satellite in built-up areas by using geometrical considerations and simple diffraction theory. By this model, first we are able to predict the probability with which a LOS path exists between the MS and the SPF (P_s). The second we can estimate the attenuation when a shadowed state (NLOS) is encountered related to physical parameters. In this model *Ps* and attenuation are related to physical parameters such as street widths and building height distributions. Therefore, by using this model, prediction of propagation parameters is achieved with very low computational complexity and simple physical data. The same building geometry model as shown in Figure 4.10 is the model of the situation to be analyzed using a physical-statistical model. The simplified situation of a physical-statistical model, however, is described in Figure 4.13 for easy understanding.

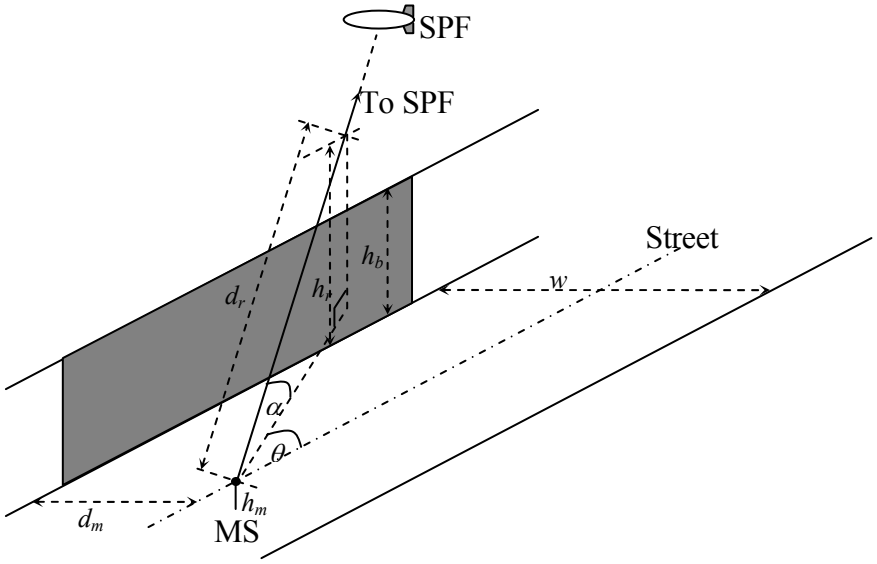

Figure 4.13 A concept of physical-statistical model.

α : elevation angle of the SPF from the MS

θ : azimuth angle of the SPF from the MS relative to the axis of the street

w : street width

d_m : perpendicular distance of the MS from the building face

h_m : the height of the phase centre of the MS antenna above local ground level

h_b : the height of the building immediately below the direct ray relative to ground level

h_r : the height of the direct ray above the building face relative to local ground level

d_r : the distance along the direct ray from the MS to the point on the ray immediately above the building.

The parameters h_r and d_r is expressed by simple trigonometry relationship as follows

$$h_r = \begin{cases} h_m + \dfrac{d_m \tan\alpha}{\sin\theta} & ; \quad for\ 0 < \theta \le \pi \\ h_m + \dfrac{(w - d_m)\tan\alpha}{\sin\theta} & ; \quad for\ -\pi < \theta \le 0 \end{cases}, \tag{4.39}$$

$$d_r = \begin{cases} \dfrac{d_m}{\sin\theta\cos\alpha} & ; \quad for\ 0 < \theta \le \pi \\ \dfrac{(w - d_m)}{\sin\theta\cos\alpha} & ; \quad for\ -\pi < \theta \le 0 \end{cases}, \tag{4.40}$$

The signal, however, may also reach the MS from a single reflection from the building face on the opposite side of the street. For that reason, the equivalent parameters are expressed by

$$h_{rr} = \begin{cases} h_m + \dfrac{(2w - d_m)\tan\alpha}{\sin\theta} & ; \quad for\ 0 < \theta \le \pi \\ h_m + \dfrac{(w + d_m)\tan\alpha}{\sin\theta} & ; \quad for\ -\pi < \theta \le 0 \end{cases}, \tag{4.41}$$

$$d_r = \begin{cases} \dfrac{(2w - d_m)}{\sin\theta\cos\alpha} & ; \quad for\ 0 < \theta \le \pi \\ \dfrac{(w + d_m)}{\sin\theta\cos\alpha} & ; \quad for\ -\pi < \theta \le 0 \end{cases}. \tag{4.42}$$

By this model an additional propagation loss incurred by shadowing attenuation is calculated based on single-knife edge diffraction theory expressed by

$$L_s = P(v_d) + \rho^2 P(v_r), \tag{4.43}$$

where ρ is the loss because of reflection, including effects due to polarization, surface roughness and the material reflection coefficient. The diffraction parameters for the direct and reflected rays, v_d and v_r respectively are given by

$$v_d = (h_b - h_r)\sqrt{\frac{2}{\lambda d_r}}, \tag{4.44}$$

$$v_r = (h_b - h_r)\sqrt{\frac{2}{\lambda d_{rr}}}. \tag{4.45}$$

The diffracted power, $P(v)$, can be expressed in terms of the Fresnel cosine and sine integral $C(v)$ and $S(v)$ as

$$P(v) = \frac{1}{2}\left(\frac{1}{2} + C^2(v) - C(v) + S^2(v) - S(v)\right). \tag{4.46}$$

We simulate a shadowing attenuation using this model as a function of building height with various elevation angles as depicted in Figure 4.14. We can see that the higher the building height the bigger the shadowing attenuation. When elevation angle is 10^0 the

shadowing attenuation appear very high even the building height is only 6 meter the attenuation is 15 dB. In the following section we therefore compare the propagation loss for SPF link obtained by using ray tracing simulation and a physical-statistical approach.

4.6 Predicted Propagation Parameters

4.6.1 Propagation Path Loss

The ray-tracing simulation result is presented as a total of propagation loss obtained from the calculation of direct LOS ray and multipath scattered ray of received electric field by vector summation using (4.36)-(4.38) [75]-[76]. Figures 4.15 (a), (b) and (c) show the numerical result of propagation path loss prediction in different azimuth angles, those are 90^0, 60^0, and 45^0, respectively. In LOS region, path loss curve is obtained from direct and single (ground or wall) reflected ray. However, in NLOS region the rays come from reflected, rooftop diffracted and combination of diffracted-reflected rays. Note there is no direct ray in a NLOS region. Azimuth of 90^0 demonstrates to be the worst scenario of propagation path loss due to building blockage. When MS in the shadow region associated to some particular elevation angles, the diffraction from rooftop is a major contributor to the received electric field. As a result, the propagation path loss dramatically increases to the value of the order of 20 dB or more compared with the LOS region.

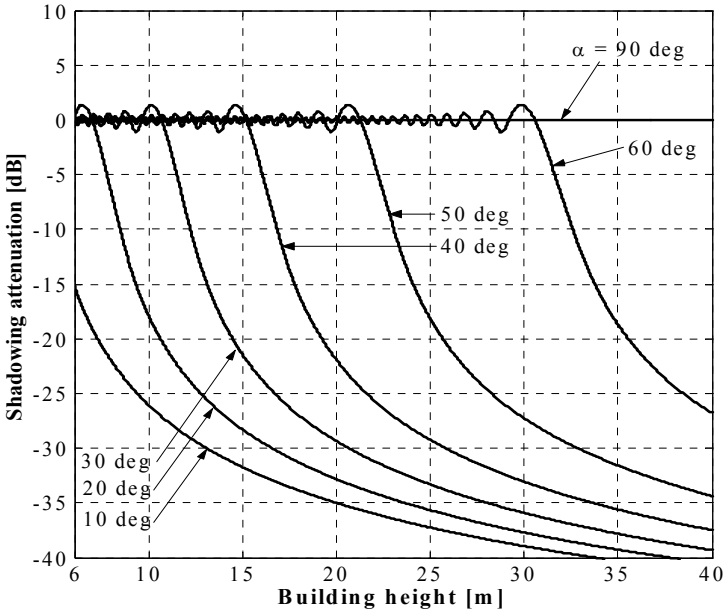

Figure 4.14 Shadowing attenuation vs. building height in several elevation angles.

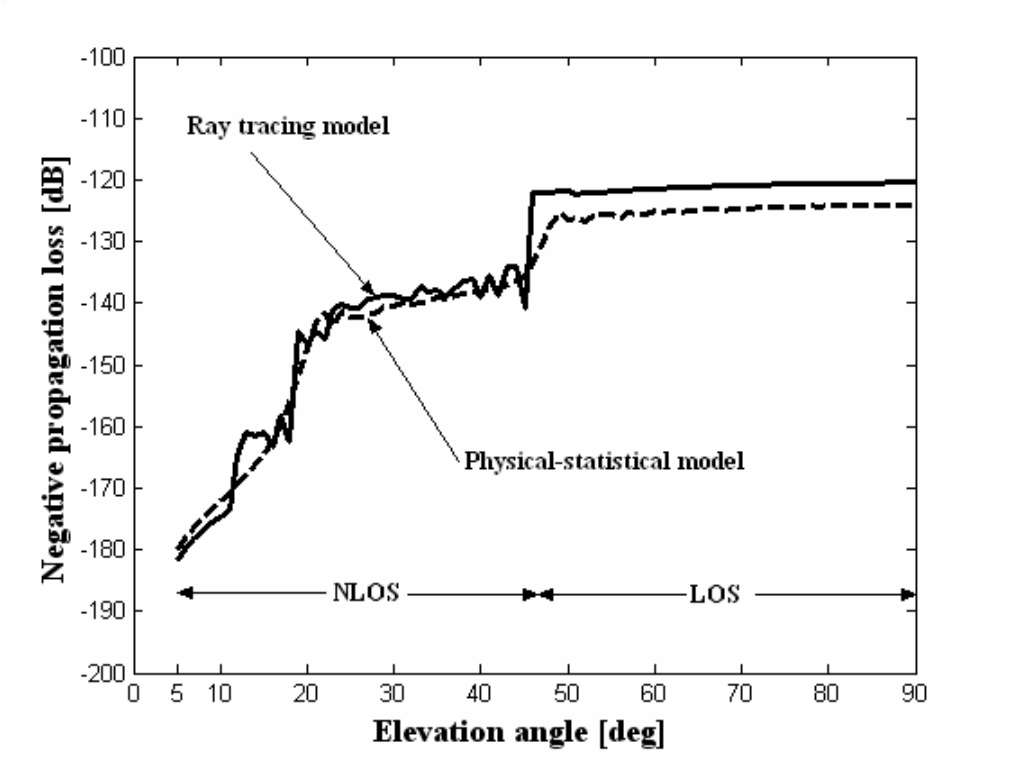
Ray tracing model
Physical-statistical model
NLOS
LOS
Negative propagation loss [dB]
Elevation angle [deg]
-100
-110
-120
-130
-140
-150
-160
-170
-180
-190
-200
0
5
10
20
30
40
50
60
70
80
90

(a)

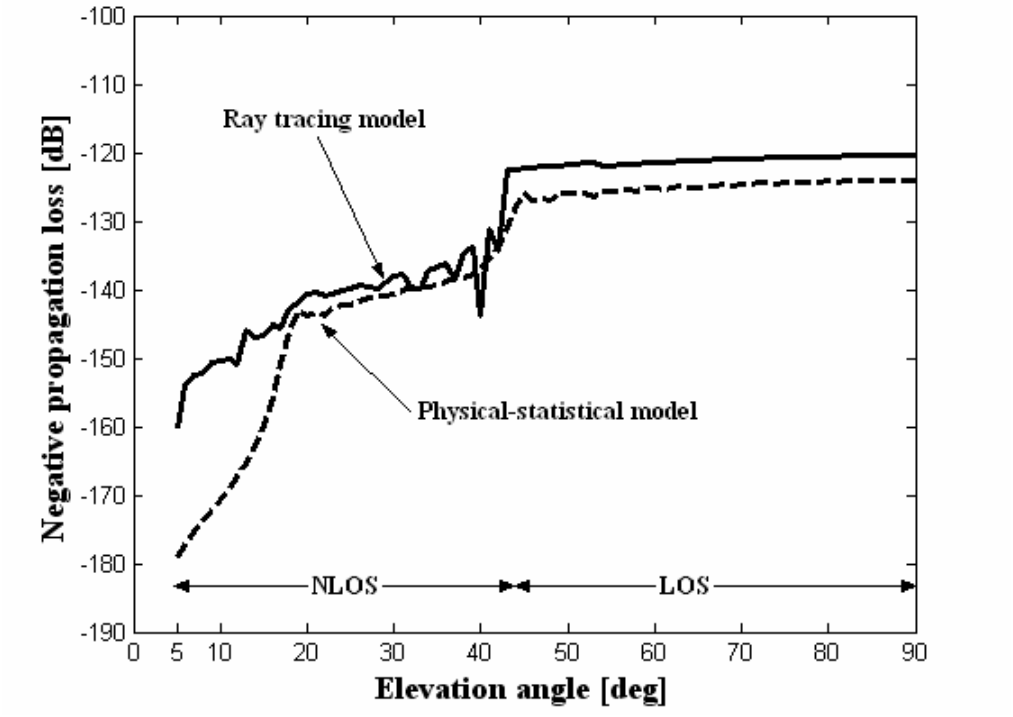
Ray tracing model
Physical-statistical model
NLOS
LOS
Negative propagation loss [dB]
Elevation angle [deg]
-100
-110
-120
-130
-140
-150
-160
-170
-180
-190
0
5
10
20
30
40
50
60
70
80
90

(b)

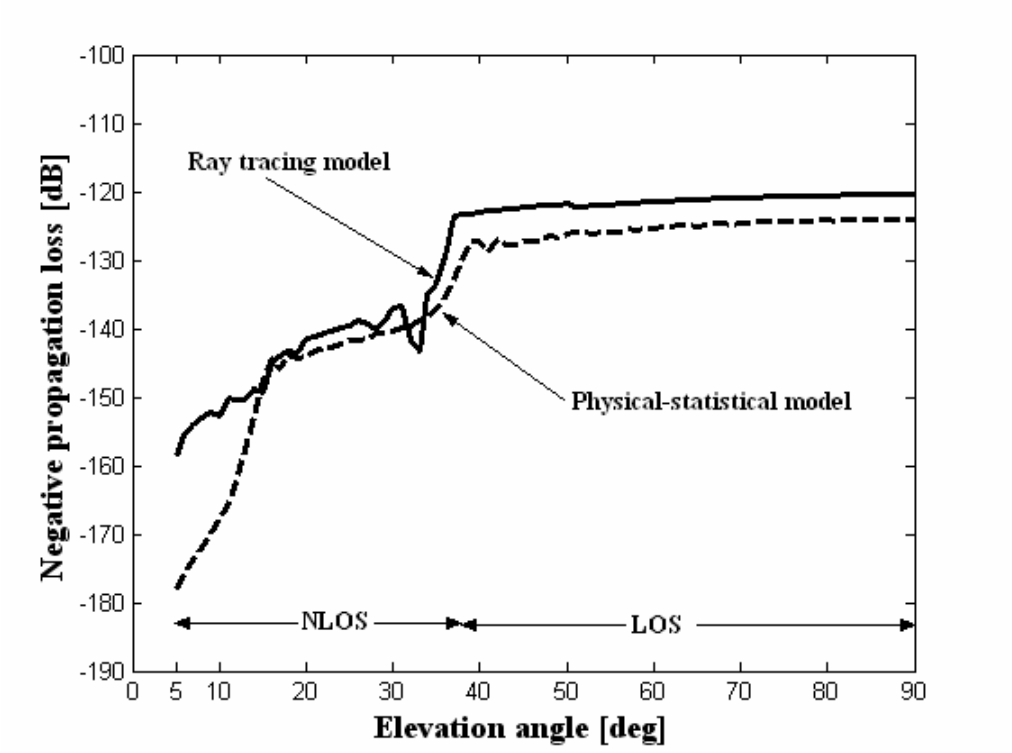

(c)

Figure 4.15 Predicted propagation path loss for azimuth: (a) 90^0; (b) 60^0; (c) 45^0.

The results show a very good agreement between our ray-tracing model and the physical-statistical model for the scenario of $\theta = 90^0$ in all elevation angles. In the LOS condition, we observe the propagation loss obtained by using ray-tracing model is about 3 dB lower than that by the physical-statistical model in all scenarios. This is due to we include the reflection from the ground and may be reflection from the building as well. In the NLOS condition, we notice the results of both model are different. For both scenario of $\theta = 60^0$ and $\theta = 45^0$, our ray-tracing model exhibit higher received power level for low elevation angle (i.e. $\alpha < 20^0$), while a very good agreement can be observed for elevation angle higher than 20^0. This is due to in our ray-tracing model the contribution of the reflection and the diffraction rays and their combination is considered. However the physical-statistical model has only considered the diffraction from rooftop of the building.

Considering the SPF coverage illustrated in Chapter 2 by (2.5), an average propagation path loss value is displayed in Table 2 for different azimuth angles. In Table 2, the propagation path loss was presented in an average value for the three regions within the coverage. Region 1 is a coverage with elevation angle greater than 45^0 (within 20 km of

horizontal distance from sub-platform point). Region 2 is an area with elevation angle between 45^0 and 15^0 (related to the horizontal distance between 20 km up to 75 km), and region 3 is the rest of the coverage (from 75 km up to 194 km in horizontal distance). From the table we can see that an azimuth angle has a little effect to the average path loss at most of high elevation angle such as in region 1. However azimuth angle has much an effect to the propagation loss at low elevation angle such as in region 2 and region 3. We observe that propagation loss in region 2 and 3 is decreasing as azimuth angle also decreases.

Table 4.3

Average propagation path loss [dB] versus elevation angle for the model in Figure 4.10.

Azimuth [degree]	Elevation angle [degree]		
	Region 1 ≥ 45	Region 2 $45 > \alpha \geq 15$	Region 3 $15 > \alpha \geq 5$
90	121.6	142.3	172.8
60	121.1	138.3	152.6
45	121.2	135.6	151.4

These results could give much contribution to the analysis of co-channel interference experienced by the MS (downlink interference) more accurately. This because of the propagation path loss is predicted in more realistic [77] compared with only assuming as a free-space path loss. For example, we will be able to calculate the co-channel interference experienced by the MS that is receiving signal from wanted platform (i.e. located at 80^0 in elevation) but also suffer from unwanted platform signal (i.e. located at 20^0 in elevation). Whereas, we found in a previous work the interference analysis for the case of IMT-2000 is based on a free space path loss assumption [78]-[79]. We will show our propagation path loss prediction employed to calculate required transmitted power at the SPF through the link budget analysis presented in the following section.

4.6.2 Estimated Power Requirement

Based on the propagation result presented above, this section presents link budget analysis for the next generation mobile communication digital CDMA-based such as IMT-2000 that

carried out by the SPF. The required bit energy per noise power spectral density can be expressed as [42]

$$\frac{E_b}{N_0} = \frac{P_T\, G_t\, G_r}{R_b\, k\, T_0\, L(\alpha,\theta)\, L_0\, M_L}, \tag{4.47}$$

where R_b denotes the information rate in bits per second, T_0 represents receiver temperature in degrees Kelvin, k is Boltzmann's constant, L_0 is cable, connector, and combiner losses, M_L represents the link margin and $L(\alpha,\theta)$ is a propagation path loss as a function of elevation and azimuth angle obtained by ray tracing simulation. In this analysis we evaluate the required transmitted power for different classes of services of the 3G-multimedia application [80]. The parameters that involved in the calculation are displayed in Table 4.4.

Table 4.4

IMT-2000 specifications and system parameters used in the calculation.

Item	**Specification**
Frequency [GHz]	2
Information rate [kbps]	8, 12.2, 16, 64, 144, 384, 2000
SPF antenna gain [dBi]	30
MS antenna gain [dBi]	0
Boltzmann's constant [J/K]	1.38x10-23
Temperature's chamber [K]	290
Link margin [dB]	15.4
Cable, connector, and other losses [dB]	2
E_b/N_0 [dB]	Max. 7.9

The results are presented in Figures 4.16 (a), (b) and (c) for different scenarios, which means different azimuth angle namely 90^0, 60^0, and 45^0, respectively. We observe in Figures 4.16 (a), the required transmitted power for different scenarios is almost similar. This means in region 1 the required transmitted power at SPF is less affected by the azimuth angle. However in region 2 and region 3 the required transmitted power is much

affected by the azimuth angle. Region 3 shows the worst scenario in which the azimuth angle is 90^0. The required transmitted power was too high and may not be able to be implemented for the SPF mobile communication. For that case, the required transmitted power would have to vary between 31.2 W (8 kbps) up to 7.80 kW (2 Mbps).

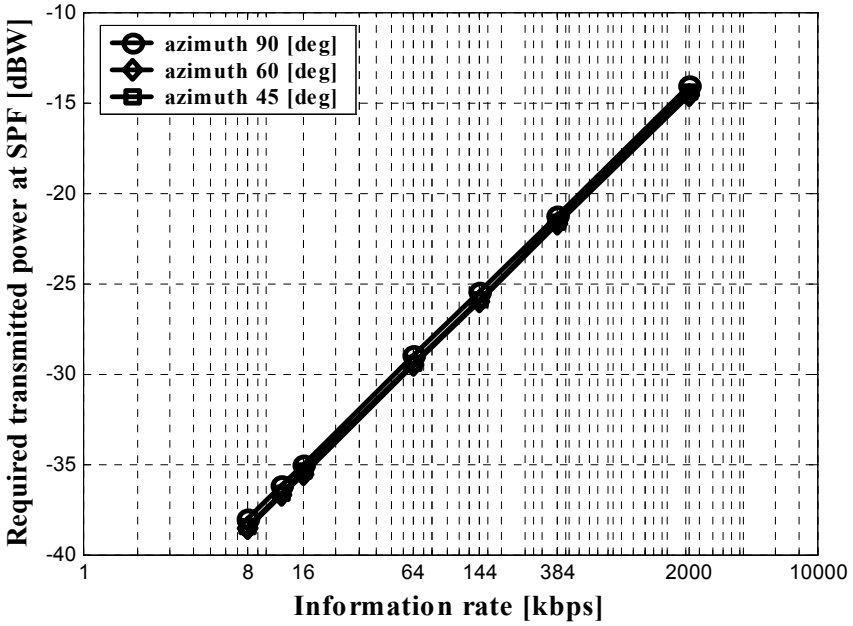

(a)

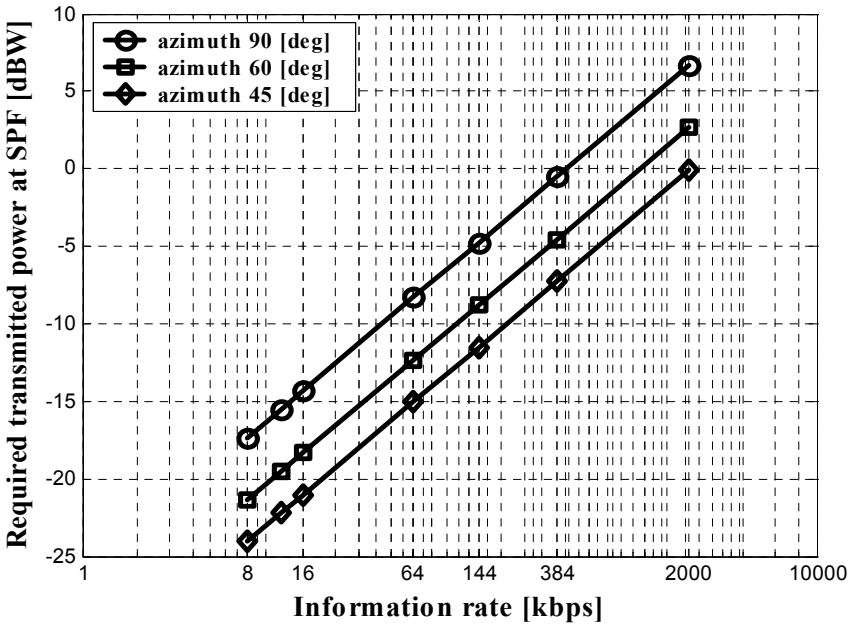

(b)

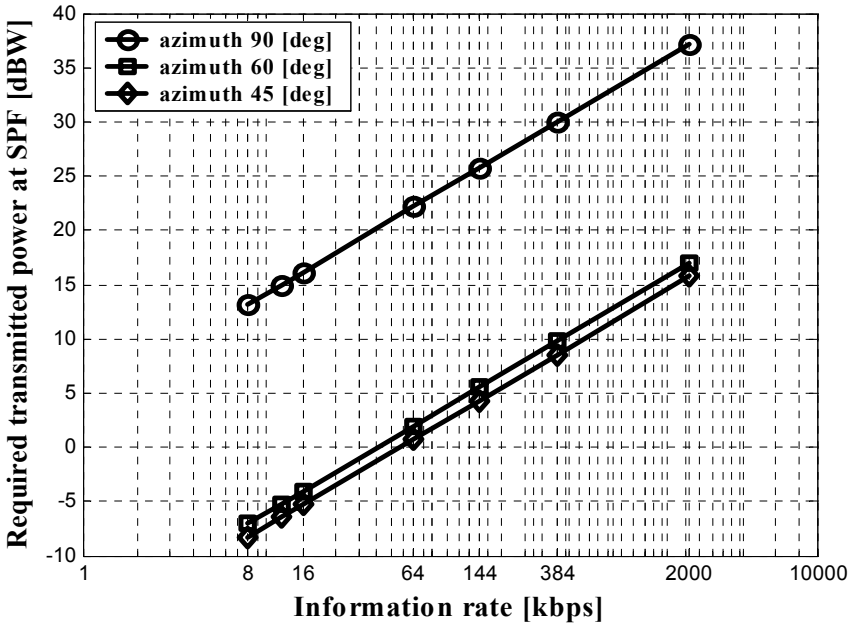

(c)

Figure 4.16 Required transmitted power at the SPF:
(a) Region 1; (b) Region 2; (c) Region 3.

4.7 Summary

In this chapter, we evaluated propagation parameters such as propagation loss and required transmit power for different type of area presented in Chapter 3 in stratospheric platform communication. Since there is no measurement campaign performed from aerial vehicle in the city, we employed site-specific model for analyses purposes by using ray tracing algorithm. Firstly, building geometry and distribution for an area under consideration are experimentally investigated at around Tokyo and Gunma Prefecture. Then, a building geometry model that has a characteristic similar with experimental result is developed for simulation. Virtual ray tracing scheme is employed with considering both reflection and diffraction mechanism from building rooftop, building face and street.

From simulation, we found that the propagation path loss is a decreasing function to both of elevation as well as azimuth angle with respect to the SPF position. The result has been confirmed by a comparison with the physical-statistical model proposed in [70] for verification. It is shown a good agreement for 90^0 of azimuth angle and mostly good agreement is observed in a high elevation angle of other azimuth angles.

Using these results, we then estimated the required transmitted power onboard the platform for the case of IMT-2000 service applications. The different scenarios which mean different azimuth angle of the simulation results show the critical limitations of the SPF system carrying the next generation mobile services. By defining the SPF coverage into three regions based on different elevation angle, it is found that the critical required transmitted power in the model is observed in the region 3 which means the fringe of coverage area in which the azimuth angle is 90^0. Such high required transmitted power may not be able to be implemented in the next generation mobile communication employing the SPF.

The current analysis regarding estimation of either performance or capacity in the stratospheric platform communication is purely based on the assumption of LOS propagation condition. Shadowing situation in the analysis is often be neglected for simplicity. However, it is required an evaluation with considering both LOS and shadowing situation. This propagation prediction result presented in this chapter would contribute in further analysis as it evaluates both conditions. Additionally, this result may also be useful for investigating the co-channel interference in which frequency reuse is employed to increase the capacity in the area of stratospheric platform communication.

Chapter 5

On the Downlink Performance of SPF Communication Channel

In this chapter we evaluate and propose the downlink performance of SPF communication channel. It is shown in [85]-[86] that for some particular situations, which refers to particular elevation and azimuth angle, the SPF communication link would need multipath mitigation technique to ensure the channel quality of being above the minimum level performance.

A simulation model is developed based on propagation parameters that were obtained through modeling and ray-tracing scheme utilization. The propagation parameters in a developed typical urban low rises environment were first derived by means of ray tracing method. Chapter 4 has provided the detail of the method. We then evaluate the downlink SPF channel in terms of BER, which include the propagation parameters in our estimation. We assume the SPF channel that carrying the next generation mobile IMT-2000 services with different information bit rate. Both LOS as well as NLOS channel situations, which are driven by elevation and azimuth angles of the platform, are considered in this evaluation.

5.1 Introduction

As we continue to step forward into the new wireless infrastructure that employs the SPF, it becomes increasingly clear that the dominant consideration in the design of systems employing such an infrastructure will be their ability to perform with adequate margin over a hostile channel. In Chapter 3 the performances of mobile SPF communication channel under LOS condition in semi-urban environment have been shown. Ricean fading distribution of the received signal was found to be the dominant channel model in such environment. In Chapter 4 evaluation to the SPF radio propagation characteristics has been extended to different area that is a typical urban low rises environment. Elevation and azimuth angles were found to be the most critical parameters in the implementation of mobile IMT-2000 services through the SPF channel from a power requirement point of view. In the system design criterion, however, BER performance is the important parameter that in general should be estimated before implementation.

In this chapter SPF downlink performance in urban low rises environment is evaluated in term of average BER over fading channel due to the fact of multipath. In urban low rises environment with a typical building geometry model, low elevation angle in a particular azimuth angle are a critical parameter to the channel characteristic. Accordingly, LOS and NLOS channel condition will be affected by the position of the platform seen by the MS. While the same method of ray tracing is performed here, a different arrangement of building geometry model from that of the model presented in Chapter 4 is considered for evaluation. The objective is to know the SPF channel parameters behavior in various types of building geometry model in the city, which is frequently different from one place to another.

SPF has recently been proposed to deliver IMT-2000 services either in remote area that is not covered by existing system or in the city as a complimentary delivery method to the existing system. While a plethora of studies of IMT-2000 has been devoted refer to existing terrestrial system, some studies can be found in satellite system [81]-[83]. However, there are only a few studies for IMT-2000 performance evaluation, which is carried out using the SPF technology [18], [78] and [84]. Moreover, there is no study yet related to the SPF channel performance in term of BER probability when it is employed to carry IMT-2000 services. Our evaluation in the sections that follow describes and explains

at the first time BER probability for the SPF channel in the city environment intended to deliver IMT-2000 services.

5.2 Overview of IMT-2000 Services

Figure 2.7 in Chapter 2 shows a frequency allocation table for SPF communication. We can see that there will be a sharing frequency between SPF system and terrestrial cellular system to deliver 3G mobile IMT-2000 services within band frequency of around 2 GHz. A study of co-channel interference analysis between both systems or between SPF and satellite system is then required. Some studies have performed such an analysis [11], [78], [81] and [84], resulting that the SPF system could operate together with the existing system under particular limitations such as separation distance or transmission power. In this chapter, however, we evaluate the performance of IMT-2000 services in a single SPF system, i.e. in the case the SPF is deployed to cover a region in which that region is not covered by the existing terrestrial system.

In a 3G mobile IMT-2000 services, the SPF will be equipped with multispot beam antenna array to create the spot beams or cells on the ground so that frequency reuse technique can be implemented. This technique constitutes a way to conserve the spectrum frequency band. IMT-2000 as an official name of the ITU for 3G published a set of performance requirements for the services of being carried out. They are shown in Table 5.1 in terms of minimum E_b/N_0, minimum BER and the environment that a certain application is going to be implemented. This third generation mobile communication systems are known as UMTS in European countries.

WCDMA and CDMA2000 are the main third generation air interface in the world and deployment has been started in Europe and Asia, including Japan and Korea, in the same frequency band, around 2 GHz. WCDMA is known in different name as UTRA within 3GPP and ETSI. The new requirements of the third generation systems which are different from second generation systems have been identified. Those are bit rates up to 2 Mbps, variable bit rate to offer bandwidth on demand, multiplexing of services with different quality requirements on a single connection (i.e. voice, video and packet data) and from delay sensitive real time traffic to flexible best-effort packet data. Other requirements for 3G are 10 % frame error rate to 10^{-6} bit error rate, should co-existence with second

generation system, support of asymmetric uplink and downlink traffic, high spectrum efficiency and should be coexistence of FDD and TDD mode. The above requirements are also expected for 3G utilization based on SPF system. Because of different geometrical configuration, detailed investigation of 3G application employing the SPF is then required. In this chapter a partial investigation to the downlink channel performance for 3G based on the SPF is evaluated.

Table 5.1

Standard QoS parameters for 3G mobile IMT-2000 [80].

R_b [kbps]	Typical Applications	Min. Required E_b/N_0 [dB]	Min. Required BER	Environment
8	Very low rate data	3	2.3×10^{-2}	Vehicular
12.2	Speech	5	6.0×10^{-3}	Vehicular
16	Speech	3	2.3×10^{-2}	Vehicular
32	Speech	3	2.3×10^{-2}	Vehicular
64	Real time data	2	3.8×10^{-2}	Vehicular
144	Real time data	1.5	4.6×10^{-2}	Vehicular
384	Non real-time data	1	5.6×10^{-2}	Pedestrian

The configuration of 3G mobile cellular system based on SPF can be seen in Figure 5.1. The MS served by the SPF spreads everywhere in the coverage. Each MS therefore has a specific elevation or azimuth angle in a way of looking to SPF. This condition leads to a different channel characteristic when they change their position due to channel fading and shadowing. Consequently, the channel performance will vary due to different channel characteristic. We here emphasis our channel performance evaluation with involving elevation and azimuth angle as a main parameter. This evaluation therefore would represent for any locations of the MS everywhere inside the SPF coverage.

5.3 Downlink Performance Evaluation

Signal transmission between SPF and a mobile terminal on the ground generally often takes place via many paths. However, due to the SPF is situated very high in the stratosphere, a significant portion of the total energy arrives at the mobile receiver by way

of a direct wave. The remaining power is received by way of a specular ground reflected wave and the many randomly scattered rays that form a diffuse wave. Therefore, a signal is received from a number of different paths. In this evaluation, the signals of the different paths are traced using well-known technique called ray tracing algorithm. As a result, all replicas of the same transmitted signal but with different amplitudes, phases, delays, and arrival angles are summed at the mobile terminal and those may be constructive or destructive.

SPF channels have many common points with satellite channels, while their path loss is much lower even compared with the case of a LEO satellite system. Compared to wireless terrestrial links, SPF links have more favorable propagation characteristics. In wireless terrestrial systems, the received power decays as a function of the transmitter-receiver distance raised to a power of four. Additionally, the Rayleigh distribution is commonly used to describe the small-scale fading envelope. In SPF links, there exists a dominant signal component such as a LOS path, and the small-scale fading envelope distribution is Ricean except for low elevation angle. We will show this characteristic based upon the model that we developed in this study. A critical parameter is the Ricean factor K, which for a fixed point of receiver K is defined as the ratio of the dominant component to the scatter contribution. Typically, the range of K is 0–20 dB for semi-urban environment for the case of SPF. However, in this chapter urban low rises environment is assumed and therefore smaller value of K is found compared with the value of K for semi-urban environment as presented in Chapter 3. Generally, the larger its value, the higher the energy gain in SPF-based systems compared to terrestrial systems, where K is close to zero (Rayleigh fading).

In uplink direction, better receiver techniques such as space diversity can be used in the BTS in their respective SPF resulting in better channel performance. However, MS usually is not equipped with receiver techniques as good as in the BTS. Therefore, here downlink performance is evaluated under the condition that a MS is not equipped with any receiver techniques. On the other word, in this chapter the downlink performance of SPF link is examined with considering only a propagation parameters obtained through ray tracing simulation without utilizing any receiver techniques.

Two channel parameters in terms of propagation loss and Ricean factor (K) as a function of elevation angle in different scenario means different azimuth angle are estimated using the building geometry model depicted by Figure 5.2. The detailed dimension and other parameters of the model under test are listed in Table 5.2.

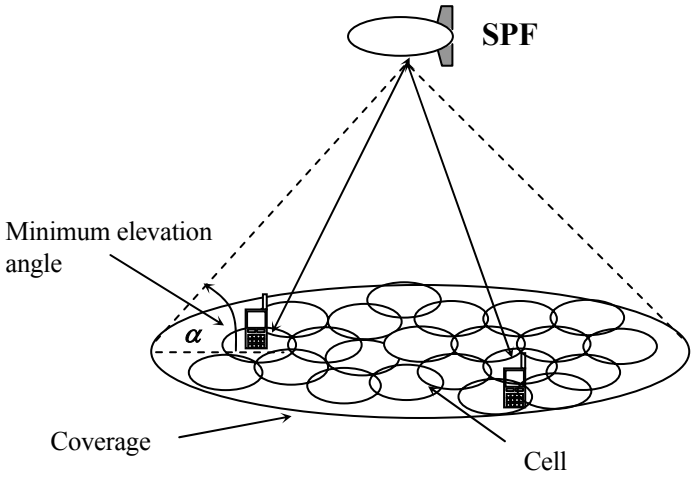

Figure 5.1 Configuration of 3G mobile cellular system based on SPF.

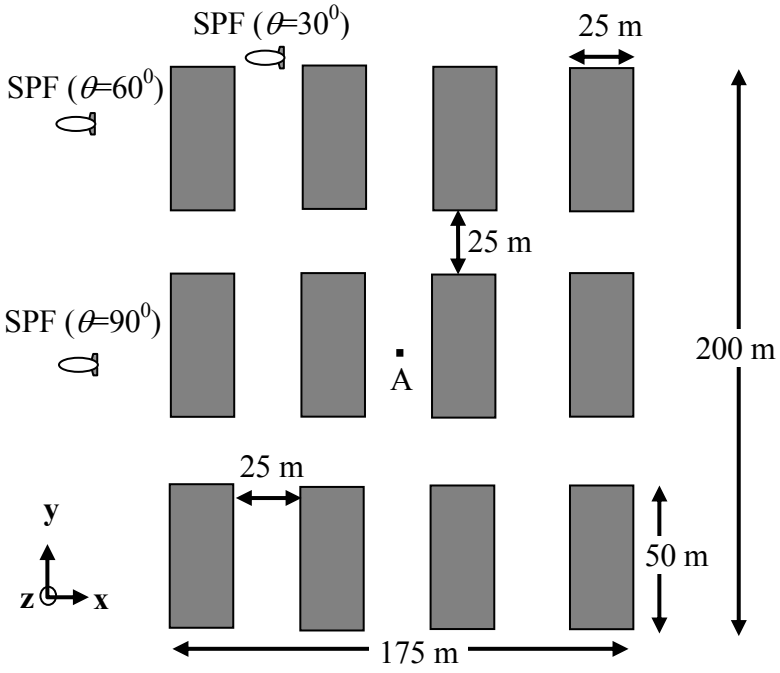

Figure 5.2 Area under test (top view).

Electrical parameters of the building and street are assumed to be the same with that of the parameters used in Table 4.2 in Chapter 4 and that refers to [65]. In this model, however, the buildings are in parallel arrangement with the street slightly narrower than in the model presented in Figure 4.10. We use the same specification of the ray tracing algorithm and assumption made in our simulation to characterize propagation parameters as previous chapter.

Table 5.2

Geometrical parameter of the model under test.

Parameters	Specifications
SPF height (h)	20 km
Frequency (f)	2 GHz
Building height (h_b)	25 m
Building width (w_b)	25 m
Building length (w_l)	50 m
Street width (w_s)	25 m
MS antenna height (h_m)	1.5 m
SPF elevation (α)	5^0 to 90^0 (in a step of 1^0)
SPF azimuth (θ)	90^0, 60^0 and 30^0

5.3.1 SPF Channel Characteristic

Figure 5.3 demonstrates the ray-tracing simulation result of the total propagation loss obtained from the calculation of a direct LOS ray and multipath scattered rays. In the figure, we can see that even though azimuth angle is different, the propagation loss in LOS situation is similar along with elevation angle variation. However in NLOS situation, different azimuth angle has resulted different propagation loss. This is due to the multi-path power of the rays may vary for different azimuth angle. The highest propagation loss occurs when azimuth angle is 90^0, and it decreases as azimuth angle also decreases. We observe in NLOS situation, the propagation loss dramatically increases by the order of 20 dB or more compared to that in LOS region. In this case we can say that the propagation loss in the SPF communication is less sensitive with the azimuth angle variation in case of

high elevation angle. However, in low elevation angle or particularly in the shadow region, the propagation loss is not only dependent but also quite sensitive to the azimuth angle variation. We have shown in our work [77] that the propagation loss characteristic is governed by both elevation and azimuth angle. The comparison with physical-statistical model proposed in [74] has also been made for verification of ray tracing simulation. Both ray-tracing and physical-statistical model show a good agreement in some cases, but there is only little difference in other case.

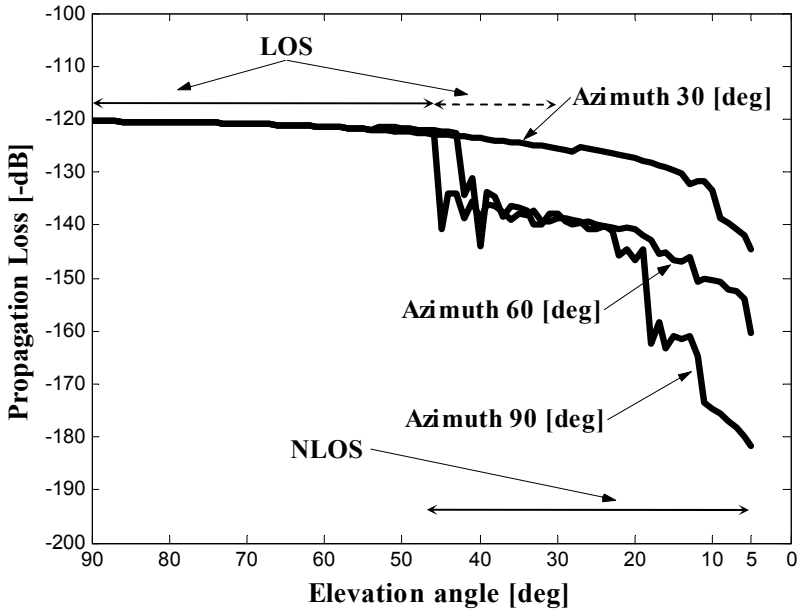

Figure 5.3 Different scenario of propagation characteristic of LOS and NLOS condition.

Fading in nomadic systems, however, is best described by the narrowband temporal Ricean factor (*K*). As mentioned, at a fixed location, the *K* is defined as the ratio of the dominant fixed component to the non-coherent scatter component within the multipath profile. However, in this study it is obtained the spatial *K* due to different location of the SPF with refer to different elevation and azimuth angle with respect to the MS location on the observed area, which characterizes the small-scale spatial variations. By using ray tracing simulation it is possible to calculate average power level for every single ray at the receiver, therefore *K* factor can be very easily to be obtained. The simple formulation of how to calculate *K* factor is expressed by

$$K = \frac{A^2}{2\sigma^2}, \tag{5.1}$$

where A^2 represents the average direct LOS power and $2\sigma^2$ is the variance or average power of the multipath components.

Since there is no direct ray in NLOS region, *K* factor goes to zero in this region, for example in low elevation angle as depicted in Figure 5.4 It is shown in a transition region between LOS and NLOS region (ranging from 36^0 up to 46^0 of elevation angle for all azimuth angle), *K* factor is gradually increased due to the presence of direct ray. From these results, it is obvious that the MS may be fail to establish the communication link with the SPF either due to a very high propagation loss or very poor condition of the channel performance indicated by a very low value of *K* factor.

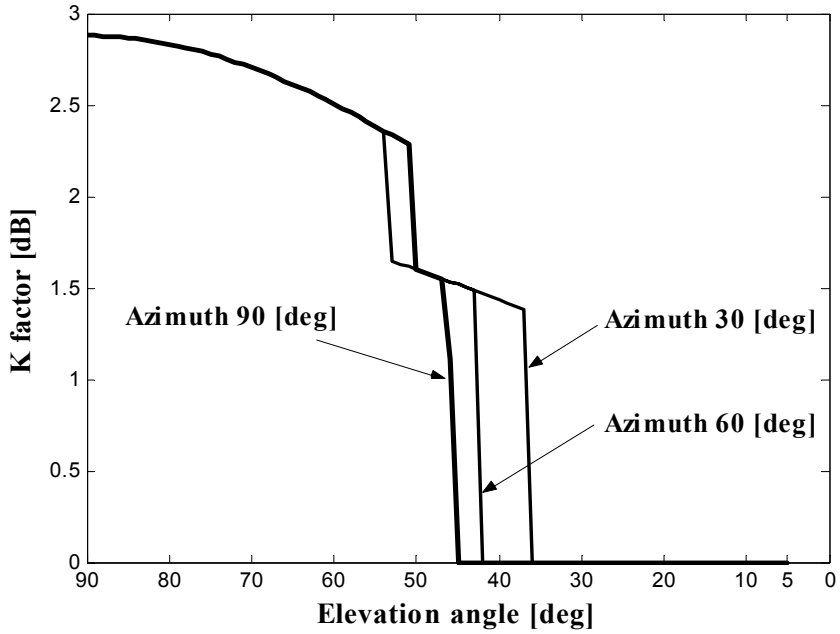

Figure 5.4 Predicted *K* factor.

5.3.2 Evaluation Model

In this section a simulation model for the performance evaluation of the downlink SPF channel is developed on the basis of the channel characteristic previously described. The scattering diagram of the simulation model is demonstrated in Figure 5.5. In the figure the downlink SPF channel has been modeled as a Rayleigh fading model for NLOS situation due to an obstacle by the building. On the other hand the channel is modeled as Ricean fading channel for LOS situation due to the presence of the direct path in most of the cases.

In a LOS state, it is well-known that receive signal amplitude (R) is characterized by the Ricean probability function (PDF) as

$$f(R) = 2cRe^{-c(R^2+1)} I_0(2cR), \quad R \geq 0, \tag{5.2}$$

where c = $1/(2\sigma^2)$, R is envelope of the received signal and amplitude of LOS component is assumed equal to 1. In the NLOS state, it is describe by the Rayleigh probability density function given by

$$f_{NLOS}(R) = 2cRe^{-cR^2}, \quad R \geq 0. \tag{5.3}$$

The resulting propagation path losses and K factors as a function of elevation and azimuth angle are then involved in the performance evaluation. Moreover, the evaluation has taken into account the information bit rates (R_b) that are basically used in IMT-2000 services, while DPSK modulation scheme is employed in our simulation.

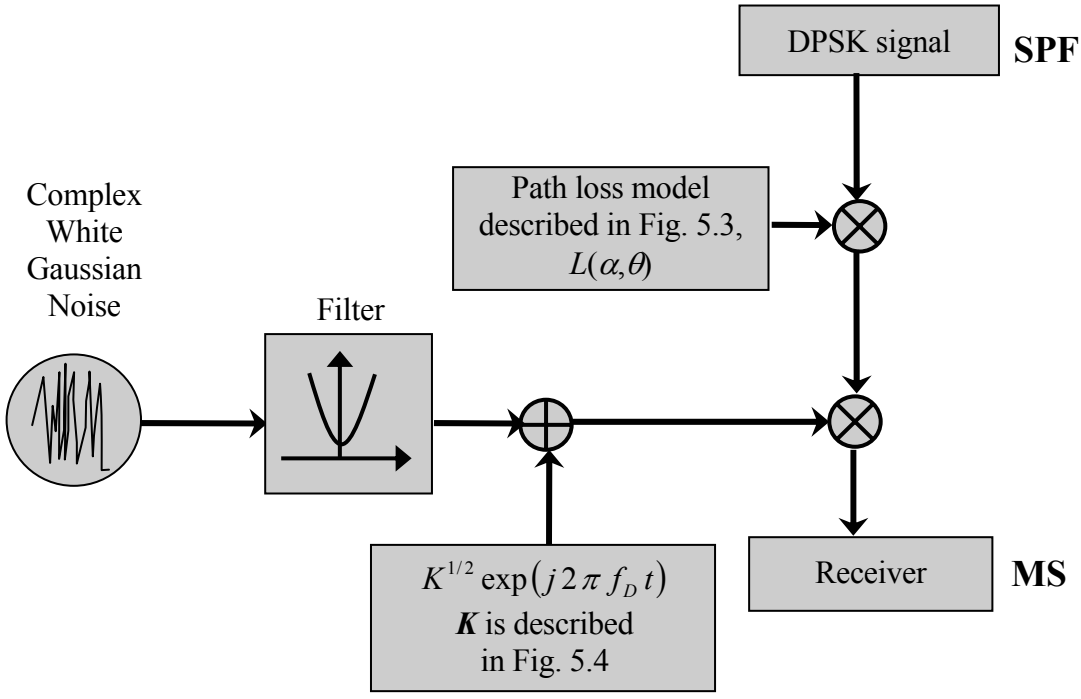

Figure 5.5 The downlink SPF channel model.

According to our proposed channel model, where the downlink SPF channel may follow Ricean distribution, the corresponding result of K factor must be used in the evaluation. A

complex white Gaussian noise generator is used to represent in-phase and quadrature signal components, with unit power. No Doppler effect is expected in this evaluation due to fixed positioning of both SPF as well as mobile user. In this case the channel may be characterized as having a frequency slow fading channel model. Therefore, the filter that we used in the simulation is designed to produce a close approximation to the classical Doppler spectrum at its output. A phasor of constant amplitude, K is Rice factor obtained in Figure 5.3 that is a function to elevation and azimuth angle, is then added in order to represent the dominant coherent part of the channel. Its output is then used to multiply the DPSK modulated signal from transmitter (SPF). Path loss model obtained in Figure 5.2 is applied to the transmitted signal in order to simulate the real condition of the channel before the signal arrives at the receiver through the long distance from the SPF to the MS on the ground.

In Table 5.3 the detailed specification of IMT-2000 for the usage in SPF system is presented. Different information bit rates refer to different IMT-2000 services are considered in the simulation. We use the antenna onboard the platform with the maximum gain of 30 dBi that complies with the antenna pattern adopted for the SPF application [9], while at the user end we assume omnidirectional antenna with 0 dBi gain.

Table 5.3

IMT-2000 Specification used in a downlink performance evaluation.

Parameter	Specification
Frequency [GHz]	2
Modulation	DPSK
Channel model	Rice fading channel (subsection 5.3.1)
Bit rate [kbps]	8, 32, 64, 384, and 2000
SPF antenna gain [dBi]	Comply to [9]
MS antenna gain [dBi]	0
Boltzmann's constant [J/K]	1.38x10-23
Temperature's chamber [K]	290
Link margin [dB]	15.4
Cable, connector, and other losses [dB]	2
E_b/N_0 [dB]	7.9

5.4 BER Performance

Figure 5.6 demonstrates some results of average BER evaluation for 90^0, 60^0 and 30^0 azimuth angles and E_b/N_0 is set equal to 7.9 dB for all bit rates. The BER curve is plotted as a function of elevation angle for five categories of bit rate. From the result, we can see that the link performance in 90^0 azimuth angle is the worst case, while in 30^0 azimuth angle is the best case. In 90^0 of azimuth angle, the performance decreases quickly when the link goes to the NLOS condition. We also observed the performance in low elevation angle such as lower than 10^0, to achieve BER equals or lower than 10^{-3}; it is only possible if the bit rate is lower than 384 kbps and azimuth angles of 30^0. This means the communication link fails or the performance is worse in all azimuth angles if elevation angle lower than 20^0 for a bit rate equals or greater than 384 kbps. On the other hand, in LOS situation such as in elevation angle greater than 45^0, it is shown an error floor in the BER curves due to the presence of multipath components for all scenarios, which means for different azimuth angle. The channel performance cannot be improved for wide band signals (i.e. 2 Mbps) due to selectivity of the channel. This result implies the need for the usage of channel impairment mitigation techniques for the application of wide band signals in SPF communication.

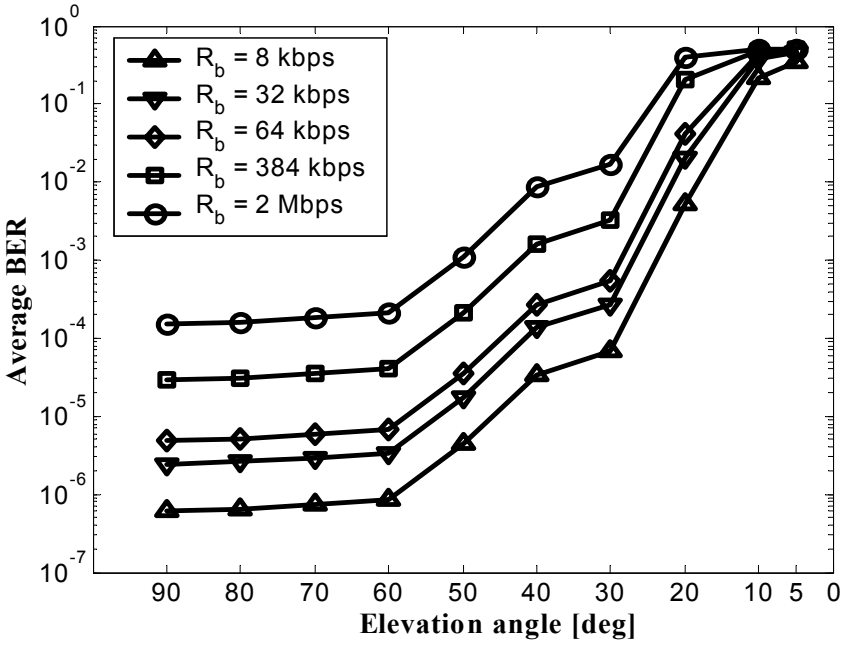

(a)

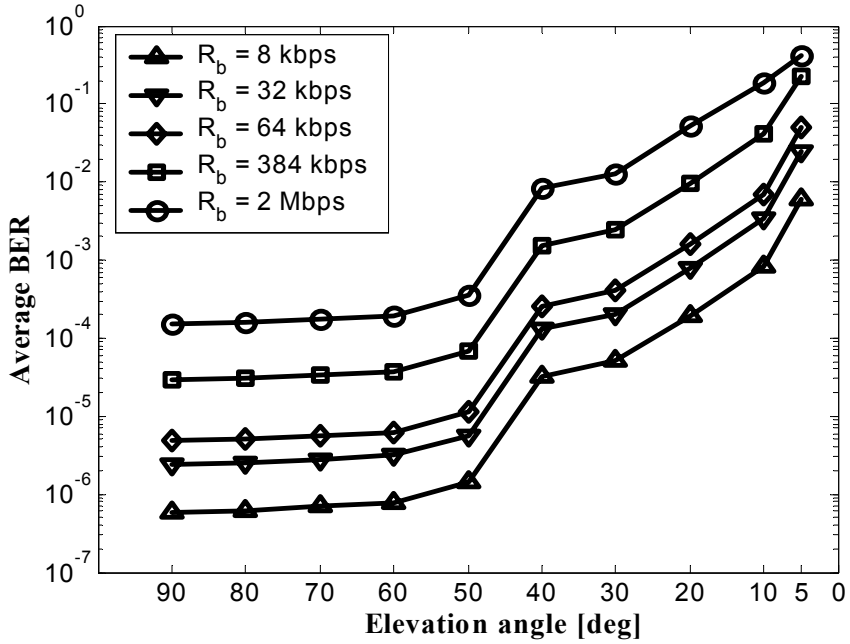

(b)

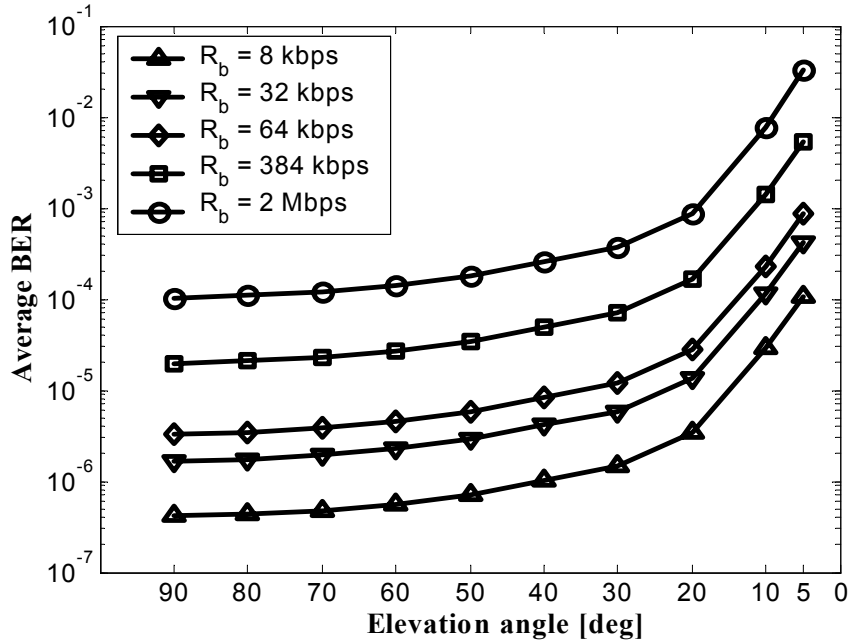

(c)

Figure 5.6 Downlink performance of IMT-2000 link in SPF channel with azimuth angle: (a) 90^0; (b) 60^0; (c) 30^0.

5.5 Summary

Downlink performance of SPF mobile channel has been evaluated and analyzed specifically for IMT-2000 services. Propagation parameters in terms of propagation loss

and *K* factor were first derived on the basis of elevation and azimuth angle with employing well-known ray-tracing method. The propagation parameters obtained in this chapter can be valid only in a low rises urban environment, which typically consist of moderate building height and narrow road in order to represent multipath environment that is a common nature in mobile channel. The propagation parameters are then used to estimate downlink channel performance for both narrowband as well as wide band signals depending on the information bit rate of the transmitted signals. From this evaluation, we found that in SPF communication, the elevation and azimuth angle in which mobile users communicate with the SPF play a very important role.

It is shown that elevation angle greater than 40^0 demonstrate better performance for all azimuth angles. However, an error floor in high elevation angle (LOS condition) due to multipath has occurred and that would require the channel impairment mitigation technique to improve the SPF channel performance. For example BER performance could not be improved by only increasing elevation angle because it shows almost similar performance when elevation angle increase from 40^0 up to 90^0 for each information bit rate. The BER improvement can only be improved by reducing the information bit rate. This situation would require multipath mitigation technique to be used in SPF downlink direction to improve the downlink channel performance.

Another important result in this chapter is that the propagation prediction result presented here may also be used for investigating the co-channel interference for the case of multiple SPF in which a frequency reuse scheme is employed to increase the channel capacity. This is because the propagation loss estimation and the channel fading characterized by Rice factor are evaluated under different elevation and azimuth angle. In this case, interference analyses can be made for multiple SPF implementations which actually located in different angle seen by mobile user on the ground.

Chapter 6

SPF CDMA Capacity Analysis

We propose an analysis of reverse link CDMA multispot beam stratospheric platforms (SPF) in this chapter [87]. The SPF is currently considered as a novel wireless technology for the development of the next generation fixed and mobile communications. The geometry of this technology is different from that of the terrestrial but rather similar to the satellite based cellular system. However, evaluation on the CDMA system capacity of this technology has not been much reported. This chapter addresses all possible multiple access interference analyses including the effects of channel fading and shadowing in order to evaluate the system capacity. Single SPF and multiple SPF model are evaluated under perfect power control and imperfect power control. The results indicate that in SPF systems the reverse link CDMA capacity is significantly reduced because of the power control imperfections. Moreover, in multiple SPF model the interference caused by the users in overlapped region is not trivial. We found that because of this problem the capacity is reduced for both speech and real-time data applications compared with the single SPF model even though the assumption of perfect power control can be made. In order to improve the system capacity we propose two methods. First is to increase the minimum elevation angle defined for each platform and the second is to employ an adaptive antenna. Both methods show significant improvement in the capacity even though in the condition of imperfect power control.

6.1 Introduction

Stratospheric Platform (SPF) has been recently proposed as a novel technology for the development of wireless fixed and mobile communication systems [7] and [88]-[91]. It is based on aerial unmanned or manned vehicles, which are able to operate at stratospheric altitudes of approximately 17-30 km for a long endurance. This novel communication infrastructure has the advantages of higher line of sight capability and wider coverage area compared with the terrestrial systems, and a much shorter propagation distance which therefore give a significant advantage of link budget compared with the satellite systems. Cellular structure on the ground of this system will be implemented by using multispot beam antenna on board the platform for cells projection [92].

One application of the SPF is the next generation 3G mobile, which basically employs CDMA system and shares the same spectrum as used in terrestrial system [9]. In terrestrial cellular system, CDMA has a many-fold increase in capacity compared with TDMA/FDMA [93]. Some fundamental differences between terrestrial and SPF links, however, have led to the necessity of further investigation. For example, in SPF CDMA system, propagation delay is slightly larger than that in terrestrial system so that an effective power control scheme may not work properly. Therefore the power control imperfections in such a system must be considered in the capacity analysis. Another difference is that in the SPF system all users located within the platform coverage are subject to the power control of the same platform even though they are located at different spot beam or cell. This is because all spot beam antennas, which refer to all base stations, are located at the same platform. For this reason, the interference caused by these users is not a function of the distance between the user and the platform, because of the influence of the power control. In multiple SPF, the users in the border of slightly outside the platform coverage have the potential too to produce interference. But, they are served by the adjacent nearest platform so that they are subject to the power control of their respective platform. In this case, these users may produce the interference power, which the level depends on the distance. Moreover, in a multispot beam SPF system, the spot beam antenna radiation pattern will play an important role. In such a case, interference level from the users outside the reference cell directly depends upon the antenna characteristics and the definition of the spot beam contour.

Although there are many literatures on terrestrial CDMA cellular system, CDMA capacity issues have not been much investigated for the case of SPF [84] and [94]-[96]. The downlink performance of such a system has been examined in [94], while the other cell interference factor and the reverse link capacity have been evaluated in [95]. However the analysis mentioned above did not consider the effects of imperfect power control and the interference from the users of adjacent platform. In [96] the extension analysis proposed in [95] is presented with considering the scenarios of multiple platform application, but the analysis was still based on the condition of perfect power control. Both forward and reverse link CDMA capacity issues have also been investigated in [84] for a SPF rural macrocell integrated within a terrestrial UMTS network. However for both forward and reverse link, it has been modeled by using an oversimplified channel model for the capacity estimation. When considering CDMA system, the most serious problem we have to deal with is the user interference or known as multiple access interference (MAI), because all users are contending the same bandwidth at the same time. Power control must be used in such a system in order to overcome the near-far effect. However, it is rather impractical to assume that there is perfect power control. Therefore, in this contribution we address a comprehensive model to calculate all possible MAI for the reverse link SPF CDMA system for both single and multiple platform scenarios. The analysis is based on the condition of perfect power control and imperfect power control. Moreover, the channel model we used in the analysis is an experimentally investigated channel model in SPF communication performed in our previous work [97]-[99].

In addition, in this chapter we propose two methods to improve the system capacity, namely by increasing minimum elevation angle defined for each platform and the method of adaptive antenna. The former method resulting in the capacity improvement, however, it has to be paid by the increasing number of required platform to cover the global coverage. The latter method is a well-known rigorous technique to enhance the capacity by means of suppressing multipath signal and interference. However, the number of elements of the array onboard the platform is limited by the array size, which is only in a few meters.

The rest of the chapter is organized as follows. Section 6.2 explains the proposed SPF system CDMA model and defines the outage probability. Both single SPF model and multiple SPF model are introduced in this section. Reverse link interference analysis is presented in Section 6.3 for both models. The analysis describes all multiple access

interferences including channel fading and shadowing experienced by the SPF system. In section 6.4, we demonstrate numerical results. Section 6.5 provides the usage of adaptive antenna and describes the numerical result in comparison with the usage of multispot beam fixed antenna. Finally conclusions are drawn in Section 6.6.

6.2 SPF CDMA and Channel Model

In this chapter we propose two SPF CDMA system model for the reverse link capacity analysis. Those are a single SPF and a multiple SPF model. Each platform is equipped with a multispot beam phased array antenna to create the spot beams or cells on the ground. The spot beam antenna characteristic complies with the ITU recommendations given in the following expression [9]

$$G(\theta) = \begin{cases} 34.8 - 3\left(\theta / 1.57\right)^2, & for\ 0^0 \le \theta \le 4.53^0 \\ 9.8, & for\ 4.53^0 \le \theta \le 5.87^0 \\ 55.95 - 60\log(\theta), & for\ 5.87^0 \le \theta \le 37^0 \\ -38.2, & for\ 37^0 \le \theta \le 90^0 \end{cases}, \qquad (6.1)$$

where $G(\theta)$ is the antenna gain in (dBi) of the spot beam with boresight angle θ.

In the single SPF model, interference is originated from the users in a reference cell and the other cell within the coverage of the platform. However, interference in multiple SPF model is produced from the users in a reference cell, the users in the other cell within the platform coverage and the users in an overlapped region. We introduce an overlapped region in multiple SPF model as a region outside the coverage but still seen by the reference SPF, as shown in Figure 6.1. We will show the interference contribution from the users located in an overlapped region, in which they cannot be neglected in the analysis.

We assume all SPF are located at an altitude of 20 km and the separation distance between each platform is 200 km. The coverage area of each platform and the size of overlapped region are then calculated directly using platform altitude, platform separation distance and the setting of minimum elevation angle defined for each platform. The lower the minimum elevation angle the bigger the coverage area and the larger the overlapped region. For analytical purposes, first we consider the minimum elevation angle for each platform is 10^0.

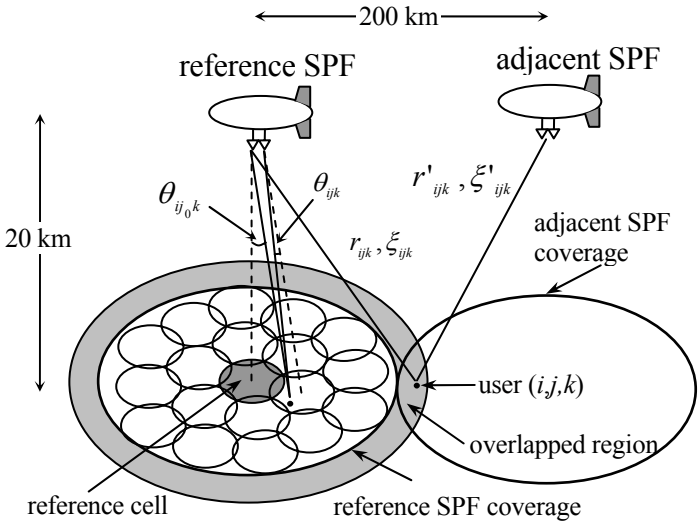

Figure 6.1 Multiple SPF model.

The transmission quality for a digital CDMA system may be described in terms of the energy per bit over total noise power spectral density E_b/N_0

$$\frac{E_b}{N_0} = \frac{W}{R}\frac{C}{I+\eta}, \tag{6.2}$$

where W is the channel bandwidth, R is the single user information bit rate, C is the received carrier power, I is the total co-channel interference power and η is the AWGN noise power.

6.2.1 Single SPF Model

First we evaluate a single SPF model. In this model, we assume that there are j cells within the platform coverage and each cell has N simultaneously active users. The cell is defined as an area, which is illuminated by the main lobe of a spot beam. The main lobe is 34.8 dBi and the intersection between adjacent cells is assumed at –3 dB contour, refer to 9.6^0 boresight angle according to the spot beam antenna characteristic presented in (6.1). We define ith user in the jth cell by a unique set of indices (i, j), where $1 \le i \le N$ and $1 \le j \le J$. Let V denotes the set of interfering users who can be seen by the platform for the user-of-interest. For this model, if the user-of-interest is denoted by (i_0, j_0) then we can express received carrier-to-total interference plus noise power ratio in (6.2) as

$$\frac{C}{I+\eta} = \frac{\beta_{i_0 j_0} EIRP_{i_0 j_0} G_{j_0}(\theta_{i_0 j_0})}{\sum_{(i,j)\in V} \beta_{ij} EIRP_{ij} G_{j_0}(\theta_{ij}) + \eta}, \tag{6.3}$$

where β_{ij}^{-1} is the attenuation in the link from user (i, j) to the reference platform, including path loss and channel fading. $EIRP_{ij}$ is the effective isotropic radiated power of the user, and $G_{j_0}(\theta_{ij})$ is the antenna gain of the spot beam covering the user-of-interest with boresight angle θ_{ij}.

6.2.2 Multiple SPF Model

In a multiple SPF model, we assume each platform service area of an M platform constellation is divided into J cells with N simultaneously active users per cell. For simplicity, the same size of coverage area for each platform under consideration is assumed in this work. The cell structure is assumed to be similar with that of the cell structure for the single SPF model. This means each cell has the same area and intersection between adjacent cells is also assumed at –3 dB contour. In this model, the ith user in the jth cell of the kth platform is identified by a unique set of indices (i, j, k), where $1 \le i \le N$, $1 \le j \le J$ and $1 \le k \le M$. Similar to the single SPF model, now let V denotes as the set of interfering users who can be seen by the serving platform for the user-of-interest, referred to as the reference platform including the users from overlapped region. We set the indices (i_0, j_0, k_0) to denote the user-of-interest in this model. The received carrier to total interference plus noise power ratio in (6.2) is then expressed as

$$\frac{C}{I+\eta} = \frac{\beta_{i_0 j_0 k_0} EIRP_{i_0 j_0 k_0} G_{j_0}(\theta_{i_0 j_0 k_0})}{\sum_{(i,j,k)\in V} \beta_{ijk} EIRP_{ijk} G_{j_0}(\theta_{ijk}) + \eta}, \tag{6.4}$$

where all parameters definition is similar to (6.3) unless subscript k in (6.4) is added to denote an adjacent platform.

For both cases (single and multiple SPF model), a threshold value of E_b/N_0 for a certain performance requirement $(E_b/N_0)_{\text{req}}$, can be specified depending on channel characteristics, modulation method, and coding scheme. We define the outage probability, Pout, as the probability of failing to achieve the required $(E_b/N_0)_{\text{req}}$ and can be expressed by

$$P_{out} = \Pr\left\{\frac{E_b}{N_0} \le \left(\frac{E_b}{N_0}\right)_{req}\right\}. \quad \textbf{(6.5)}$$

The SPF CDMA system capacity, referred to as the average number of users per cell N, is then linked to the outage probability, i.e. $N = f(P_{out})$, and can be determined by a certain requirement on the outage probability.

6.2.3 SPF Channel Model

In (6.3) and (6.4), β_{ij}^{-1} and β_{ijk}^{-1} should take account the path loss and the channel fading for each user. In order to estimate the system capacity in more realistic, we should know the characteristic of the SPF channel, which is predicted to different from that of the terrestrial channel but rather similar to the satellite channel. We have experimentally characterized the SPF channel in our previous work [97]. It was found that the Ricean fading channel is an appropriate model for the case of SPF link with K factor varies depending on the elevation angle and the frequency. This value of K factor is then should be involved in the interference analysis. In simulation, however, the computation becomes too complicated if each user is assigned with different value of K due to their unique position, refer to specific elevation angle. To solve this problem, we take a mean value of K for different elevation angles.

6.3 Reverse Link Interference Analysis

We notice the most important difference between the multispot beam SPF and cellular terrestrial scenarios lies in the interference mechanism. For a multispot beam SPF CDMA system, the users will be under power control of their respective spot beam, i.e. their respective base station. However, in SPF system all base stations are located on the location within a distance of few meters corresponds to the aperture of the phased array antenna onboard the platform. Thus, the user signal within the coverage of their respective spot beam will traverse the same path towards all base stations and experience approximately the same shadowing. Such a situation is not applicable for the users within the overlapped region, for example in multiple platforms scenario. Users in overlapped region are considered belong to adjacent SPF so that they will be under power control of their respective spot beam in their respective platform. These users will experience

different shadowing with the users in the reference SPF and therefore they can contribute to produce interference to the user at the reference platform.

Due to fading and shadowing, even an unshadowed user may experience a nontrivial degree of power control error (PCE) for a multispot beam SPF CDMA system. The power control error, λ, can be modeled as a lognormal distribution, i.e., $\lambda = e^{\delta}$, where δ is a zero-mean Gaussian random variable with standard deviation σ_{δ}. In the case of perfect power control the logarithmic standard deviation is 0 dB. After averaging over the fast fading, E_b/N_0 can be expressed as

$$\frac{E_b}{N_0} = \frac{W}{R}\frac{P_0 e^{\delta_{i0,j0,k0}}}{I_{intra} + I_{inter} + \eta}, \tag{6.6}$$

where P_0 is the nominal received power with ideal power control. I_{intra} is the interference originated from users within the reference cell and I_{inter} is the interference originated from users within the other cell. A reference cell is assumed at the nadir of the platform, served by the reference base station.

6.3.1 Intracell Interference

When we consider perfect power control, the total interference power from the users inside the reference cell can be given as

$$I_{intra} = \upsilon (N-1) P_0, \tag{6.7}$$

where υ denotes the voice activity factor, which is 1 with probability ψ and 0 with probability 1-ψ. In practical situation, the average received power at the spot beam antenna onboard the platform may not be the same for each user signal. Therefore, the total interference from users located within the reference cell under imperfect power control condition can be expressed by

$$I_{intra} = \sum_{i=1}^{N-1} \upsilon P_0 e^{\delta_i}, \tag{6.8}$$

where δ_i is the Gaussian random variable of the received signal of the ith user.

6.3.2 Intercell Interference

The total interference power from other cell includes interference power from the other cell within the overlapped region. This interference power is given as

$$I_{\text{int}er} = \sum_{k=2}^{M} \sum_{j=1}^{J} \sum_{i=1}^{N} \upsilon P_0 e^{\delta_{ij}} \gamma_{ijk}^2 + \sum_{k=2}^{M} \sum_{j=1}^{J} \sum_{i=1}^{N} \upsilon P_0 e^{\delta_{ijk}} \gamma_{ijk}^2 \chi_{ijk}^2 , \tag{6.9}$$

where γ_{ijk}^2 is the power discrimination due to spot beam antenna radiation pattern and χ_{ijk}^2 is the power control factor for users in the overlapped region. Note the second term of (6.9) is neglected for the single SPF model analysis, which means that there is no overlapped region.

According to the spot beam antenna radiation diagram that we consider here, the distribution of spot beam antenna gain over a cell region is not uniform. The users in each cell must have additional power gain which is proportional to $1/G_j(\theta_{ijk})$, where $G_j(\theta)$ is the jth spot beam antenna gain to equalize the received power at their own spot beam antenna. However, the reference spot beam will suffer from this power gain. The power discrimination factor γ_{ijk}^2 due to reference spot beam antenna gain is then given by [100]

$$\gamma_{ijk}^2 = \frac{G_{j_0}(\theta_{ij_0k})}{G_j(\theta_{ijk})}, \tag{6.10}$$

where θ_{ij_0k} is the off-boresight angle relative to the reference spot beam as depicted in Figure 6.1.

Now let we consider the power control factor χ_{ijk}^2 to account for the interference brought by the users in the overlapped region, which are served and power controlled by an adjacent platform. Here we cannot ignore the distance, shadowing (A), and channel fading of the user relative to their respective platform. The shadowing state in platform communication may have a similarity with that of the satellite system [101]. For example the users in the overlapped region may be shadowed to both his own serving platform and the reference platform, may be shadowed to neither platform, or may be shadowed to one,

but not to the other. For such a user to both the reference platform and their own platform, we can express the power control factor as [100]

$$\chi_{ijk}^2 = \left(\frac{r'_{ijk}}{r_{ij_0k}}\right)^{\mu}\left[A^2 e^{\xi'_{ijk}-\xi_{ijk}} + A(1-A)\frac{e^{\xi'_{ijk}}}{1+K} + A(1-A)e^{-\xi_{ijk}}(1+K) + (1-A)^2\right], \quad (6.11)$$

where r'_{ijk} and r_{ijk} denote the distance from the users to their own serving platform and reference platform, respectively. ξ'_{ijk} and ξ_{ijk} is random variable modeling the shadowing effect corresponding to these two paths. The shadowing is modeled to follow Gaussian distribution with mean μ_ξ and standard deviation σ_ξ in dB. μ is the path loss exponent, in which μ = 2 is considered in our work. If we consider the shadowing to be taken as different values for the users at different elevation angles, the analysis will become too complicated. Thus, we assume the shadowing varies only with the region in which the user is. This means the value of shadowing for the users within the reference cell (at the nadir) is smaller than that within the other cell inside the coverage of the reference platform. Moreover, shadowing of the users within the coverage of the reference platform is smaller than that within the overlapped region.

It is reasonable that the total MAI component can be approximated as a Gaussian random variable when the number of users in each cell (N) is become large. Therefore, the mean of total MAI (I) component normalized to P_0 (I/P_0) can be expressed as

$$\mu_I = \psi\left[c_1\left(N-1+\sum_{(i,j,k)}\gamma_{ijk}^2\right) + c_2\sum_{(i,j,k)}(r'_{ijk}/r_{ijk})^2\gamma_{ijk}^2\right], \quad (6.12)$$

where

$$c_1 = E[e^{\delta}] = Ae^{\alpha^2\sigma_s^2} - Ae^{\alpha^2\sigma_{us}^2} + e^{\alpha^2\sigma_{us}^2}, \quad (6.13)$$

is the expectation value to account power control imperfection of both shadowed users and unshadowed users with standard deviation σ_s and σ_{us}, respectively.

$$c_2 = E[\chi_{ijk}^2]/\left(r'_{ijk}/r_{ijk}\right)^2 = A^2 e^{\alpha^2\sigma_\xi^2} + A(1-A)\frac{e^{\alpha\mu_\xi+\alpha^2\sigma_\xi^2/2}}{1+K} + A(1-A)e^{-\alpha\mu_\xi+\alpha^2\sigma_\xi^2/2}(1+K)+(1-A)^2, \quad (6.14)$$

is the parameter to account power control factor imperfection for the users within the overlapped region, where α=(ln10)/10 and the parameter of A is the shadowing probability.

Similarly, we can derive the variance of normalized MAI (I/P_0) and is given by the following expression

$$\sigma_I^2 = \psi\left[(d_1-\psi c_1^2)\left(N-1+\sum_{(i,j)}\gamma_{ijk}^4\right)+(d_2-\psi c_2^2)\sum_{(i,j,k)}(r'_{ijk}/r_{ijk})^4\gamma_{ijk}^4\right], \quad (6.15)$$

where

$$d_1 = E[(e^\delta)^2] = Ae^{2\alpha^2\sigma_s^2} - Ae^{2\alpha^2\sigma_{\mu s}^2} + e^{2\alpha^2\sigma_{\mu s}^2}, \quad (6.16)$$

and

$$d_2 = E[\chi_{ijk}^4]/\left(r'_{ijk}/r_{ijk}\right)^4 = A^2 e^{4\alpha^2\sigma_\xi^2} + A(1-A)\frac{e^{2\alpha\mu_\xi+2\alpha^2\sigma_\xi^2}}{1+K} + A(1-A)e^{-2\alpha\mu_\xi+2\alpha^2\sigma_\xi^2}(1+K)^2+(1-A)^2, \quad (6.17)$$

Both d_1 and d_2 are the second moment to account power control imperfection for the users within the coverage of the reference platform and within the overlapped region, respectively.

Based on the definition in (6.5), we can express the outage probability for the reverse link SPF CDMA as

$$P_{out} = \Pr\left\{\frac{W}{R}\frac{e^{\delta_{i_0j_0k_0}}}{I_{intra}/P_0 + I_{interr}/P_0 + \eta/P_0} \le \left(\frac{E_b}{N_0}\right)_{req}\right\} = \Pr\{I_{intra}/P_0 + I_{interr}/P_0 \ge \varsigma\}, \quad (6.18)$$

where

$$\varsigma = \frac{W}{R}\left[\frac{e^{\delta_{i0,j0,k0}}}{(E_b/N_0)_{req}} - \frac{1}{E_b/\eta_0}\right], \tag{6.19}$$

where E_b/η_0 is the bit energy-to-AWGN spectral density ratio. Since the Gaussian distribution of $(I_{intra}+I_{inter})/P_0$ with mean μ_I and variance σ_I^2, we can obtain the outage probability conditioned on the power control error of the user-of-interest, $e^{\delta_{i0,j0,k0}}$, as expressed by

$$P_{out}|\delta = \frac{1}{2}erfc\left(\frac{\varsigma - \mu_I}{\sqrt{2\sigma_I^2}}\right), \tag{6.20}$$

where $erfc(\lambda)$ is the error function given by

$$erfc(\lambda) = 1 - \int_0^{\lambda} \frac{2}{\sqrt{\pi}} \exp\left(-x^2\right) dx\,. \tag{6.21}$$

6.4 Numerical Result

The CDMA capacity is determined by evaluating (6.20) numerically for different parameters. We evaluate the system capacity in the reverse link for two different classes in 3G mobile services as presented in Table 6.1.

Table 6.1

QoS parameters for 3G multimedia services that we used in the analysis.

R [kbps]	Typical Application	Min. Required $(E_b/N_0)_{req}$ [dB]
12.2	Speech	5
144	Real-time data	1.5

We assume all the numerical results obtained in this contribution refer to a voice activity factor of 3/8. We also set the total bandwidth W = 5 MHz and the bit energy-to-AWGN spectral density ratio E_b/η_0 = 20 dB. We choose the probability of shadowing (A) is 0.3, and we use the Rice factor (K), which was obtained from our experiment result for the case

of SPF channel presented in [97]. The PCE standard deviation for unshadowed users (σ_{us}) is assumed 1 dB.

6.4.1 Capacity for Single SPF Model

We evaluate the effect of multiple access interference in a single SPF model by at first calculating other-cell interference factor. The other cell interference factor is defined as the interference power produced by the users belonging to the other cells divided by that produced by the users within the reference cell. Table 2 demonstrates simulation result of the mean value of the other cell interference for different power control error standard deviation (σ_s). It can be observed that the other cell interference factor is increased as the power control error becomes large.

In Figure 6.2 and 6.3 the outage probability is plotted for the situation of perfect power control and imperfect power control with the information bit rate of 12.2 kbps (speech) and 144 kbps (real-time data), respectively. It is clear that the system capacity heavily depends on the accuracy of power control scheme. If the perfect power control could be achieved, the number of users per cell supported at $P_{out} = 10^{-2}$ would be 93 users for speech and 17 users for real-time data. If the assumption of perfect power control is not held, the values of N will decrease dramatically. The system capacity drops by at least 17% and 20% every 1 dB increase in PCE standard deviation for speech and real-time data services, respectively.

Table 6.2

Mean value of the other cell interference factor for single SPF model.

PCE Standard deviation (σ_s)	R = 12.2 kbps	R = 144 kbps
0 dB	0.24	0.26
1 dB	0.32	0.35
2 dB	0.39	0.43
3 dB	0.48	0.52

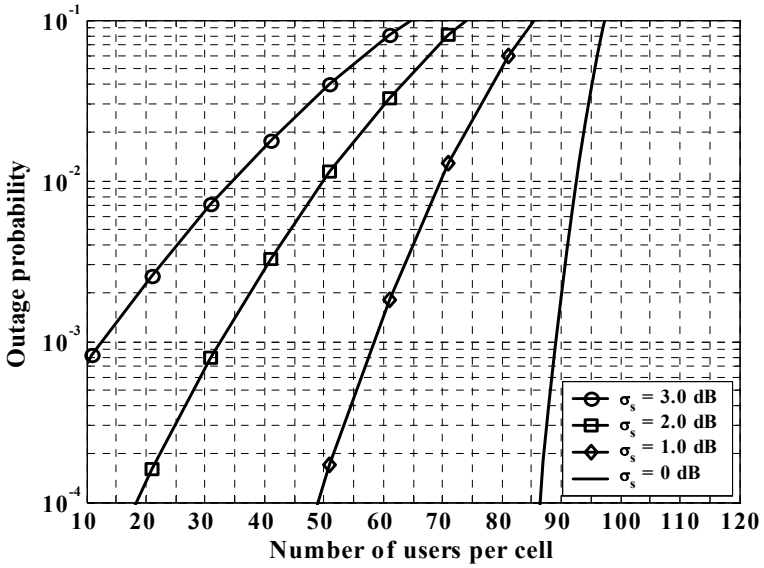

Figure 6.2 Effect of PCE standard deviation on the outage probability for a single SPF CDMA model (R = 12.2 kbps, E_b/N_0 = 5.0 dB).

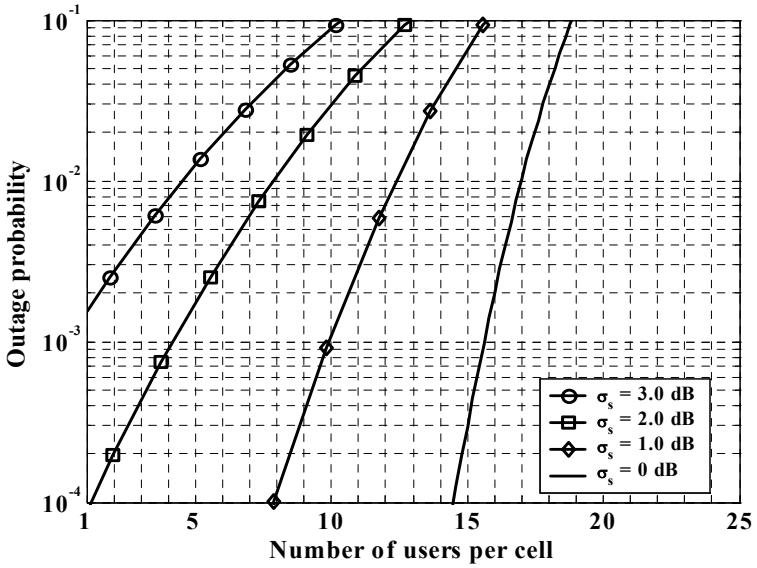

Figure 6.3 Effect of PCE standard deviation on the outage probability for a single SPF CDMA model (R = 144 kbps, E_b/N_0 = 1.5 dB).

6.4.2 Capacity for Multiple SPF Model

Now let we evaluate the system capacity for a model of multiple SPF. For the SPF constellation we considered, when the minimum elevation angle is 10^0, the mean values of the other cell interference factor for the overlapped region is found 0.11. This value must be taken into account with the interference from the other cell within the coverage of the

reference platform. In this model, PCE standard deviation (σ_s) is considered to vary every 0.5 dB so as to represent small variation of the power control imperfection. As a result, in Figure 6.4 and 6.5 the outage probability is plotted for different class of services. Compared with the result obtained for single SPF model, if perfect power control can be achieved, the number of users supported at $P_{out} = 10^{-2}$ would reduce by at least 14% for speech services and 12% for real-time data. This capacity reduction in multiple SPF model is because of the interference from the users within the overlapped region belonging to the nearest adjacent platform. This amount of capacity reduction is not trivial in the particular system when the bandwidth is very critical.

One approach to solve this problem is to increase the minimum elevation angle of the platform's coverage. This scheme is able to reduce the size of the overlapped region so that additional interference from this region can be decreased. In Figure 6.6 we demonstrate that the system capacity, i.e. for speech services, can be improved by increasing the minimum elevation angle defined for each platform. The system capacity can be increased so as become close to the capacity of single SPF model if the minimum elevation angle changes from 10^0 to 20^0. However, such scheme would increase the number of platforms in the constellation that are required in order to provide global coverage.

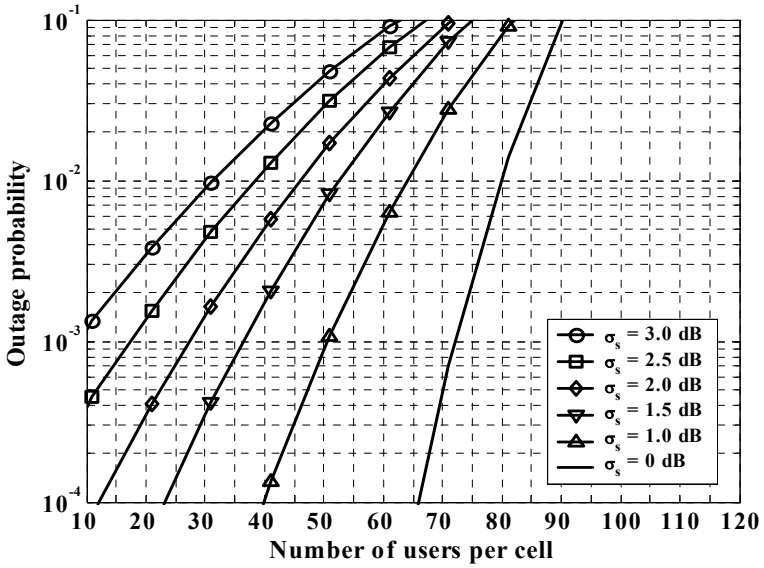

Figure 6.4 Effect of PCE standard deviation on the outage probability for a multiple SPF CDMA model (R = 12.2 kbps, E_b/N_0 = 5.0 dB, minimum elevation angle 10^0).

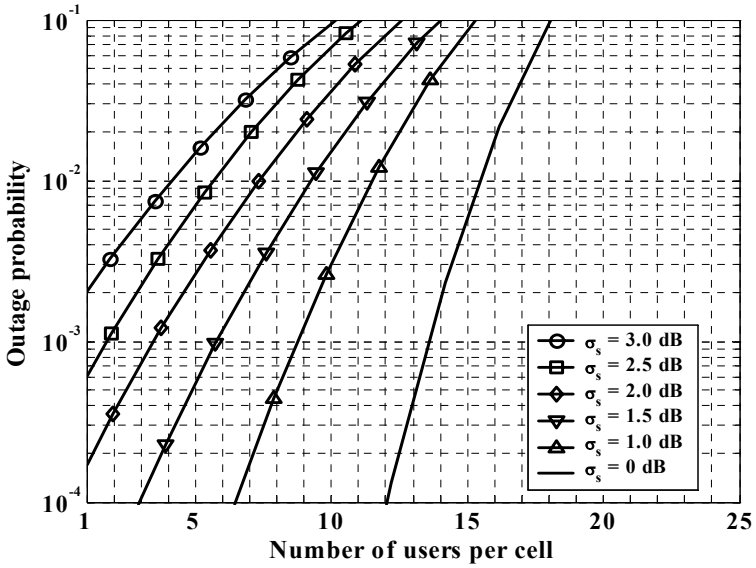

Figure 6.5 Effect of PCE standard deviation on the outage probability for a multiple SPF CDMA model (R = 144 kbps, E_b/N_0 = 1.5 dB, minimum elevation angle 10^0).

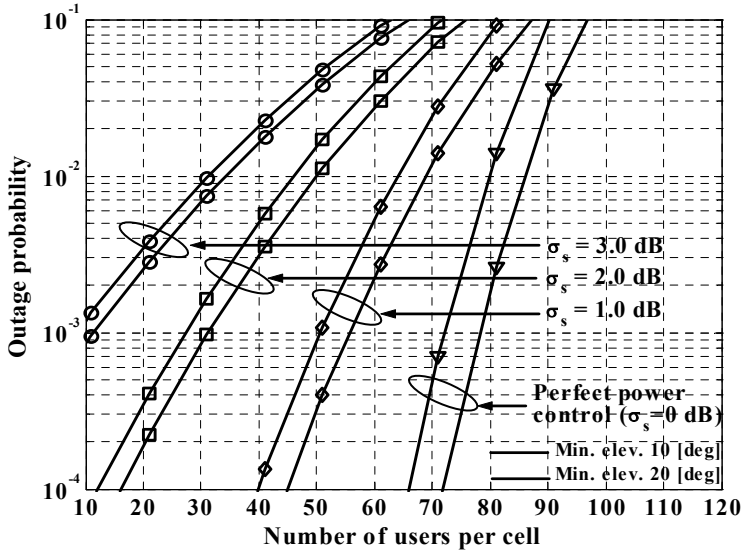

Figure 6.6 Effect of PCE standard deviation on the outage probability for a multiple SPF CDMA model (R = 12.2 kbps, E_b/N_0 = 5.0 dB and min. elevation angle 10^0 and 20^0)

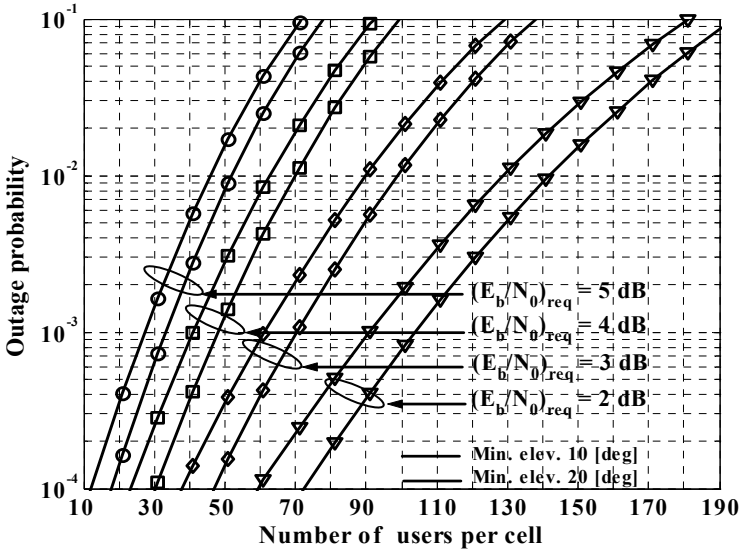

Figure 6.7 Effect of E_b/N_0 on the outage probability for a multiple SPF CDMA model (R = 12.2 kbps, σ_s = 2 dB and min. elevation angle 10^0 and 20^0)

The specification of $(E_b/N_0)_{req}$ is another parameter that affecting the system capacity. The influence of $(E_b/N_0)_{req}$ on the system capacity is illustrated in Figure 6.7. From the figure, we observe that the system capacity is increased significantly by decreasing the required threshold of E_b/N_0. In a multiple SPF model with the minimum elevation angle 10^0, the system capacity will increase by at least 30% at $P_{out} = 10^{-2}$ for every 1 dB decrease in $(E_b/N_0)_{req}$. When the minimum elevation angle increases to 20^0, a proportional increasing in capacity can also be obtained by decreasing the value of $(E_b/N_0)_{req}$.

6.5 Capacity Performance with Adaptive Antenna Arrays

We have considered CDMA capacity in SPF system, which is equipped with multi-beam phased array antenna whose radiation pattern characteristics follow the reference model specified in [9]. The array antenna that we used has a static beam and the results have indicated that the interference from users outside the reference cell is attenuated by the spot beam antenna characteristics. Interference level is found not trivial because the desired spot beam antenna suffers from the power gain of the users outside the reference cell. In this condition the users in each cell outside the reference cell must have an additional in power to equalize the received power at their own spot beam antenna due to the distribution of the antenna gain over a cell region is not uniform. If user (i, j, k) has an off-boresight angle

$\theta_{ijk}^{(j)}$ relative to his own spot beam, the additional power gain is then proportional to $1/G_j(\theta_{ijk}^{(j)})$, where $G_j(\theta)$ is the *j*th spot beam antenna gain.

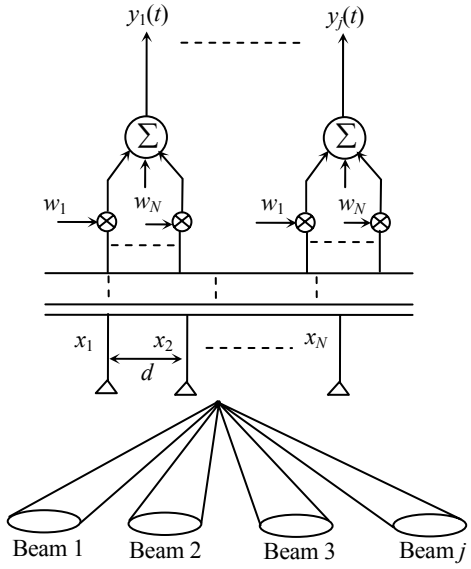

Figure 6.8 System model for SPF adaptive antenna.

It is possible to implement flexible beam steering that is intended for each of the user terminals by means of adaptive array antennas onboard the platform [92]. It represents the special cases of cellular communication in the sense of that all base stations are co-located in one platform and operated in a free space environment. The latter case is associated with that there is no scatterers present, and where the wave arriving at the array can be represented by simple plane waves with constant amplitude. Therefore the propagation channel between users and base stations antenna depends only on the direction of the wave arrival. In such a case the propagation channel is given by a steering vector whose components are the relative phases and amplitudes of a single wave at each of the antenna elements. This following sub-section aims at evaluating the SPF CDMA capacity under the condition of employing adaptive antenna.

6.5.1 Adaptive Antenna Model for the SPF

When adaptive antenna arrays are employed at the base station, directional beams can be formed to the desired user to reduce the interference level by allowing users to transmit lower power. Figure 6.8 shows a model of linear adaptive array antenna onboard the platform. The array is having *L* elements with a spacing of *d* and generates *j* receiving

beams. The arrays response in any direction is found by calculating the magnitude of the array output y when the channel is set to the array vector for that direction as expressed by

$$y = \vec{w}_{opt}^{H} \bullet \vec{x}, \tag{6.22}$$

where $\vec{x}$ is the array response vector which is a function of direction of arrival (θ) of each element. $\vec{w}_{opt}^{H}$ represents the transpose complex conjugate of an optimum value of adaptive weight vector, which is associated with each user (i, j, k). For an array of L elements at the base station, the array response vector $\vec{x} = \vec{a}(\theta)$ is an L x 1 vector expressed as

$$\vec{x} = \vec{a}(\theta) = \left[a_1, a_2, a_3, ..., a_L\right]^T, \tag{6.23}$$

where for mth element the array response is

$$a_m = \exp\left(-i\frac{2\pi}{\lambda} m d \sin\theta\right) = \exp\left(-ikmd\sin\theta\right). \tag{6.24}$$

It is then possible to direct the maximum gain of the array factor in the desired direction by adjusting the weight vector. We used well-known correlation matrices of the received signal to compute the direction-of-arrival [102] rather than the sub-space algorithms of direction finding, such as MUSIC or ESPRIT. This is because the number of users, in SPF CDMA system, usually exceeds the number of antenna array elements due to the space limitation onboard the platform for the array size. After getting the weight vector for the user-of-interest, $w_{i_0 j_0 k_0}$, then the power discrimination factor γ_{ijk}^2 in (6.10) has to be modified and is given by

$$\gamma_{ijk}^2 = \left| w_{i_0 j_0 k_0}^{H} \, a\left(\theta_{ijk}^{j_0}\right) \right|^2. \tag{6.25}$$

6.5.2 Capacity with Adaptive Antenna

In order to estimate CDMA capacity by employing adaptive antennas, we use the same specification of parameters as used in section 4. In this sub-section, however, we assume that a directional beam in the direction of desired user is formed by adaptive algorithms, which also cover the reference cell. Sidelobes level is assumed to exist with a certain level much lower than the main lobe. For comparison purposes, fixed multi-beam antenna

radiation pattern adopted by ITU is also considered. Voice with the information bit rate of 12.2 kbps in a single SPF model and multiple SPF model is calculated under the standard deviations of power control error 2.0 dB and 1.0 dB for shadowed and unshadowed users, respectively, is considered.

Figure 6.9 shows numerical results with the comparison of using original array antenna proposed in [9] and adaptive antenna with various sidelobes level for a single SPF model. It is found that for 10^{-2} outage probability, about 50 users can be supported in each cell when the fixed multi-beam antenna is employed. When adaptive antenna with the sidelobe level of 30 dB lower than the maximum gain is employed, the number of users supported in the system increase up to 58 users per cell. A slightly improved in capacity is observed due to a little difference of the sidelobe level between fixed antenna and adaptive antenna. When the sidelobe level of adaptive antenna is increased, however, the capacity is improved significantly. For example the system capacity can reach 78 users per cell when the sidelobe level is –35 dB. Furthermore, if the sidelobe level can be decreased to –40 dB and –45 dB, the number of users per cell will go up greatly to 10^{0} and 138 users, respectively.

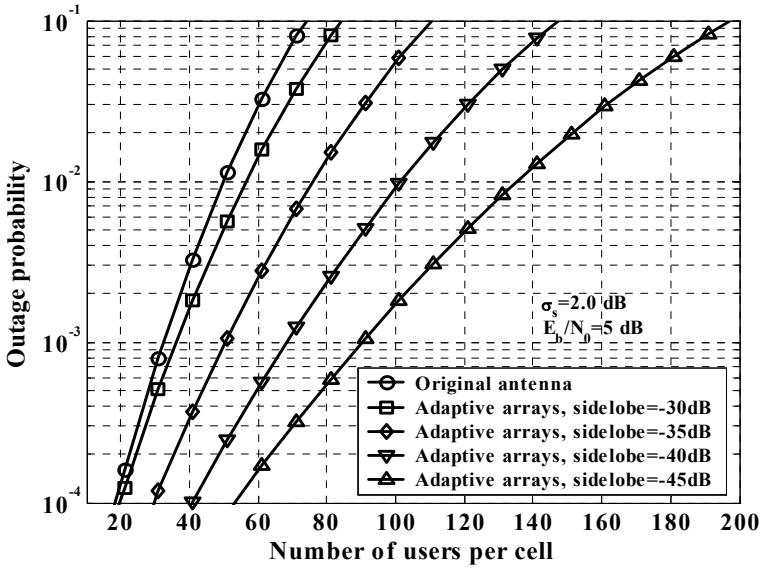

Figure 6.9 Effect of adaptive antenna on the outage probability for single SPF CDMA model with different sidelobe level (R = 12.2 kbps, σ_s = 2 dB, min. elevation angle 10^{0}).

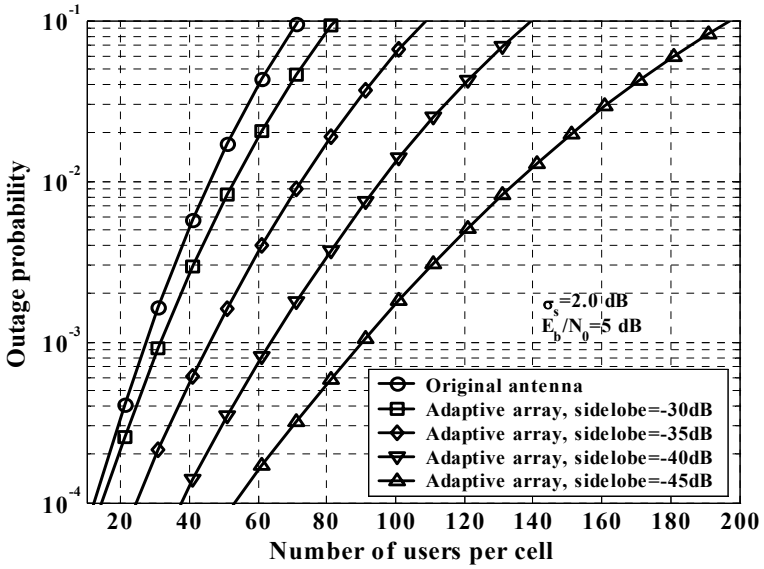

Figure 6.10 Effect of adaptive antenna on the outage probability for multiple SPF CDMA model with different sidelobe level (R = 12.2 kbps, σ_s = 2 dB, min. elevation angle 10^0).

Figure 6.10 demonstrates the capacity improvement by using adaptive antenna in multiple SPF model. The tendency of capacity improvement because of the usage of adaptive antenna is similar as of in the single SPF model. Moreover, when the adaptive antenna with sidelobe of –45 dB is employed, we found that the capacity for multiple SPF model is equal with that of the capacity for single SPF model. This is because an adaptive antenna can work properly to suppress the interference produced by the users outside the reference coverage of the desired platform.

6.6. Summary

This chapter has demonstrated an analysis of the reverse link CDMA system capacity in a multispot beam SPF environment. All possible multiple access interference including the effects of channel fading and shadowing are addressed in order to evaluate the system capacity. We utilized the proposed Rise fading model for SPF that we obtained in terms of K presented in Chapter 3 to account multiple access interference in the analysis.

The system capacity of a single SPF model and multiple SPF model is evaluated in terms of the outage probability requirement. We considered the power control imperfection in the analysis due to the fact that there is no practical perfect power control even though for the

LOS condition. It is found that because of the effect of imperfect power control, the system capacity for both models is significantly reduced.

In multiple SPF model, multiple access interference produced by the users within an overlapped region is also nontrivial reduction of the system capacity. Therefore, the capacity reduction caused by these users has to be compensated. One solution is to increase the minimum elevation angle defined for each platform's coverage. For the model we consider, with the setting of minimum elevation angle is 20^0, the system capacity can be improved so as nearly as the capacity brought by the single SPF model.

However, the increasing of minimum elevation angle means the required number of platform is also increased to cover global coverage. For the reason, adaptive antenna has been proposed in this study to solve the system capacity reduction problem due to the interference produced by the users within the other cell. The improvement in the capacity can be achieved depending on the setting of sidelobe level of the adaptive array antenna.

Chapter 7

Conclusion and Future Work

7.1 Conclusion

Limitation possessed by conventional wireless terrestrial and satellite systems has prompted researchers to seek a new alternative wireless delivery method. SPF is found to be the most promising candidate because it has many advantages over the existing wireless technology. We have provided a brief overview of SPF communication in comparison to terrestrial and satellite system. Some advantages over the existing wireless system are highlighted. However, there are some important things that still significant to be investigated in order this novel technology becomes into real. One of the most important things is investigation to the channel characteristic as a fundamental requirement for a proper system design of wireless communication employing this novel technology.

We have shown the SPF channel characteristic both in semi-urban as well as in urban low rises environment. In semi-urban environment, we proposed a definition and describe an analysis of the SPF channel model that is based on field experiment in which the situation is mostly dominated by LOS propagation. We then characterize the channel and the result shows that Ricean fading channel is a proper model because the presence of LOS situation in many places in the measurement. For the environment in which the measurement is

conducted, we found that Rice factor (K) is a function of elevation angle and frequency carrier. Based on that channel model, we also found by computer simulation that the channel performance under DPSK and DQPSK modulation scheme for elevation angle greater than 40^0 yields better performance. This channel characteristic may only be valid to an environment, which there is no obstacle between SPF and the user on the ground.

In Chapter 4, we have evaluated radio propagation loss of communication link between SPF and user in urban low rises environment, in which propagation path is often blocked by obstacles, i.e. by the buildings. By using well-known ray tracing technique, propagation loss is evaluated under various elevation and azimuth angles. This various conditions are intended to represent the many situations of the users in a way of looking to the SPF because of the street orientation on the ground. Result of evaluation using ray tracing technique is then compared with another technique for verification. This technique is called physical-statistical method. Both ray tracing technique and physical-statistical methods show a good agreement in propagation loss evaluation. Another important parameter of wireless system design is power consumption. This is estimated by using link budget analysis taking example that the SPF delivers IMT-2000 services to the mobile users on the ground. It is shown that elevation and azimuth angles are important parameters to estimate the power. We found from simulation that because of small elevation angle, i.e. lower than 20^0 and azimuth angle is 90^0, the power consumption is too high and therefore it might be impossible in the SPF scenario.

Bit error rate probability is another parameter in a wireless system design. We have therefore evaluated the downlink performance of the SPF communication link for the area of urban low rises environment in Chapter 5. At this time, however, we used different building geometry model from the one used in Chapter 4. Results of propagation parameters evaluated by ray tracing algorithm is then utilized in the downlink BER estimation. The BER curve is plotted as a function of elevation angle for five categories of information bit rate employed in 3G IMT-2000 services. It is shown in low elevation angle (NLOS situation) such as lower than 20^0, the communication link fails or the performance is very poor in all azimuth angles for an information bit rate equals or greater than 384 kbps. On the other hand, in LOS situation such as elevation angle greater than 45^0, it is shown an error floor in the BER curves due to the presence of multipath components. The

downlink channel performance cannot be improved for wide band signals, i.e. 2 Mbps information bit rate, due to selectivity of the channel.

In Chapter 6, by using channel model proposed in Chapter 4, we have presented CDMA capacity analysis in multibeam and multiple SPF. Analysis is performed under comprehensive multiple access interference considering fading, shadowing and imperfect power control. We examine a reverse link capacity of CDMA system employing single and multiple SPF model in terms of outage probability as a function of number of users. It is shown in multiple SPF model that the users in overlapped region, which power controlled by adjacent platform, have non-trivial contribution of interference to the reference platform. The increasing of minimum elevation angle is then proposed as a solution to reduce interference effects generated by these users. The method shows very effective, however the number of the SPF might be increased because of the coverage area become smaller. This problem, therefore, would be not only costly but also environmentally unacceptable. To cope with this problem we proposed to use adaptive antenna array onboard the platform without need to increase the minimum elevation angle. This technique shows to be very effective so that the capacity of multiple SPF is increased approaching to the capacity of single SPF.

7.2 Future Work

There are several issues that have not been considered in this study and therefore need to be further investigated. In Chapter 3, Rice factor (K) is estimated using the method that ignores the noise. In real implementation, it needs to include noise in estimation of K in order to improve the accuracy of channel characterization for the SPF communication. Additionally, in this chapter channel performance evaluation has been assumed under the condition that the SPF stays in fixed position and MS moves slowly. Therefore, the channel is modeled under slow and flat fading channel. In real system, wind in the stratosphere may drift the SPF to move and also MS on the ground may have certain velocity so that the performance evaluation should be made under fast and frequency selective fading channel.

Ray tracing technique is employed in Chapter 4 and 5 with neglecting the diffraction from vertical corner of the building under test. In low elevation angle, however, this mechanism

has important contribution to improve the accuracy of propagation estimation using ray tracing. Moreover, wide band channel information such as power delay profile is a foremost channel modeling nowadays and possible to be predicted by using ray tracing algorithm. It might become an interesting topic as the SPF channel model has been scarcely addressed in the literature especially in a wideband channel modeling.

Finally, the material presented in this thesis is mainly based on the experiment when the SPF is not in actual position as it is intended in real implementation. In short years to come, the channel modeling should be made not only by simulation but also it has to be proven by using a real data measurement obtained from the SPF at actual position in the stratosphere.

Bibliography

[1] William C.Y. Lee, *Mobile Communications Design Fundamentals*. New York: John Wiley & Sons, 1993.

[2] B. Walke, P. Seidenberg, M. P. Althoff, *UMTS The Fundamentals*. New Jersey: John Wiley & Sons, 2003.

[3] Theodore S. Rappaport, *Wireless Communications Principles & Practice*. New Jersey: Prentice Hall PTR, 1996.

[4] Dennis Roddy, *Satellite Communications*. New York: McGraw-Hill, 2001.

[5] Michael O. Kolawole, *Satellite Communication Engineering*. New York: Marcel Dekker, 2002.

[6] Ray E. Sheriff and Y. Fun Hu, *Mobile Satellite Communication Networks*. West Sussex England: John Wiley & Sons, 2001.

[7] G. M. Djuknic, J. Freidenfelds, and Y. Okunev, "Establishing wireless communications services via high altitude aeronautical platforms: A concept whose time has come?," *IEEE Communications Magazine*, vol. 35, no. 9, pp. 128-135, September 1997.

[8] R. Miura and M. Oodo, "Wireless communications system using stratospheric platforms," *Journal of Communications Research Laboratory*, vol. 48, no. 4, pp. 33-48, 2001.

[9] "Minimum performance characteristics and operational conditions for high altitude platform stations providing IMT-2000 in the bands 1885-1980 MHz, 2010-2025 MHz, and 2110-2170 MHz in the Regs. 1 & 3 and 1885-1980 MHz and 2110-2160 MHz in Reg. 2," *ITU-R M. 1456*, 2000.

[10] "Preferred characteristics of systems in the fixed service using high altitude platform stations operating in the bands 47.2-47.5 GHz and 47.9-48.2 GHz," *Recommendation ITU-R F.1500*, 2000.

[11] M. Oodo, R. Miura, T. Hori, T. Morisaki, K. Kashiki, M. Suzuki, "Sharing and compatibility study between fixed service using high altitude platform stations (HAPS) and other services in the 31/28 GHz bands," *Wireless Personal Communications*, vol. 23, pp. 3-14, 2002.

[12] ITU, Radio Regulations, Articles 1, no. 1-66A, 1998.

[13] http://www2.nict.go.jp/mt/b181/english/link-e.html

[14] http://www.capanina.org/

[15] http://www.skytowerglobal.com/begin.html

[16] http://www.kari.re.kr/

[17] http://www.etri.re.kr/

[18] M. Oodo, H. Tsuji, R. Miura, M. Maruyama, and M. Suzuki, "Experiment of IMT-2000 using stratospheric flying solar-powered airplane," in *Proceedings IEEE Global Telecommunication Conference* (*GLOBECOM*), vol. 2, December 2003, pp. 1152-1156.

[19] M. Oodo, R. Miura, T. Hori, T. Morisaki, K. Kashiki, and M. Suzuki, "Sharing and compatibility study between fixed service using high altitude platform stations (HAPS) and other services in the 31/28 GHz bands," *Wireless Personal Communications*, vol. 23, pp. 3-14, 2002.

[20] R. Miura, M. Maruyama, M. Suzuki, H. Tsuji, M. Oodo, and Y. Nishi, "Experiment of telecom/broadcasting mission using a high-altitude solar-powered aerial vehicle pathfinder plus," in *Proceedings of the 5th International Symposium on Wireless Personal Multimedia Communications* (*WPMC*), vol. 2, October 2002, pp. 469-473.

[21] P. L. Rice, A. G. Longley, K. A. Norton, and A. P. Barsis, "Transmission loss predictions for tropospheric communication circuits," *NBS Tech Note 101*; two volumes; issued May 7, 1965.

[22] A. G. Longley and P. L. Rice, "Prediction of tropospheric radio transmission loss over irregular terrain; A computer method," *ESSA Technical Report*, ERL 79-ITS 67, 1968.

[23] A. G. Longley, "Radio propagation in urban areas," *OT Report*, pp. 78-144, 1978.

[24] R. Edward and J. Durkin, "Computer prediction of service area for VHF mobile radio networks," *Proceedings of the IEE*, vol. 116, no. 9, pp. 1493-1500, 1969.

[25] C. E. Dadson, J. Durkin, and E. Martin, "Computer prediction of field strength in the planning of radio systems," *IEEE Transactions on Vehicular Technology*, vol. 24, no. 1, pp. 1-7, February 1975.

[26] T. Okumura, E. Ohmori, and K. Fukuda, "Field strength and its variability in VHF and UHF land mobile services," *Review Electrical Communication Laboratory*, vol. 16, no. 9-10, pp. 825-873, September-October 1968.

[27] M. Hata, "Empirical formula for propagation loss in land mobile radio services," *IEEE Transactions on Vehicular Technology*, vol. 29, no. 3, pp. 317-325, August 1980.

[28] European Cooperation in the Field of Scientific and Technical Research EURO-COST 231, "Urban transmission loss models for mobile radio in the 900 and 1800 MHz bands," *Revision 2*, *The Hague*, September 1991.

[29] J. Walfisch and H. L. Bertoni, "A theoretical model of UHF propagation in urban environments," *IEEE Transactions on Antennas and Propagation*, vol. 36, no. 12, pp. 1788-1796, October 1988.

[30] M. J. Feuerstein, K. L. Blackard, T. S. Rappaport, S. Y. Seidel, and H. H. Xia, "Path loss, delay spread, and outage models as functions of antenna height for microcellular system design," *IEEE Transactions on Vehicular Technology*, vol. 43, no. 3, pp. 487-498, August 1994.

[31] R. M. Barts and W. L. Stutzman, "Modeling and simulation of mobile satellite propagation," *IEEE Transactions on Antennas and Propagation*, vol. 40, no. 4, pp. 375-382, April 1992.

[32] L. Ippolito, "Millimeter wave propagation measurements from the applications technology satellite (ATS-V)," *IEEE Transactions on Antennas and Propagation*, vol. 18, no. 4, pp. 535-552, July 1970.

[33] M. J. Miller, B. Vucetic, and L. Berry, *Satellite Communications; Mobile and Fixed Services*. Norwell, Massachusetts: Kluwer Academic Publisher, 1993.

[34] W. J. Vogel and J. Goldhirsh, "Mobile satellite system propagation measurements at L-band using MARECS-B2," *IEEE Transactions on Antennas and Propagation*, vol. 38, no. 2, pp. 259-264, February 1990.

[35] E. Lutz, D. Cygan, M. Dippold, F. Dolainsky, and W. Papke, "The land mobile satellite communication channel-recording, statistics, and channel model," *IEEE Transactions on Vehicular Technology*, vol. 40, no. 2, pp. 375-386, May 1991.

[36] K. P. Phillips, "An overview of propagation factors influencing the design of mobile satellite communication systems," *IEE Electronic and Communication Engineering Journal*, vol. 9, no. 6, pp. 281-288, December 1997.

[37] F. Dovis, R. Fantini, M. Mondin, and P. Savi, "Small-scale fading for high altitude platform (HAP) propagation channels," *IEEE Journal on Selected Areas in Communications*, vol. 20, no. 3, pp. 641-647, April 2002.

[38] S. Shimamoto, T. Mikoshiba, S. Takakusagi, M. Hayashi, and H. Shiba, "Performance evaluations of communication systems employing stratospheric aircrafts and LEO satellites," *IEICE Transactions on Communications*, vol. E81-B, no. 12, pp. 2343-2350, December 1998.

[39] S. R. Saunders, *Antennas and Propagation for Wireless Communication Systems*. New York: John Wiley & Sons, 1999.

[40] M. Patzold, *Mobile Fading Channels*. New York: John Wiley & Sons, 2000.

[41] K. K. Talukdar and W. D. Lawing, "Estimation of the parameters of the Rice distribution," *Journal of Acoustical Society of America*, vol. 89, no. 3, pp. 1193-1197, 1991.

[42] John G. Proakis, *Digital Communications*. New York: McGraw Hill, 2000.

[43] COST 231 Final report, "Digital mobile radio: COST 231 view on the evolution towards 3rd generation systems," *Commission of the European Communities and COST Telecommunications*, Brussels, 1999.

[44] K. Low, "Comparison of urban propagation models with CW-measurements," in *Proceedings of IEEE Vehicular Technology Conference*, vol. 2, May 1992, pp. 936-942.

[45] M. F. Ibrahim and J. D. Parsons, "Signal strength prediction in built-up areas," in *Proceedings IEE*, 130F (5), 377-384, 1983.

[46] K. Allsebrook and J. D. Parsons, Mobile radio propagation in British cities at frequencies in the VHF and UHF bands," *IEEE Transactions on Vehicular Technology*, vol. 26, no. 4, pp. 313-323, November 1997.

[47] G. Y. Delisle, J. -P. Lefevre, M. Lecours, J. -Y. Chouinard, "Propagation loss prediction: A comparative study with application to the mobile radio channel," *IEEE Transactions on Vehicular Technology*, vol. 34, no. 2, pp. 86-96, May 1985.

[48] F. Ikegami, T. Takeuchi, and S. Yoshida, "Theoretical prediction of mean field strength for urban mobile radio," *IEEE Transactions on Antennas and Propagation*, vol. 39, no. 3, pp. 299-302, March 1991.

[49] S. R. Saunders, and F. R. Bonar, "Prediction of mobile radio wave propagation over buildings of irregular heights and spacings, *IEEE Transactions on Antennas and Propagation*, vol. 42, no. 2, pp. 137-144, February 1994.

[50] S. R. Saunders, and F. R. Bonar, "Explicit multiple building diffraction attenuation function for mobile radio wave propagation," *IEE Electronics Letters*, vol. 27, no. 14, pp. 1276 – 1277, July 1991.

[51] S. Y. Seidel and T. S. Rappaport, "Site-specific propagation prediction for wireless in-building personal communication system design," *IEEE Transactions on Vehicular Technology*, vol. 43, no. 4, pp. 879 – 891, November 1994.

[52] W. Honcharenko, H. L. Bertoni, J. L. Dailing, J. Qian, and H. D. Yee, "Mechanisms governing UHF propagation on single floors in modern office buildings," *IEEE Transactions on Vehicular Technology*, vol. 41, no. 4, pp. 496 – 504, November 1992.

[53] W. K. Tamand V. N. Tran, "Propagation modeling for indoor wireless communication," *IEE Electronics & Communication Engineering Journal*, vol. 7, no. 5, pp. 221 – 228, October 1995.

[54] J. W. Mckown and R. L. Hamilton, Jr., "Ray tracing as a design tool for radio networks," *IEEE Network Magazine*, vol. 5, no. 6, pp. 27-30, Nov. 1991.

[55] S. Y. Tan and H. S. Tan, "A theory for propagation path-loss characteristics in a city-street grid," *IEEE Transactions on Electromagnetic Compatibility*, vol. 37, no. 3, pp. 333-342, August 1995.

[56] S. Y. Tan and H. S. Tan, "Improved three-dimension ray tracing technique for microcellular propagation," *IEE Electronics Letters*, vol. 31, no. 17, pp. 1503-1505, August 1995.

[57] S. Y. Tan and H. S. Tan, "Propagation model for microcellular communications applied to path loss-measurements in Ottawa city streets," *IEEE Transactions on Vehicular Technology*, vol. 44, no. 2, pp. 313-317, May 1995.

[58] K. Rizk, J. F. Wagen, and F. Gardiol, "Two-dimensional ray tracing modeling for propagation prediction in microcellular environments," *IEEE Transactions on Vehicular Technology*, vol. 46, no. 2, pp. 508-518, May 1997.

[59] G. Liang and H. L. Bertoni, "A new approach to 3-D ray tracing for propagation prediction in cities," *IEEE Transactions on Antennas and Propagation*, vol. 46, no. 6, pp. 853-863, June 1998.

[60] G. E. Athanasiadou, A. R. Nix, and J. P. McGeehan, "A microcellular ray tracing propagation model and evaluation of its narrow-band and wide-band predictions," *IEEE Journal on Selected Areas in Communications*, vol. 18, no. 3, pp. 322-335, March 2000.

[61] M. C. Lawton and I. P. McGeehan, "The application of a deterministic ray Launching algorithm for the prediction of radio channel characteristics in small-cell environments," *IEEE Transactions on Vehicular Technology*, vol. 43, no. 4, pp. 955-969, November 1994.

[62] J. McKown and R. L. Hamilton, "Ray tracing as a design tool for radio networks," *IEEE Network Magazine*, vol. 5, no. 6, pp. 27-30, November 1991.

[63] R. A. Valenzuela, "Ray tracing prediction of indoor radio propagation," in *Proceedings IEEE International Symposium on Personal, Indoor, and Mobile Radio Communications* (*PIMRC*), vol. 1, 1994, pp. 140-144.

[64] S. C. Kim, B. J. Guarino, T. M. Willis III, V. Erceg, S. J. Fortune, R. A. Valenzuela, L. W. Thomas, J. Ling and J. D. Moore, "Radio propagation measurements and prediction using three-dimensional ray tracing in urban environments at 908 MHz and 1.9 GHz," *IEEE Transactions on Vehicular Technology*, vol. 48, no. 3, pp. 931-946, May 1999.

[65] H. L. Bertoni, *Radio Propagation for Modern Wireless Systems*. New Jersey: Prentice Hall PTR, 2000.

[66] J. D. Kraus, *Electromagnetics*. New York: McGraw-Hill, 1984.

[67] J. B. Keller, "Geometric theory of diffraction," *Journal of the Optical Society of America*, vol. 52, pp. 116–130, 1962.

[68] R. G. Kouyoumjian and P. H. Pathak, "A uniform theory of geometric diffraction for an edge in a perfectly conducting surface," in *Proceedings of the IEEE*, vol. 62, pp. 1448–1461, November 1974.

[69] W. Honcharenko and H. L. Bertoni, "Prediction of wideband RF propagation characteristics in buildings using 2D ray tracing," in *Proceedings IEEE Vehicular Technology Conference*, vol. 1, July 1995, pp. 931-946.

[70] A. Falsafi, K. Pahlavan and Y. Ganning, "Transmission techniques for radio LAN's-a comparative performance evaluation using ray tracing," *IEEE Journal on Selected Areas in Communications*, vol. 14, no. 3, pp. 477-491, April 1996.

[71] H. Meng, P. Koushik and T. S. Rappaport, Comparative study of indoor and outdoor site-specific propagation prediction models," *Technical Report MPRG-TR-93-07*, Virginia Tech, February 1993.

[72] Yoshitomo Ishijima, *A Study on Mobile Communication for High Altitude Platform Station*. Master Thesis, Graduate School of Global Information and Telecommunication Studies, Waseda University, September 2002.

[73] F. Tila, P. R. Shepherd and S. R. Pennock, "2 GHz propagation and diversity evaluation for in building communications up to 4 MHz using high altitude platforms

(HAP)," in *Proceedings IEEE Vehicular Technology Conference*, vol. 1, 2001, pp. 121-125.

[74] S. R. Saunders and B. G. Evans, "A physical-statistical model for land mobile satellite propagation in built-up areas," in *Proceedings of the 10th IEE Antennas and Propagation Conference*, vol. 2, April 1997, pp. 44 – 47.

[75] Iskandar and Shigeru Shimamoto, "Urban site path loss prediction for mobile communications employing stratospheric platforms," in *Proceedings of the 8th IEEE International Symposium on Signal Processing and Its Application* (*ISSPA*), August 2005, pp. 267-270.

[76] Iskandar and Shigeru Shimamoto, "Ray tracing for urban site propagation in stratospheric platform mobile communications," in *Proceedings of the 11th IEEE Asia-Pacific Conference on Communications* (*APCC*), October 2005, pp. 212-216.

[77] Iskandar and Shigeru Shimamoto, "Prediction of propagation path loss for stratospheric platforms mobile communications in urban site LOS/NLOS environment," in *Proceedings IEEE International Conference on Communications* (*ICC*), vol. 12, June 2006, pp. 5643-5648.

[78] J. M. Park, D. S. Oh, Y. S. Kim and D. S. Ahn, "Evaluation of interference effect into cellular system from high altitude platform station to provide IMT-2000 service," in *Proceedings IEEE Global Telecommunication Conference* (*GLOBECOM*), vol. 1, December 2003, pp. 420-424.

[79] S. Masumura and M. Nakagawa, "Joint system of terrestrial and high altitude platform station (HAPS) cellular for W-CDMA mobile communication," *IEICE Transactions Communications*, vol. E.85, no. 10, pp. 2051-2058, October 2002.

[80] H. Holma and A. Toskala, *W-CDMA for UMTS: Radio Access for Third Generation Mobile Communications*. West Sussex, England: John Wiley and Sons, 2004.

[81] Y. F. Hu, R. E. Sheriff, E. Del Re, R. Fantacci, and G. Giambene, "Satellite-UMTS traffic dimensioning and resource management technique analysis," *IEEE Transaction on Vehicular Technology*, vol. 47, no. 4, pp. 1329-1341, November 1998.

[82] N. Efthymiou, Y. F. Hu and R. E. Sheriff, "Performance of intersegment handover protocols in an integrated space/terrestrial-UMTS environment," *IEEE Transactions on Vehicular Technology*, vol. 47, no. 4, pp. 1179 – 1199, November 1998.

[83] P. Taaghol, B. G. Evans, E. Buracchini, D. Gaudinaro G., J. H. Lee and C. G. Kang, "Satellite UMTS/IMT2000 W-CDMA air interfaces," *IEEE Communications Magazine*, vol. 37, no. 9, pp. 116-126, September 1999.

[84] E. Falletti, M. Mondin, F. Dovis and D. Grace, "Integration of a HAP within a terrestrial UMTS network: interference analysis and cell dimensioning," *Journal of Wireless Personal Communications*, vol. 24, pp. 291-325, 2003.

[85] Iskandar and Shigeru Shimamoto, "On the downlink performance of stratospheric platform mobile communications channel," in *Proceeding IEEE Global Telecommunications Conference* (*GLOBECOM*), November 2006.

[86] Iskandar and Shigeru Shimamoto, "On the performance of IMT-2000 communication link based on stratospheric platforms," *Indonesian Journal* (*Makara*) *series on Technology*, vol. 10, no. 1, pp. 1-10, April 2006.

[87] Iskandar and Shigeru Shimamoto, "Analysis of CDMA capacity for multiple stratospheric platform mobile communications under imperfect power control and fading," in *Proceedings IEEE Wireless Communications and Networking Conference* (*WCNC*), March 2007.

[88] S. Ohmori, Y. Yamao, and N. Nakajima, "The future generations of mobile communications based on broadband access technologies," *IEEE Communications Magazine*, vol. 38, no. 12, pp. 134-142, December 2000.

[89] D. Avagnina, F. Dovis, A. Ghiglione, and P. Mulassano, "Wireless networks based on high-altitude platforms for the provision of integrated navigation/communication services," *IEEE Communications Magazine*, vol. 40, no. 2, pp. 119-125, February 2002.

[90] T. C. Tozer and D. Grace, "High-altitude platforms for wireless communications," *IEE Electronics and Communication Engineering Journal*, vol. 13, no. 3, pp. 127-137, June 2001.

[91] J. Thornton, D. Grace, C. Spillard, T. Konefal, and T. C. Tozer, "Broadband communications from a high altitude platform: The European helinet programme," *IEE Electronics and Communication Engineering Journal*, vol. 13, no. 3, pp. 138-144, June 2001.

[92] M. Oodo, R. Miura, and Y. Hase, "On board DBF antenna for stratospheric platform," in *Proceedings IEEE Conference on Phased Array System and Technology*, May 2000, pp. 125-128.

[93] K. S. Gilhousen, I. M. Jacobs, R. Padovani, A. J. Viterbi, L. A. Weaver, Jr., and C. E. Wheatley III, "On the capacity of a cellular CDMA system," *IEEE Transactions Vehicular Technology*, vol. 40, pp. 303-312, May 1991.

[94] B. E. Jabu and R. Steele, "Cellular communications using aerial platforms," *IEEE Transactions Vehicular Technology*, vol. 50, no. 3, pp. 686-700, May 2001.

[95] Y. C. Foo, W. L. Lim, R. Tafajolli, and L. W. Barclay, "Other cell interference and reverse link capacity of high altitude platform station of CDMA system," *IEE Electronic Letters*, vol. 36, issue 22, pp. 1881-1882, October 2000.

[96] T. C. Hong, B. J. Ku, J. M. Park, and D. S. Ahn, "Reverse link capacity of the WCDMA system using high altitude platform stations," in *Proceedings IEEE Wireless Communications and Networking Conference* (*WCNC*), vol. 1, March 2005, pp. 195-200.

[97] Iskandar and Shigeru Shimamoto, "Channel characterization and performance evaluation of mobile communication employing stratospheric platform," *IEICE Transactions on Communications*, vol. E89-B, no. 3 pp. 937-944, March 2006.

[98] Iskandar and Shigeru Shimamoto, "The channel characterization and performance evaluation of mobile communication employing stratospheric platform," in *Proceedings IEEE/ACES Wireless Communications and Applied Computational Electromagnetics Conference* (*WCACEM*), April 2005, pp. 828-831.

[99] Iskandar and Shigeru Shimamoto, "The channel characterization of mobile communication employing stratospheric platform," in *Proceedings of the 12th International Conference on Telecommunication System–Modeling and Analysis* (*ICTSM*), July 2004, pp. 293-298.

[100] H. Fu, G. Bi and K. Arichandran, "Performance of multibeam CDMA-based LEO satellite systems with imperfect power control," *International Journal of Satellite Communications*, vol. 16, pp. 155-167, 1998.

[101] E. Lutz, "Other-cell interference in satellite power-controlled CDMA uplink," in *Proceedings of the 5th IEEE International Mobile Satellite Conference*, June 1997, pp. 83-88.

[102] Ami Harada, *Studies on Techniques for High-efficiency Frequency Utilization in Wireless Communication Systems*. PhD. Dissertation, Graduate School of Global Information and Telecommunications Studies, Waseda University, July 2004, Chapter 4.

Publications

Journal Papers

[1] Iskandar and Shigeru Shimamoto, "Channel characterization and performance evaluation of mobile communication employing stratospheric platform," *IEICE Transactions on Communications*, vol. E89-B, no. 3, pp. 937-944, March 2006.

[2] Iskandar and Shigeru Shimamoto, "On the performance of IMT-2000 communication link based on stratospheric platforms," *Indonesian Journal* (*Makara*) *Series on Technology*, vol. 10, no. 1, pp. 1-10, April 2006.

International Conferences

[3] Iskandar and Shigeru Shimamoto, "Analysis of CDMA capacity for multiple stratospheric platform mobile communications under imperfect power control and fading," in *Proceedings IEEE Wireless Communications and Networking Conference* (*WCNC*) *2007*, Hong Kong, China, March 2007.

[4] Iskandar and Shigeru Shimamoto, "On the downlink performance of stratospheric platform mobile communications channel," in *Proceedings IEEE Global Telecommunications Conference* (*GLOBECOM*) *2006*, San Francisco, USA, November 2006.

[5] Iskandar and Shigeru Shimamoto, "Prediction of propagation path loss for stratospheric platforms mobile communications in urban site LOS/NLOS environment," in *Proceedings IEEE International Conference on Communications* (*ICC*) *2006*, Istanbul, Turkey, vol. 12, June 2006, pp. 5643-5648.

[6] Iskandar and Shigeru Shimamoto, "Ray tracing for urban site propagation in stratospheric platform mobile communications," in *Proceedings of the 11th IEEE Asia-Pacific Conference on Communications* (*APCC*) *2005*, Perth, Australia, October 2005, pp. 212-216.

[7] Iskandar and Shigeru Shimamoto, "Urban site path loss prediction for mobile communications employing stratospheric platforms," in *Proceedings of the 8th IEEE International Symposium on Signal Processing and Its Application* (*ISSPA*) *2005*, Sydney, Australia, vol. 1, August 2005, pp. 267-270.

[8] Iskandar and Shigeru Shimamoto, "The channel characterization and performance evaluation of mobile communication employing stratospheric platform," in *Proceedings of IEEE/ACES Wireless Communications and Applied Computational Electromagnetics Conference* (*WCACEM*) *2005*, Hawaii, USA, April 2005, pp. 828-831.

[9] Iskandar and Shigeru Shimamoto, "The channel characterization of mobile communication employing stratospheric platform," in *Proceedings of the 12th International Conference on Telecommunication System–Modeling and Analysis* (*ICTSM*) *2004*, Monterey, USA, July 2004, pp. 293-298.